Design, Fabrication and Testing of Novel Medical Facemasks to Prevent Covid-19

by

Laine Alby

A thesis submitted to the Graduate Faculty of
Auburn University
in partial fulfillment of the
requirements for the Degree of
Master of Science

Auburn, Alabama
May 7, 2022

Keywords: textiles, COVID-19, facemask,
filtration, medicine, novel

Approved by

Sabit Adanur, Chair, Professor of Mechanical Engineering
Jeffrey Suhling, Professor and Department Chair of Mechanical Engineering
Jay Khodadadi, Professor of Mechanical Engineering
Jordan Roberts, Senior Lecturer of Mechanical Engineering

Abstract:

The nation is going through an unprecedented time due to the Coronavirus pandemic. One of the most effective ways to prevent viral spread is to use face masks and respirators. Available reusable face masks are often not as effective as single-use coverings, which are costly and environmentally irresponsible. Currently, there is limited knowledge available on the performance of fabrics used in masks. Filtration efficiencies as a function of aerosol particulate sizes in 10 nm to 10 μm range are relevant for respiratory virus transmission but lack evaluation. The purpose of this research is to develop novel face masks and respirators to fight the pandemic based on scientific and engineering principles. In this research, novel medical face masks are designed, produced, and tested to reduce the spread of COVID-19 while improving on deficiencies present in currently used textile reusable face coverings. The project incorporates additive manufacturing, computer aided design (CAD), third party testing of both Bacterial Filtration Efficiency (BFE) and differential pressure measurements, and laser-visualization tools for illuminating leakage.

Acknowledgements

I would first like to thank my advisor Dr. Sabit Adanur for allowing me the opportunity to investigate a current and modern field relevant to the COVID-19 pandemic as well as the opportunity to pursue my master's degree. I also would like to thank my additional committee members, Dr. Jeff Suhling, Dr. Jay Khodadadi, and Dr. Jordan Roberts for their contribution.

Additionally, a special thanks is given to Dr. Vrishank Raghav of Auburn University's Aerospace Engineering Department and his research team including postdoctoral candidate Dr. Sarah Willis and graduate student Will McAtee for their help and experimental setup for laser visualization. Also, I would like to thank Dr. Ramsis Farag for allowing me to use the optical microscope and scale in his lab to aid my research.

I also wish to extend my thanks to Ajay Jayswal for his help with the initial research and design stages of the mask as well as his contribution to a stimulating and encouraging work environment in the lab. Thank you to my friends and family as well, who have been supportive throughout my research time and have encouraged me in my pursuits.

Finally, the financial support from the Alabama Department of Economic and Community Affairs (ADECA) is gratefully acknowledged.

Table of Contents

List of Tables:

List of Figures:

CHAPTER 1: INTRODUCTION

The coronavirus pandemic (COVID-19) has introduced unprecedented new challenges in virus transmission prevention. Initially, the pandemic was thought to be caused close contact with an infected individual who presented symptoms. However, the virus began to spread more quickly than anticipated. On January 30, 2020, SARS-CoV-2 was described in several individuals who were believed to have been infected by a traveler who had returned recently from China, yet the traveler did not present any symptoms of the virus [1]. This brought attention to the scientific community the possible danger of virus transmission by asymptomatic patients and fueled the search for a solution to the swift spread of the virus across the world.

Face masks and respirators have been considered one of the most effective methods of transmission limitation to prevent coronavirus from spreading throughout the population [2]. As resources became more limited during the pandemic, many fabric face coverings were produced to supplement traditional face masks and respirators such as N-95 masks or surgical masks. However, very limited knowledge existed detailing the filtration performance of various fabrics that could potentially be used to construct these masks. Additionally, masks alone have been considered to only have a small effect on reducing transmission rates unless they are highly effective and widely used, emphasizing the need for effective masks that do not cause strain on the user when worn [3].

Since 2019, there have been 490,853,129 recorded cases of COVID-19 globally, with a cumulative 6,155,344 deaths caused by the disease [4]. In the United States alone, over 79 million cases have been recorded, with almost 200,000 recorded in the last week as of April 6, 2022. Deaths in the United States have reached 974,431, which is perilously close to one million deaths that can be attributed to the devastation of the COVID-19 pandemic. For comparison,

India has recorded over 43 million cases with over half a million recorded deaths, Brazil has recorded almost 30 million cases and over 600,000 deaths, France has recorded over 25 million cases and almost 140,000 deaths, and Germany has recorded over 21 million cases with over 130,000 deaths.

Figure 1 demonstrates the effects of COVID-19 around the world. Darker blue countries denote countries who have recorded a greater number of cases since the onset of the COVID-19 pandemic, whereas lighter blue countries have recorded fewer cases. The graphic also demonstrates over 1 million cases recorded in the last 24 hours that the website was viewed, which was on April 12, 2022, demonstrating that the virus is still very much plaguing the world now and solutions are still necessary to halt the spread.

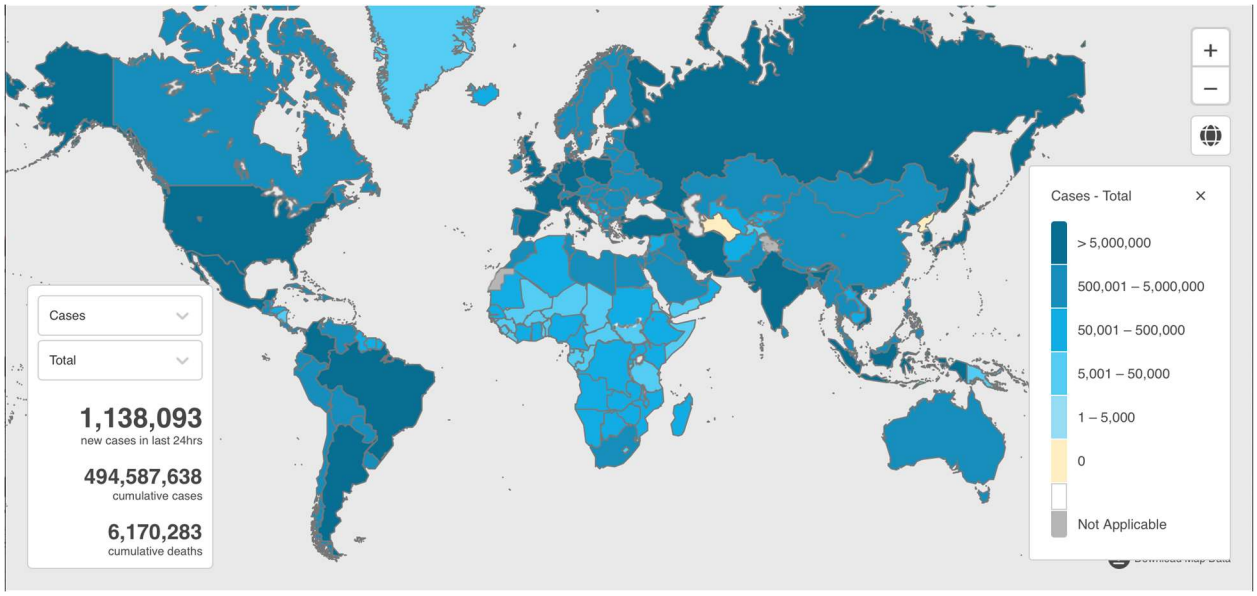

Figure 1: Coronavirus cases recorded around the world [5]

Figure 2 demonstrates the daily trends in cases for the United States and corresponding events from the general timeline of COVID-19 events that may have induced changes in the trends. For example, in April 2020, when the CDC first recommended mask wearing outside of the home, the number in cases plateaus, but increases in June as restrictions are eased [6]. This

encourages the idea that wearing masks can decrease the spread of COVID-19, and also emphasizes the magnitude of the COVID-19 pandemic in the United States alone.

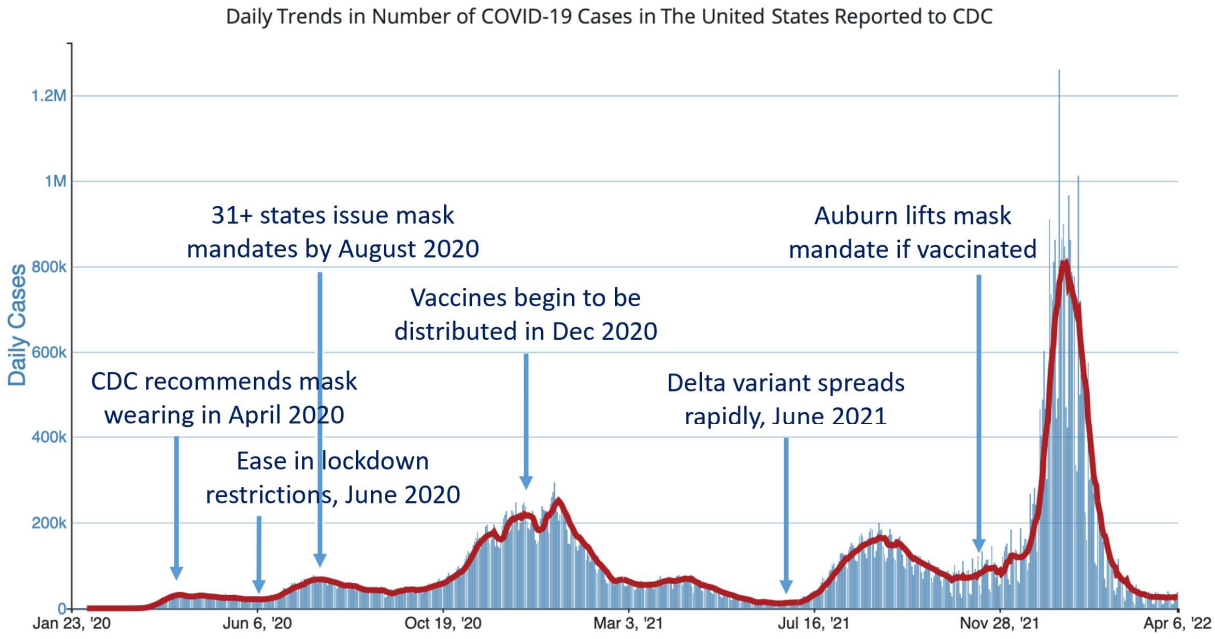

Figure 2: Daily trends in COVID-19 cases in the U.S. since January 2020 [6]

Constructing and producing a mask design that is both effective, reusable, and comfortable could decrease the transmission of this devastating virus. The world has suffered many losses from the pandemic to date and pursuing methods of decreasing the power of this virus will only have positive repercussions. Considering limited resources and strain placed on production of masks during a worldwide pandemic, constructing a mask that can be replicated at home and reused many times is a vital part of design considerations for a novel mask. Therefore, the aim of this research is to design, fabricate, and test novel face masks to prevent the spread of COVID-19 using textiles and in a format that can be reproduced at home, but to also ensure the mask is comfortable and effective.

Additionally, it is important to note that the results of this study can be applied to fields stretching beyond the prevention of the spread of COVID-19. If a comfortable, effective, and

reusable mask were to be constructed, it could help medical professionals in their day-to-day work to have proper protective equipment without having to replace it as often. Additionally, the mask could be worn in fields where hazardous particulate is often encountered, such as demolition groups who may encounter asbestos and need proper protection to prevent inhalation of particulate. Fabric filters could even be used for household filtration of air conditioning units, creating a more sustainable option for these often-replaced filters. This could in turn be extended to cabin air filters of cars, or filters for high-volume air conditioning equipment in hospitals or industrial applications.

CHAPTER 2: LITERATURE REVIEW

2.1 Introduction

The following literature review aims to evaluate deficiencies in current cotton mask designs as well as investigate methods utilized previously to combat these deficiencies. The information collected will then be used to construct a test a novel mask design that has superior performance in filtration efficiency and breathability as compared to those available on the market today.

First, general filtration theory will be investigated to examine important parameters used to evaluate mask performance. Next, testing methods used to evaluate these parameters will be detailed. Following, current ASTM standards for barrier face coverings will be detailed to ensure the design fits current expected standards that other face masks are expected to meet. Literature impacting the design of the novel face mask will then be evaluated, including both the fit and construction of the design as well as the materials and composition that will best protect the user and others from the spread of COVID-19. Any gaps in available literature found detailing these areas will be identified so that the current investigation can explore these.

Finally, prior art will be identified. It is important to know what patents are published currently on similar designs to that being explored, as the aim of the project is to construct a novel mask design. A provisional patent has been applied for considering the design proposed in this project and examining available prior art will help in patent searching performed on this design to help determine if proceeding with a patent application is desired.

2.2 Background

In the background section of this literature review, information that gives fundamental understanding to aspects of the project is detailed. This includes the basis for filtration theory, parameters and testing methods used for evaluation, and common standards set for mask and face coverings by various organizations.

2.2.1 Filtration Theory

Fibrous filters prevent the flow of contaminants in multiple ways. Fibrous filters are defined as simple, economical devices that are capable of removing sub-micrometer particles from gas streams, which is particularly useful in medical applications such as face coverings or respirators. Because of the very small size of the particles in question, various parameters can affect performance of these filters including particle shape, aggregate morphology, flow regime, humidity, fiber size, and particle loading [7].

Porosity is an important parameter in regulating the collection efficiency that is intended. Porosity is defined as the total volume of air over the fabric volume and decreasing the porosity of the material increases the filter performance but doing so requires more back pressure to ensure the same flow rate through the filter [8]. Literature also states that pressure drop is proportionate to the filter thickness and inversely proportional to the cross-sectional area [9].

To understand filter design, the concept of single-fiber efficiency is important. This concept describes the fraction of particles collected by a unit length of a fiber, and it is calculated as follows:

$$E = 1 - \exp\left[\frac{-4\alpha\eta L}{\pi d_f(1-\alpha)}\right] \quad \text{Eq. 1}$$

where η is the single fiber efficiency, L represents the filter thickness, α represents the packing density or solidity of the filter, and d_f is the fiber diameter. The construction and

porosity of the fabric build off this concept to provide the filtration capacity of the fabric.

An ideal fibrous filter has a high collection efficiency value and a low pressure drop value. Collection efficiency is often a function of particle size, and it is defined as the fraction of entering particles that are collected by the filter. The parameters investigated in this project that reflect on this idea are bacterial filtration efficiency and initial filtration efficiency, which will be further defined in this literature review. For high-efficiency filters, as the mask for this project is intended to be, penetration is a helpful indicator of this as well, and it is defined as 1 minus the collection efficiency [7].

To construct this value, various capture mechanisms are at work. Particles may deposit on a fiber through inertial impaction, interception, Brownian motion, gravitational settling, and electrostatic forces. These mechanisms are illustrated in Figure 3.

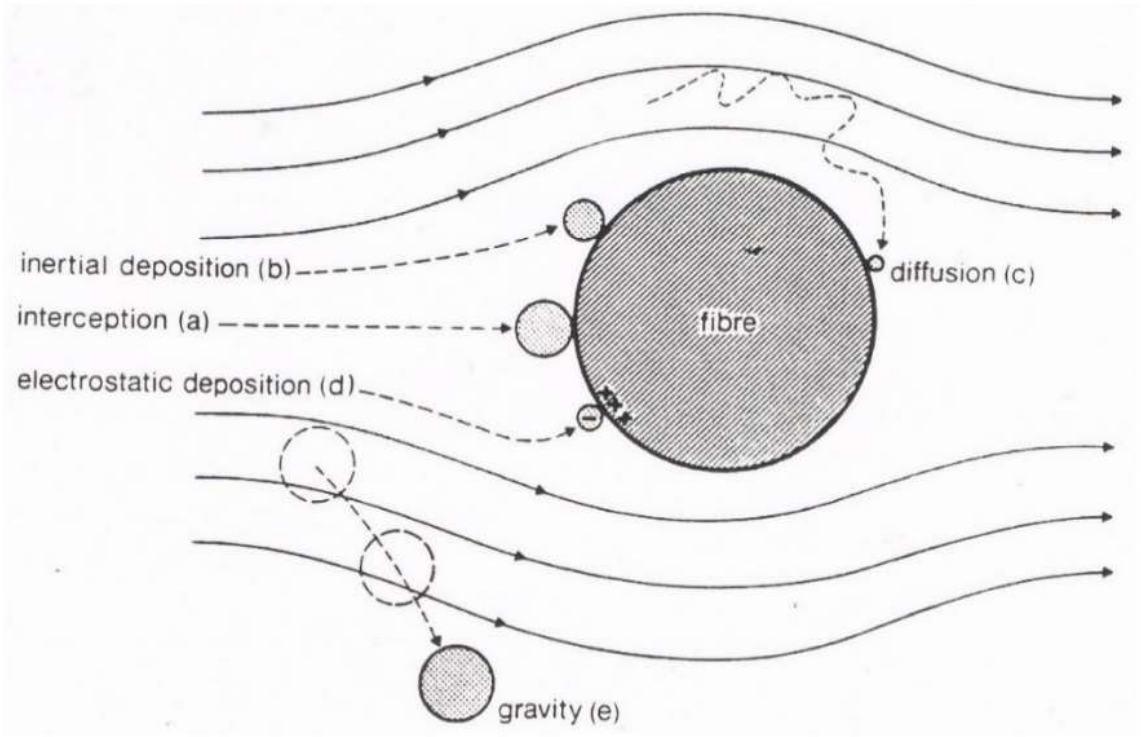

Figure 3: Filtration mechanisms [8]

Inertial impaction occurs when a particle departs from its original gas streamline and hits

a fiber, thereby not passing through the filter material. Interception occurs because particles have finite size, and when the particle comes within one particle radius of the fiber surface, deposition occurs even if it remains on its original gas streamline. Brownian motion, or random motion of small particles suspended in fluid, can be sufficiently strong enough to divert a particle from its streamline and into a fiber. Gravitational settling can contribute to filtration capture, but this effect is often negligible for nanoparticles due to their small size and mass. Electrostatic forces occur when fibers carry electric charges, which can polarize fibers and cause charged particles to divert towards fibers. However, the project in question regards a fabric that is intended to be washable, and electrostatic forces would not apply in this situation.

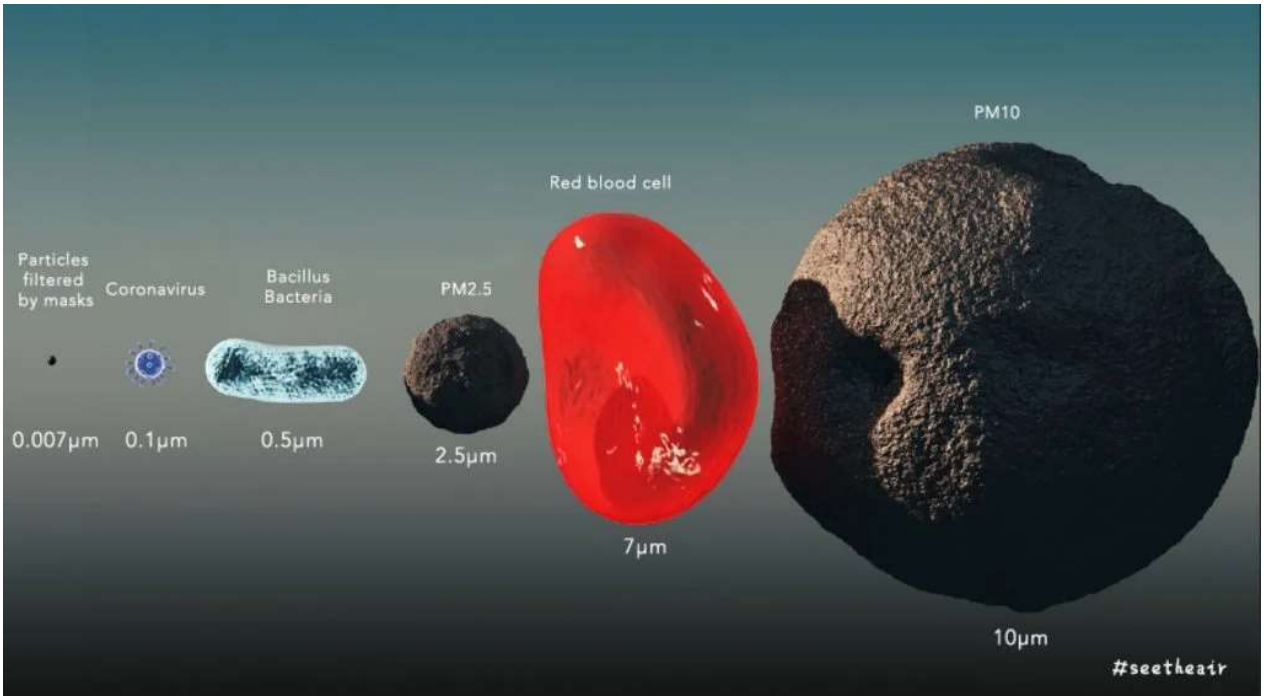

Figure 4: Common particle sizes and comparison [10]

Therefore, it important to know the pore size of the material as well as the pore size of the particles that are intended to be arrested by the filter material. Pore size is described as the spaces formed at yarn interstices in woven or knitted fabrics or between fibers in nonwoven filters [8]. When the particle is smaller than that of the pore size, the aforementioned capture

mechanisms become increasingly important. Common particle sizes are shown in Figure 4.

2.2.2 Parameters and Testing Methods

The first parameter evaluated is breathability. Differential pressure is used to evaluate this parameter, and it is calculated as follows:

$$\Delta P = \frac{X_{m1} - X_{m2}}{4.9} \quad \text{Eq. 2}$$

where X_{m1} represents the lower pressure side of the material, X_{m2} represents the higher-pressure side, 4.9 is the area in square centimeters of the test material, and ΔP is the differential pressure per square centimeter of the material in Pascals. Tests are performed on at least 10 samples.

This differential pressure measurement is used to quantify the breathability of the material. Table 1 shows maximum allowed values for this differential pressure or breathability value for various standards for different mask types in the US, EU, and China [11].

As shown, N95 type masks generally have a specified inhalation and exhalation resistance value in Pascals, which can be divided by 4.9 cm^2 to estimate the breathability value as compared to other mask types, where surgical masks have lower differential pressure measurements and are therefore considered easier to breathe through. Europe is the only region with a standard for cloth mask material masks. In conclusion, the desired value for the mask designed in this project would be closer to that of a surgical mask, and less than that of an N95 mask to maximize comfort of the user.

Table 1: Maximum allowed pressure differentials for various masks per US, EU, and China [11]

	N95, FFP2, KN95		Surgical/medical mask material	Cloth mask material
	Inhalation	Exhalation		
NIOSH[1]	343 Pa (85 L/min)	245 Pa (85 L/min)	---	---
ASTM	---	---	[2] 50/60/60 Pa/cm^2 (245/294/294 Pa) (8 L/min)	---
EU[3]	240 Pa (95 L/min) 70 Pa (30 L/min)	300 Pa (160 L/min)	[4] 40/40/60 Pa/cm^2 (196/196/294 Pa) (8 L/min)	70 Pa/cm^2
China[5]	350 Pa (85 L/min)	250 Pa (85 L/min)	49 Pa/cm^2 240 Pa (8 L/min)	---

1. NIOSH = U.S. National Institute for Occupational Safety and Health; 42CFR84.
2. Surgical mask barrier levels 1, 2, and 3, respectively. Units (Pa) assume area is 4.9 cm^2.
3. EU = European Union; EN 149; EN 14683; CWA 17553.
4. Medical masks type I, II, and IIR, respectively. Units (Pa) assume area is 4.9 cm^2.
5. China National Standards; GB2626; YY0469.

The next parameter evaluated is filtration efficiency of the mask. For this test, ASTM F2101-19 – Test Method for Evaluating the Bacterial Filtration Efficiency (BFE) of Medical Face Mask Materials, Using a Biological Aerosol of Staphylococcus *aureus* is used to evaluate the filtration efficiency.

Filtration efficiency is calculated using the following equation:

$$FE = \left(1 - \frac{G_2}{G_1}\right) * 100\% \qquad \text{Eq. 3}$$

where FE is filtration efficiency, G_1 is the concentration of tested bacteria upstream, and G_2 is the concentration downstream of the textile sample [12]. Table 2 demonstrates the typical

filtration efficiencies for N95, FFP2, and KN95 masks.

Table 2: Particle filtration efficiency test criteria for N95, FFP2, and KN95 Masks [11]

	N95 (42CFR84)	*FFP2 (EN 149)*	*KN95 (GB2626)*
Filtration efficiency	≥ 95%	≥ 94%	≥ 95%
Particles	Polydisperse NaCl	Polydisperse NaCl	Polydisperse NaCl
Flow rate	85 L/min	95 L/min	85 L/min
Tested by	NIOSH	Manufacturer	Manufacturer
No. FFRs tested	20	9	15
Fit-test: Total inward leakage	Not required	≤ 8%	≤ 8%

Additionally, there are three levels of ASTM barrier classifications for filtration efficiencies that determine the effectiveness of the face covering or respirator as shown in Table 3.

Table 3: ASTM criteria for 3 barrier levels for surgical masks [11]

	ASTM Level 1	ASTM Level 2	ASTM Level 3
Fluid resistance (mmHg)	80	120	160
Filtration efficiency (%) (PFE or BFE)	≥ 95	≥ 98	≥ 98
Differential pressure, (Pa/cm^2) (8 L/min)	< 50	< 60	< 60
Flame spread	Class 1	Class 1	Class 1

It is desirable to maximize the filtration efficiency obtained by the designed mask to a level that is comparable to an N95 mask, but without sacrificing a lower differential pressure value. Different fabrics and configurations can be tested to achieve this.

It is important to note that the breathability values and filtration efficiency values are obtained assuming the mask has a perfect fit to the user's face. Gaps in the mask can allow air to escape, thus decreasing filtration efficiency values and breathability values such that the mask cannot filter to the level it has been tested at. Therefore, it is integral that the mask be designed to

fit the user in the best way possible.

2.2.3 ASTM Standards for Barrier Face Coverings

In February of 2021, new standards were released by the global standards organization ASTM International regarding barrier face coverings that do not meet requirements for medical face coverings or respirators. These new standards were constructed in regards to face coverings made in response to the COVID-19 pandemic by ASTM's committee on personal protective coverings and equipment to introduce requirements for these barrier face coverings regarding "design and general construction criteria, particle filtration efficiency levels, sizing and fit testing criteria, labeling instructions, and guidance on cleaning and recommended periods of use" [13].

A guideline for design requirements was published with the standards release. First, general construction guidelines are detailed, and the mask designed needs to meet the criteria listed as well as specific criteria regarding reusable face masks [14]. First, the mask must cover the wearer's nose and mouth and fit snugly without gaps. The mask material must be non-irritating, non-toxic, and cannot post a flammability hazard. They should be free of sharp edges. Washable coverings should be durable enough to withstand repeated wear and laundering. Additionally, coverings with replaceable filters should have a means for preventing improper filter placement. The covering cannot have vents, valves, or open pathways, and the design should minimize flow of air around the perimeter for a better seal.

Next, details of a retention system are described. The covering should have a means of keeping the mask over the wearer's nose and mouth over a range of activities. The retention system must either be made from elastic materials or provide for adjustment for proper fit.

Then, sizing is described. Multiple sizes are permitted but not required and can be in different sizes for each population group or for specific population groups, like children.

Next, leakage assessments are required to be disclosed. A self-declaration is required that reports a reduction in leakage around the perimeter of the covering, and the design analysis on which the declaration is made must apply to the mask in a new state and after the maximum number of laundering or cleaning cycles specified for the design.

Finally, performance requirements are detailed. Barrier face coverings must meet the requirements specified in Table 4 both in a new condition and after the maximum specified laundering or cleaning cycles.

Table 4: Barrier face covering minimum performance requirements [14]

Performance Property	Criteria	Test Method Section
Sub-micron particulate filtration efficiency	≥20 %	8.1
Airflow resistance, inhalation	≤15 mm H_2O	8.2

Additionally, there are two levels of classification for performance of the barrier face masks, which are detailed in Table 5.

Table 5: Separate classification of barrier face covering performance properties [14]

Performance Property	Level 1 (Lower Performance)	Level 2 (Higher Performance)
Sub-micron particulate filtration efficiency[C] (Effectiveness of barrier face covering for capturing small particles; larger percentages indicate higher performance)	≥20 %	≥50 %
Airflow resistance (Indicative of ease of breathing while wearing barrier face covering; lower resistances indicate more breathable products)	≤15 mm H_2O[D]	≤5 mm H_2O

[A] Each performance property is classified separately; there are four possible sets of classifications. A barrier face covering can have:
(1) Level 1 performance for both properties,
(2) Level 1 performance in sub-micron particulate filtration efficiency and Level 2 performance in airflow resistance,
(3) Level 2 performance in sub-micron particulate filtration efficiency and Level 1 performance in airflow resistance, and
(4) Level 2 performance for both properties.
[B] As noted in 8.1.4.2 and 8.2.4, the performance properties are calculated from the lowest measured filtration efficiency and highest measured airflow resistance of all test specimens (including specimens subjected to the maximum number of laundering and cleaning cycles, as specified by the manufacturer).
[C] Testing results per procedures in 8.1 based on Subpart K of 42 CFR Part 84.
[D] Airflow resistance in range of 5 to 15 mm H_2O can be perceived as difficult for long-term wearing by some individuals, including children or adults that have specific medical conditions that cause difficulty in breathing.

The product must include visual rating schemes to demonstrate performance of the face covering. Various options are offered in the standards report, as shown in Figure 5.

Option 1

Property	Level 1 (Lower Performance)	Level 2 (Higher Performance)	"My Mask"
Filtration Efficiency	≥ 20%	≥ 50%	Level 2: 60%
Breathability	≤ 15 mm H_2O	≤ 5 mm H_2O	Level 1: 8 mm H_2O

Option 2

Property	Level 1 (Lower Performance)	Level 2 (Higher Performance)	"My Mask"
Filtration Efficiency	≥ 20% F1	≥ 50% F2	F2
Breathability	≤ 15 mm H_2O B1	≤ 5 mm H_2O B2	B1

Option 3

Property	Level 1 (Lower Performance)	Level 2 (Higher Performance)
Filtration Efficiency	F1	F2
Breathability	B1	B2

FIG. X3.1 Package Label—Tabular Options

Figure 5: Possible visual rating schemes for showing performance classifications of barrier face coverings [14]

A continuum option is also demonstrated, which gives mask producers the ability to show performance on a colored scale as shown in Figure 6. This could be an effective way to demonstrate that the product performs well without providing too much crowding information.

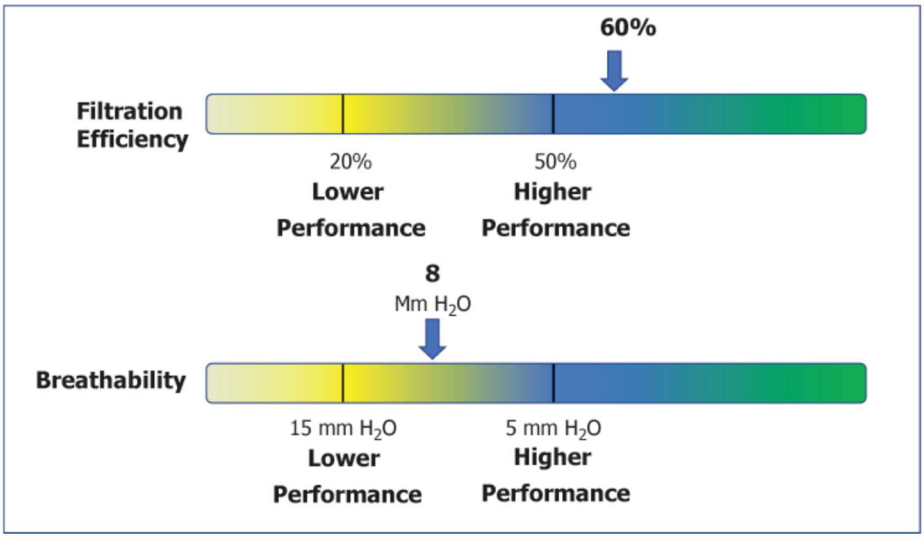

Figure 6: Package label - continuum option [14]

2.3 Mask Design

In the Mask Design section of this literature review, important recent literature regarding aspects of mask design will be noted and discussed such that results of previous experimentation and construction can ensure a functional and well performing mask in this project. Additionally, the importance of fit on the performance of masks will be discussed through the employment of various studies to demonstrate the importance of constructing a well-designed mask without leakage. Literature identifying appropriate fabric types and filter materials will also be detailed.

2.3.1 Impact of Fit on Measured Parameters

Since the beginning of the COVID-19 outbreak, many studies have been performed on the filtration performance of improvised mask materials as well as current mask materials, but mostly in ideal-fit scenarios. However, these masks may not provide the correct performance measures when the face covering is worn, including gaps and issues with fit. This can give the user a false impression of the level of protection they have from COVID-19 transmission when wearing the covering in a high-risk environment [15].

In this study, the filtration efficiency of various respirators, masks, and filter media were examined against the smallest estimated size of virus-carrying particles, around 60 nanometers in size, at a base efficiency level that does not include fit parameters and then again on a mannequin to measure efficiency during use. The masks examined include an N95 mask (3M 8511), a generic dust mask (Rite Aid MaxiMask), a medical mask (Medline), a KN95 respirator (SupplyAid), a handmade 600-thread count cotton mask with a coffee filter (Melitta), paper shop towel filter (Scott), Filtrete 1500 filter (3M), surgical wrap filter (Haylard), vacuum filter bag filter (Shop-Vac), N95 nonwoven material filter (Hollingsworth and Vose), and FTR467 UPLA material filter (APC Filtration, Inc).

Figure 7 depicts the base filtration efficiency of each tested fabric, which measure as low as 17.4% to as high as 99.98%.

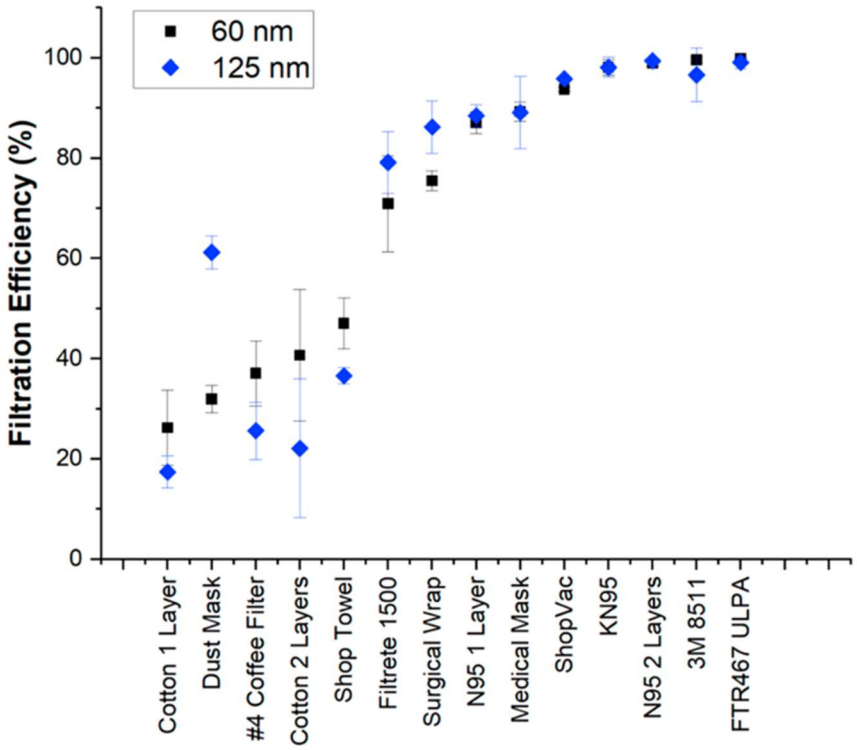

Figure 7: Base filtration efficiency of tested fabrics [15]

A single layer of the 600-thread count cotton measured the lowest filtration efficiency at a base level, but the two layers of cotton increased the range of filtration efficiencies. Testing one single layer of the N95 nonwoven material increased this range significantly to a level like that of a medical mask.

However, once the N95 nonwoven material was inserted into the cotton mask, and the masks were tested on a mannequin form to ensure fit is incorporated into the measured filtration efficiency, the following filtration efficiencies were measured as shown in Figure 8.

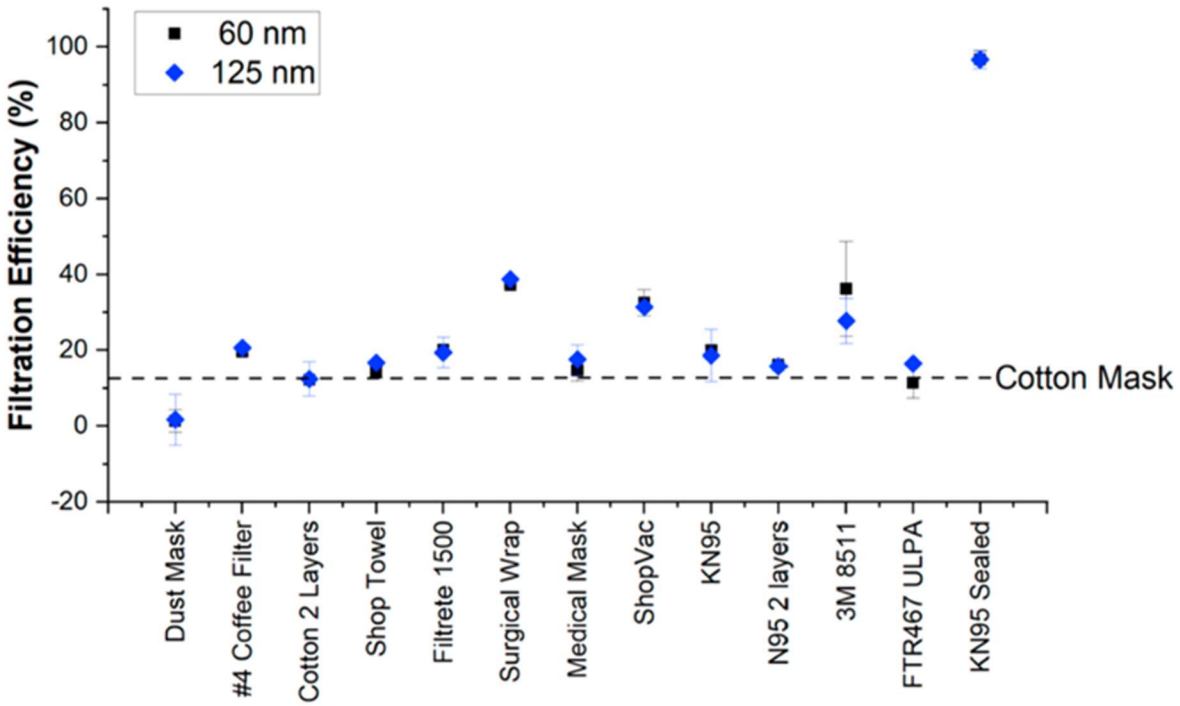

Figure 8: Filtration efficiencies of mask filter materials including fit effects [15]

To compare, the filtration efficiency of the KN95 respirator was evaluated when sealed against the head form, and the resulting efficiency was very near the base KN95 filtration efficiency reported in Figure 7.

This study effectively demonstrated the importance of fit in the filtration efficiency of a cotton face mask and emphasized that the regions with the greatest leakage potential include the nose bridge, the chin, and the jawline.

Various studies have investigated fit modifications that can help reduce leakage and retain the base level of filtration efficiency of the mask material. A research team at Northeastern University investigated the effect of adding a nylon overlayer to surgical-style masks and other homemade cloth masks on the filtration efficiency of the design by utilizing an abridged testing process that can allow for quicker testing of mask compositions during the pandemic [16].

The experimental setup included a user who would wear the mask first as designed,

without the nylon overlayer, and a grommet was fastened to the center of the mask and used to measure particle count of the air inside the mask. Next, the nylon overlayer is used to fit the mask snugly against the user's face. When the experiment was performed on an N95 respirator, a poorly fitted N95 mask measured at a mean removal efficiency of 90.6%, while a well fitted N95 mask measured around 99%. For standard medical-type masks without the overlayer, a mean removal efficiency of 50-75% was achieved. However, with the addition of the overlayer, this increased to 86-90% on average. This highlighted the importance of quality of fit over the brand or quality of materials used for the medical face masks.

Next, these same metrics were used to test a variety of 15 different cloth masks. The masks were separated into three groups based on their style: one for cone-shaped or N95-type masks, one for duck-bill style masks, and one for pleated surgical-style masks. The cone style masks demonstrated the best average performance as shown in Figure 9.

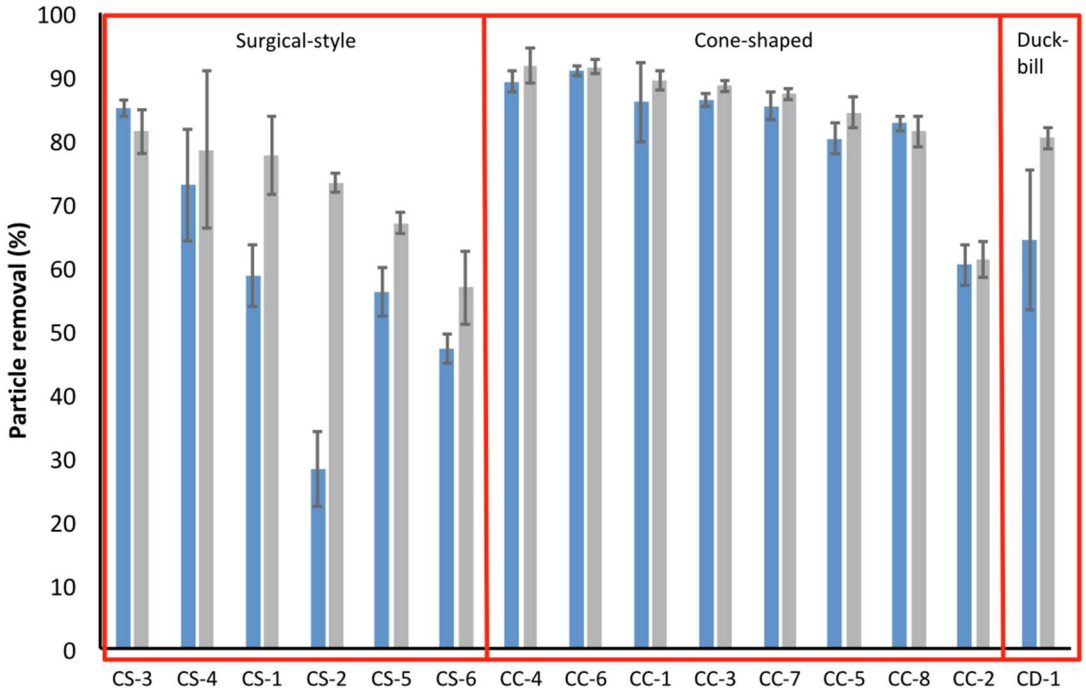

Figure 9: Particle removal rate: cloth masks of 3 styles [16]

The blue bars in the figure reflect the removal rate with normal wear, and the gray

represent removal rate with the added nylon overlayer.

This study concluded that the fit of cotton face masks is variable depending on fit and quality of materials, but that fit is an important factor in use of all masks, ranging from N95 masks to surgical masks. The cone-shaped masks provided the best removal rate, which could provide evidence that this style mask design has a better fit than surgical-style masks, and that the masks increased in removal rate once a nylon overlayer was used to fit them snugly to the user's face. When fit is excellent and the materials of good quality, a very high removal rate can be accomplished using a cotton mask.

Finally, various studies have implemented fit modifications to existing mask designs to evaluate the effect these have on eliminating gaps. A fit factor assessment was performed using a PortaCount pro testing machine and human subjects before and after applying the following fit modifications to source control masks, shown in Figure 10 [17].

Figure 10: Fit modifications [17]

The source control masks tested included two disposable medical masks, one reusable 2-ply cloth mask, one cotton 3-ply cloth mask, and one reusable 4-ply cloth mask. The resulting fit factors determined are shown in Table 6.

Table 6: Human and mannequin mask fit factors evaluated during mask fit tests [8]

Face Covering	Modification	Human Fit Factor		Manikin Fit Factor	
		mean	SD	mean	SD
Medical mask 1	No modification	1.6	0.5	2.0	0.2
	Crossed	1.1	0.2	2.2	0.4
	Bracket	1.0	0.0	2.3	0.1
	Strap	5.4	3.2	2.9	0.4
	Toggle	4.0	2.0	4.1	0.6
	Knotted & tucked	6.0	1.5	4.0	0.9
	Double mask	4.2	2.6	6.7	2.0
	Brace	7.2	1.0	6.1	2.0
Medical mask 2	No modification	1.8	0.4	2.9	0.7
	Crossed	1.1	0.2	2.3	0.6
	Bracket	1.6	0.5	2.2	0.1
	Strap	3.3	1.2	3.1	0.6
	Toggle	6.0	5.8	5.3	1.6
	Knotted & tucked	6.3	3.6	4.8	0.7
	Double mask	2.1	1.1	7.0	2.9
	Brace	13.3	3.7	7.2	1.3
2-ply cloth mask	No modification	1.4	0.3	1.5	0.0
	Brace	2.0*	0.0	2.0	0.3
3-ply cloth mask	No modification	1.3	0.5	1.5	0.1
	Brace	2.0	0.0	2.1	0.3
4-ply cloth mask	No modification	1.5	0.6	2.6	0.5
	Brace	4.6*	1.5	3.6	0.7

*Fit factor was determined to be statistically significant ($P < .05$) when comparing a fit modified face mask to the corresponding no modification control.

The most effective fit modification to the surgical masks tested was the addition of a brace. The brace addition increased the human fit factor of both medical masks by at least 6 times the original fit factor, and it increased the fit factor of each cloth mask as well. Therefore, a brace would be the most effective addition to the mask to improve fit and help increase

performance to that of the filtration efficiency and breathability estimated using ASTM testing methods.

2.3.2 Fabric selection

To construct a well-performing face covering, fabric selection is an integral part of the design that affects its filtration capabilities, especially when an inner filter layer is not considered. For that reason, various studies were investigated regarding the capabilities of commonly available fabrics and their performance in filtration and breathability for the application of constructing face masks. Since the pandemic started, many research groups have investigated this topic to address the limited availability of traditionally used face mask and filtration materials. The strain placed on providing medical-grade face coverings limited availability to the general public, causing them to utilize fabrics available in their own homes. Additionally, utilizing a fabric that is produced currently in Alabama will encourage textile industry and production in the state, promoting economic growth in the state.

Standard mask testing methods, consisting of ASTM F2101-14, using the model virus bacteriophage MS2 were used to test the viral filtration efficiency of various fabric masks as well as commercially available disposable, surgical, and N95 masks. Of the fabric masks, one included a pocket filter, which was tested without a filter, with a dried baby wipe, and with a section of a vacuum cleaner bag. The results of testing concluded that the best performing mask was the pocket filter mask, composed of cotton, when it contained the vacuum bag section as its filter medium. With an aerosol size of 6 micrometers, the viral filtration efficiency was 99.5%, and with an aerosol size of 2.6 micrometers the filtration efficiency was 98.8%. These values are both very close to the advertised efficiency of surgical masks. However, the most important element of this efficiency value is proper fit, which was not explored in this study. Results of this

study are demonstrated in Table 7 [18].

Table 7: Average viral filtration efficiency (VFE) of different types of fabric masks compared with N95, surgical, and disposable masks determined using ASTM F2101-14 standard method with bacteriophage MS2 as the challenge virus [18]

Mask	Average Viral Filtration Efficiency for an Average Aerosol Size of 6.0 μm ($VFE_{(6.0\ \mu m)}$) (%) [Range]	Average Viral Filtration Efficiency Calculated with the Larger Aerosols Excluded to Give an Average Aerosol Size of 2.6 μm ($VFE_{(2.6\ \mu m)}$) (%) [Range]	Description [1]
N95	99.9 [99.8–100]	99.3 [98.6–99.7]	KN95 (nonmedical device GB2626-2006)
Surgical 1	99.9 [99.8–100]	99.5 [98.7–99.5]	Level 1 single use surgical mask (according to AS 4381:2015 Nelson Laboratories, USA, bacterial filtration efficacy (BF) average 98.2%, minimum 97.1% as per ASTMF1862)
Surgical 2	99.6 [99.3–99.8]	98.5 [98.3–98.6]	Surgical face mask (99.9% BFE [2])
Disposable 1	99.9 [99.9–100]	99.7 [99.7–99.9]	Disposable face mask (nonmedical GB/T32610-2016)
Fabric 1	54.4 [54.3–54.6]	65.8 [64.1–67.6]	Three layered masks made of 100% cotton
Fabric 2	67.3 [54.8–92.1]	90.9 [86.5–94.3]	Denim face mask—double layer stretchy cotton
Fabric 3	93.6 [92.1–96.3]	89.0 [86.1–90.5]	100% hemp outer layer, poly membrane mid layer, and organic cheesecloth inner layer
Fabric 4	50.3 [49.7–51.2]	63.6 [51.8–75.0]	Two layers of 100% Mulberry Silk
Fabric 5	54.9 [55.4–55.7]	93.32 [86.9–97.7]	Washable fabric face mask with pocket for filter made from cotton and poplin fabric
Fabric 5 + dried baby wipe	98.5 [97.7–99.6]	97.6 [97.0–98.5]	Fabric 5 with a dried baby wipe inserted into the pocket
Fabric 5 + vacuum cleaner bag	99.5 [98.9–99.9]	98.8 [96.9–99.8]	Fabric 5 with a section of a vacuum cleaner bag inserted into the pocket
Fabric 6	98.6 [97.7–99.6]	99.1 [98.3–99.7]	Made using the Victorian DHHS design [13]. Two layers of reusable shopping bag (nonwoven polypropylene) and one layer of cotton

All masks were tested in triplicate except Fabric 1, which was tested in duplicate. The average aerosol size that the masks were tested against was 6.0 μm and the viral filtration efficiency was calculated using this aerosol size and then again with the larger aerosol excluded to give an average aerosol size of 2.6 μm to better represent the size of aerosols that reach the lower respiratory system. [1] Description information was collected from the mask packaging or seller website. [2] Bacterial filtration efficiency.

In an additional study, 15 types of natural and synthetic fabrics were used to construct masks of either single layers, double layers of the same fabric, or combination layers of multiple fabrics to determine filtration efficiency. The most thoroughly investigated fabric is cotton, in which various thread-per-inch (TPI) values were tested in different layers. Lower TPI cotton (80TPI) performed much worse than higher TPI cotton (600TPI). Full results are shown in Table

8 [19].

Table 8: Filtration efficiencies of various test specimens at a flow rate of 1.2 CFM and the corresponding differential pressure across the specimen [19]

	flow rate: 1.2 CFM		
	filter efficiency (%)		pressure differential
sample/fabric	<300 nm average ± error	>300 nm average ± error	ΔP (Pa)
N95 (no gap)	85 ± 15	99.9 ± 0.1	2.2
N95 (with gap)	34 ± 15	12 ± 3	2.2
surgical mask (no gap)	76 ± 22	99.6 ± 0.1	2.5
surgical mask (with gap)	50 ± 7	44 ± 3	2.5
cotton quilt	96 ± 2	96.1 ± 0.3	2.7
quilter's cotton (80 TPI), 1 layer	9 ± 13	14 ± 1	2.2
quilter's cotton (80 TPI), 2 layers	38 ± 11	49 ± 3	2.5
flannel	57 ± 8	44 ± 2	2.2
cotton (600 TPI), 1 layer	79 ± 23	98.4 ± 0.2	2.5
cotton (600 TPI), 2 layers	82 ± 19	99.5 ± 0.1	2.5
chiffon, 1 layer	67 ± 16	73 ± 2	2.7
chiffon, 2 layers	83 ± 9	90 ± 1	3.0
natural silk, 1 layer	54 ± 8	56 ± 2	2.5
natural silk, 2 layers	65 ± 10	65 ± 2	2.7
natural silk, 4 layers	86 ± 5	88 ± 1	2.7
hybrid 1: cotton/chiffon	97 ± 2	99.2 ± 0.2	3.0
hybrid 2: cotton/silk (no gap)	94 ± 2	98.5 ± 0.2	3.0
hybrid 2: cotton/silk (gap)	37 ± 7	32 ± 3	3.0
hybrid 3: cotton/flannel	95 ± 2	96 ± 1	3.0

[a]The filtration efficiencies are the weighted averages for each size range—less than 300 nm and more than 300 nm.

Although the cotton/chiffon silk combination had the highest filtration efficiency, the pressure differential was very high, indicating it may be uncomfortable for users to breathe through. In considering comfort level for the mask user, differential pressures are optimal when they are the lowest, but a lower differential pressure can often sacrifice performance of bacterial filtration efficiency. In conclusion, the best materials for constructing a fabric mask include higher TPI cotton and chiffon fabrics with tighter weaves and lower porosity. However, it is noted that improper fit can reduce the efficiency of the mask by up to 50%. Therefore, ensuring proper sealing of the mask is vital to retaining good filtration efficiency values.

It is also important to note that the 2-layer cotton design produced a mask with a high filter efficiency, especially above 300 nm at 99.5%. The pressure differential exhibited by this combination was 2.5, which lies in the middle of the range of combinations tested. This exhibits a two-layer cotton fabric design as a promising combination for the novel mask design of this

study, and cotton is a well-known product produced in Alabama's textile production industry. Therefore, this combination would be important to investigate for this study.

In a similarly designed study, 11 common household fabrics were gathered and tested to evaluate efficiency and breathability [20]. The fabric types are characterized in Table 9, which demonstrates the weight, thread count, porosity, and water soaking speed of each fabric type investigated for the study.

Table 9: Characterization of fabrics tested for breathability [20]

Sample Description	Fiber Content [Fabric Construction]	Weight (g/m^2)	Thread Count (threads per inch)	Porosity (%), mean ±SD, n = 9	Water Soaking Speed (mm^2/s)
Medical Mask: FM-EL style	polypropylene [non-woven]	53.9	n/a	n/a	0
Fabric 1: Used shirt	100% cotton [knit]	114.2	200	0.7 ± 0.1	10.0
Fabric 2: New undershirt	100% cotton [knit]	111.5	45	4.5 ± 0.1	0
Fabric 3: New quilt cloth	100% cotton [woven]	89.1	150	10.8 ± 0.2	10.1
Fabric 4: Used undershirt	75% cotton, 25% polyester [knit]	148.2	85	5.5 ± 0.2	160.7
Fabric 5: Used shirt	70% cotton, 30% polyester [woven]	107.5	200	0.1 ± 0.1	1.6
Fabric 6: New T-shirt	60% cotton, 40% polyester [knit]	183.2	75	1.1 ± 0.3	72.4
Fabric 7: New quilt cloth	35% cotton, 65% polyester [woven]	95.4	180	4.8 ± 0.2	23.6
Fabric 8: new bedsheet	100% polyester [woven]	81.1	180	5.8 ± 0.8	28.5
Fabric 9: New dishcloth	80% polyester, 20% polyamide [napped]	380.5	n/a	n/a	6.2
Fabric 10: Used shirt	silk [woven]	49.9	220	4.3 ± 0.1	6.7
Fabric 11: Used shirt	silk [woven]	49.4	200	2.2 ± 0.5	5.8

The fabric performances were then evaluated for each material, and breathability was also evaluated. Results for the fabric types tested are shown in Table 10. The results of this quantitative study support that cotton fabrics show higher filtration efficiency, supporting its use in the masks constructed for this project in particular. This study again emphasizes the importance of proper fit of the masks and did not include this as a factor in its study.

Table 10: Results of droplet blocking efficiency and breathability measurements [20]

Sample description	ε (%) at 25 mm (high momentum droplets)			β (mm/Pa s)
	Minimum[a]	Median	Maximum	Mean ±SD, n = 3
Medical Mask	96.4	98.5	99.9	1.83 ± 0.15
Fabric 1: Used shirt, knit, 100% C	87.9	96.8	99.8	1.37 ± 0.06
Fabric 2: New undershirt, knit, 100% C	41.1	81.9	95.2	10.70 ± 0.66
Fabric 3: New quilt cloth, woven, 100% C	30.6	71.7	93.3	8.67 ± 0.12
Fabric 4: Used undershirt, knit, 75% C - 25% PE	28.9	72.5	92.5	11.97 ± 0.25
Fabric 5: Used shirt, woven, 70% C - 30% PE	81.2	93.6	99.7	1.80 ± 0.00
Fabric 6: New T-shirt, knit, 60% C - 40% PE	42.0	83.1	98.3	7.23 ± 0.55
Fabric 7: New quilt cloth, woven, 35% C - 65% PE	55.2	81.8	96.4	5.07 ± 0.21
Fabric 8: New bedsheet, woven, 100% PE	74.9	94.8	99.7	3.23 ± 0.06
Fabric 9: New dishcloth, napped, 80% PE - 20% PA	90.0	98.2	99.8	6.53 ± 0.21
Fabric 10: Used shirt, woven, 100% S	70.8	92.9	99.5	3.90 ± 0.36
Fabric 11: Used shirt, woven, 100% S	81.1	98.7	99.8	2.10 ± 0.61
Fabric 2 - 2 Layers	78.3	94.1	98.3	5.53 ± 0.35
Fabric 2 - 3 Layers	96.8	98.9	99.8	3.77 ± 0.06
Fabric 6 - 2 Layers	94.0	98.1	99.6	3.87 ± 0.06
Fabric 6 - 3 Layers[b]		>98.1		2.63 ± 0.06
Sample description	ε (%) at 300 mm (low momentum droplets)			
	Minimum[a]	Median	Maximum	
Medical Mask	95.2	99.7	99.9	
Fabric 6	82.5	94.2	99.3	
Fabric 6 - 2 Layers[b]		>94.2		

C: cotton, PE: polyester, PA: polyamide, S: silk.

[a]Outliers (see Fig. 3) are ignored. Minimum values tabulated correspond to the lower ends of whiskers in the box plots of Fig. 3. (Maximum values are data maxima. There were no outliers in the upper quartiles.)

[b]For these tests, the average number of fluorescent beads per image was below the detection limit. Hence, the expected value based on the median efficiency of one fewer layer of the same fabric is reported.

Adjustments made to the previous study were done so to reflect more realistic settings for masks in use. For example, lower differential pressures were used to reflect the unfitted cloth masks that are more often used, reflecting typical leakage. However, conclusions remained the same: higher thread count is better, and multiple layers improves filtration. Airflow resistance was also measured in this experiment [21]. The results for the filtration efficiencies for each fabric tested is demonstrated in Table 11.

Table 11: Filtration efficiencies of individual fabrics as a function of particle size at three different pressure differentials [21]

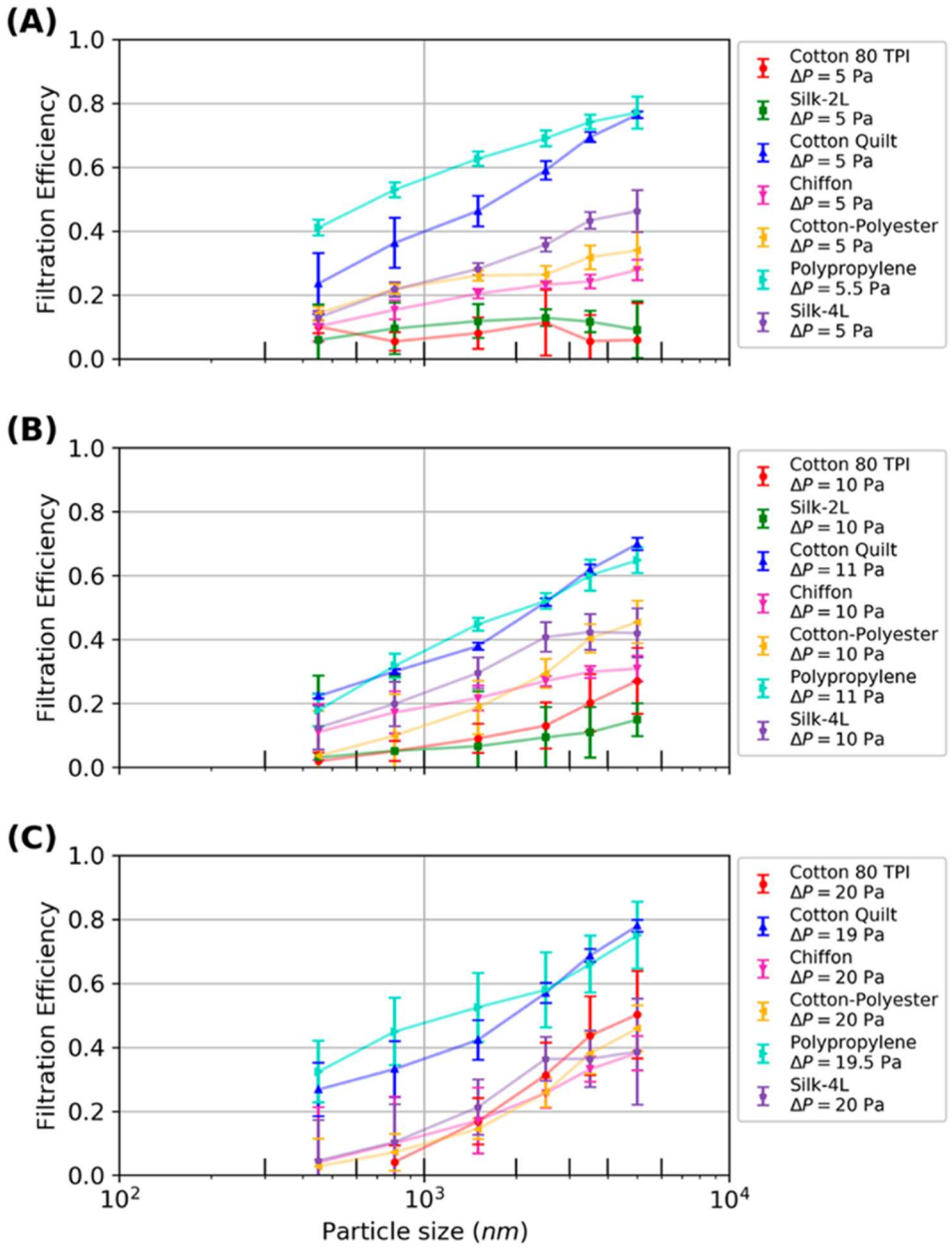

This study indicates that a cotton quilt composed of multiple layers of cotton as well as an inner batting layer performed best with a variety of particle sizes, including smaller particle sizes, indicating a design of multi-layer cotton with an interior filter layer would be beneficial to investigate.

2.4 Prior Art

In the Prior Art section of this literature review, existing patent literature will be evaluated to see what prior art exists regarding similar devices as the one described in this project. Evaluating prior art is an important step in filing for a patent, and patents could contain claims that encompass too many aspects of the created device, preventing patentability of the device.

2.4.1 DE202020101979U1 – Face protection, especially protective mask

This German patent was granted in 2020 to the assignee Krall and Roth Services GmbH and Co KG, and it describes a respiratory protection mask for mouth-nose protection. An image of the device is shown in Figure 11.

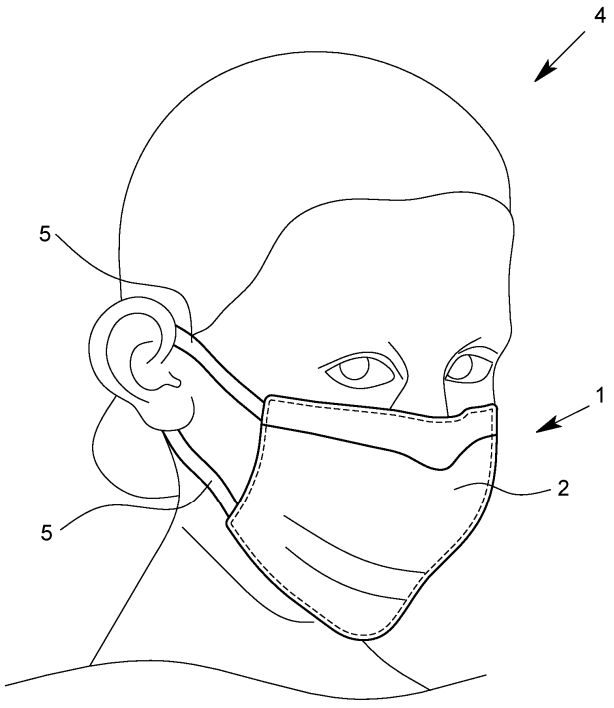

Figure 11: Device described in DE202020101979U1 [22]

The claims encompass masks that intend to reduce the secretion of infectious pathogens from the mouth and nose in the case of an epidemic such as COVID-19 that have at lease one

outer and inner layer provided. These layers must be breathable fabric, and between them must lie a mask pocket for exchangeable reception. The claim is extended to include all fabric types, including nonwoven fabrics, for the outer and inner layer.

It also includes designs with wash-permanent biocidal finishes and extends the entire design to being washable and reusable. The filter pocked opening can be oriented in any direction, and it can be assembled in any method.

The patent also details a nose clip that can be used in the design to provide for adaptation to the facial contour of the user.

2.4.2 DE202020101788U1 – Multi-layer mask with reversible, removable multi-layer filter for repeated use and cleaning options

This German patent was granted to the assignee Sci Kontor GmbH in 2020 [23]. An image of the device detailed is shown in Figure 12.

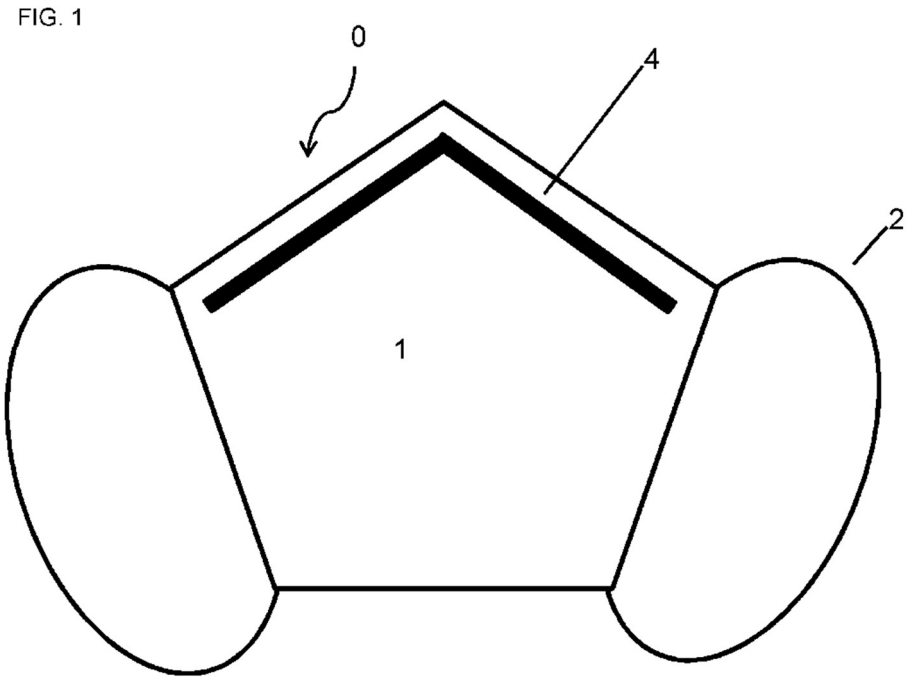

Figure 12: Device detailed in DE202020101788U1 [23]

This patent describes a multi-layer mask that specifically has an outer layer of textile fabric, an inner layer of textile fabric, and a pocket for a sheet-like multi-layer filter to be inserted. It is similar to the previous patent described but has more specific requests for fabric capabilities and describes a multi-layer filter for insertion. This patent also describes the device as being potentially washable and mentions a coating layer containing silver particles.

2.4.3 DE202020106904U1 – Mouth and nose protective mask

This German patent was granted in 2020 to the assignee Ferdinand Stuekerjuergen & Co KG GmbH [24]. An image of the described device is shown in Figure 13.

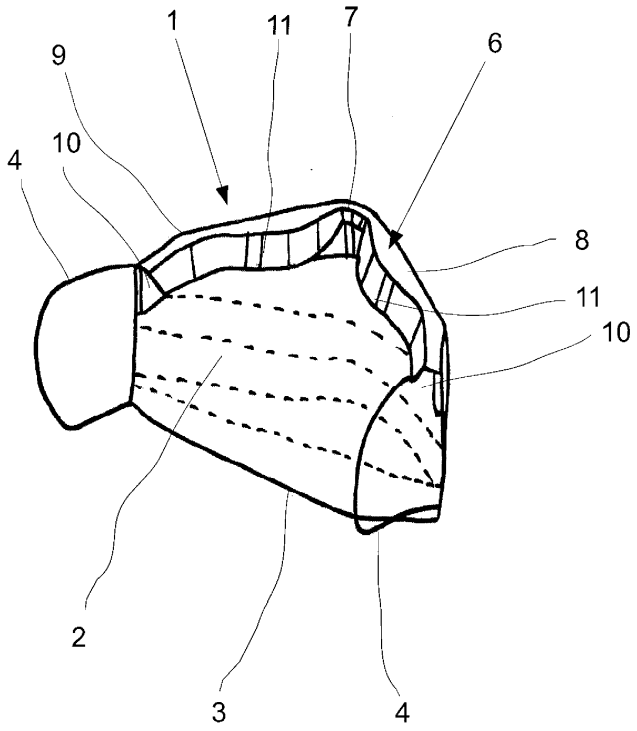

Figure 13: Device described in DE202020106904U1 [24]

This device in particular must comprise of a cover of flexibly held material that extends of the bridge of the nose and over the mouth characterized by a detachable insert on the inside of the upper edge. This insert would be shaped to the user's face contour. This insert could be

attached using Velcro-like tape and could be made of a soft plastic. Although this does not describe a fabric pocket, it does describe an insert.

2.4.4 US7614399B2 – Body conforming textile holder and filter article

US patents with similarities to the project were also examined. This patent was granted to the assignee RUSL LLC in 2009 [25].

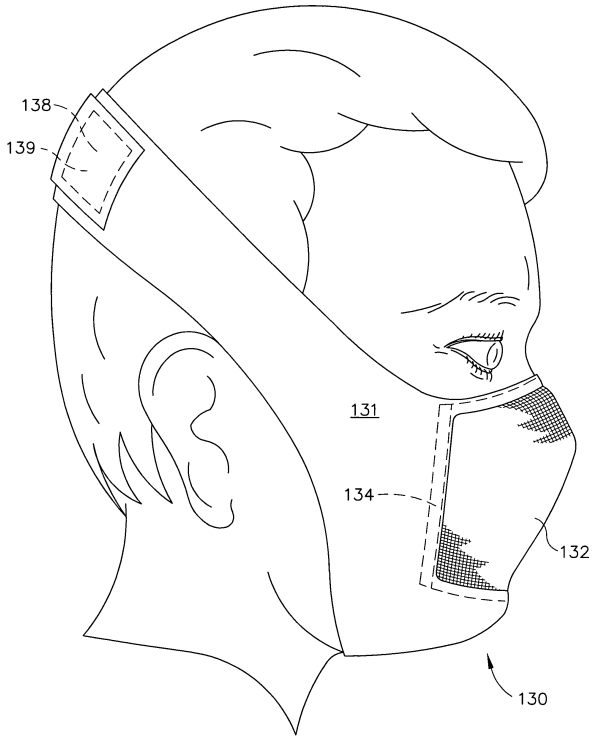

Figure 14: Device described in US7614399B2

This patent describes a device that is designed to hold an article in close body contact, and it is both body-conforming and washable. It is intended to keep a filter article close to a user's mouth and nostrils as well. The holder can be of any fabric, and the filter can be of any material. There is a pocket available for holding the filter.

This patent does not include a brace method or plastic piece that would contour to the user's nose bridge.

2.4.5 GE Additive design by Mark Fuller

A GE Additive design employee named Mark Fuller constructed a mask design in 2020 that can be 3D-printed in a matter of minutes, and he also published publicly available files for users to print the design at home [26]. The mask consists of a rectangular plastic brace piece that houses any household available filter material. The design is shown in Figure 15.

Figure 15: GE Additive mask design [26]

The brace design specifically holds similarities. He intended for the design to be produced quickly, and to mold to a large variety of users. Additionally, he details an option process of forming the frame of the mask through heating it, either by heating the mask in the microwave, with an iron, or submerging it in hot water. Then, he encourages users to place the mask against their face and allow the brace to cool to adjust the fit exactly and prevent leakage.

CHAPTER 3: MASK DESIGN AND PROTOTYPES

In this chapter, each design iteration for the mask body and brace will be described in detail. Each iteration centered around the idea of constructing a textile mask body with a removable filter piece as well as a brace of some sort that could help eliminate leakage along the nose bridge. Changes were made to each iteration according to performance defects, issues with comfort, or in attempt to simplify the manufacturing process.

In each iteration, it was important to consider various mask aspects that would affect the marketability of the mask as well as its effectiveness. For example, the comfort level of the mask is important because it is intended to be sold to the public, so it is desirable to produce a mask that is comfortable to wear for long periods. Additionally, the mask needs to retain functionality and not sacrifice this for comfort. The mask design must also be easily repeated if it is to be manufactured at a large scale. Therefore, changes can be made to the design to make the sewing process simple. Also, if the design is to be repeated by users at home, it is ideal that the mask be easy to replicate so that users at home who lack sewing experience may be able to reproduce this mask as well.

For each iteration, the materials and equipment used will be detailed. Additionally, modifications to the materials such as coatings added will also be explained. Brace designs will be demonstrated and detailed as well as changes that were made in that iteration. Finally, the mask design will be shown in detail including the construction process, detailing any changes made from the previous design. The overall design will be discussed, and proposed changes will be suggested, noting the defects of the design and what could be done differently. The final iteration is the design containing all improvements discussed that will have the best performance and level of comfort for the user.

3.1 First Prototype

3.1.1 Materials

For the first mask design iteration, the mask body was shaped around the idea of incorporating a brace structure designed to keep the mask away from the user's mouth to provide comfort as well as to better seal the mask at the nose bridge and chin. The brace was printed with PLA filament using the Lulzbot TAZ Pro 3D printer shown in Figure 16. The 3D printer utilizes SolidWorks-produced STL parts that are uploaded into a desktop software called Cura that is produced by TAZ. The parts can then be oriented and scaled, and print settings can be added before being printed using a USB drive on the printer itself.

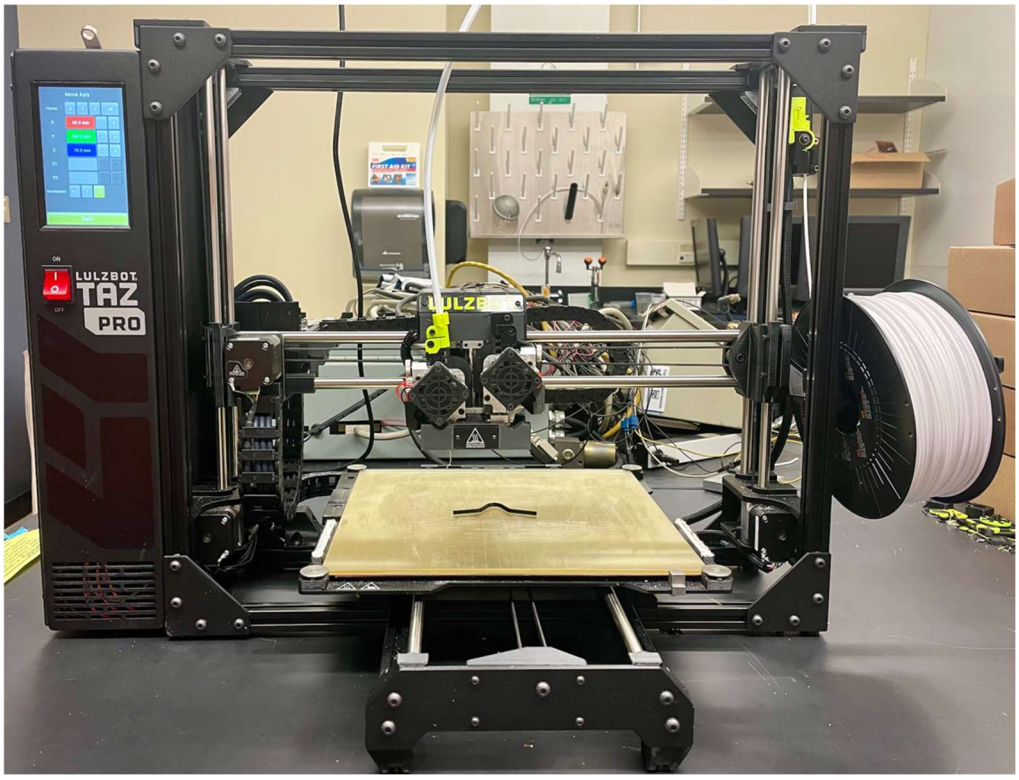

Figure 16: Lulzbot TAZ Pro 3D Printer

The mask body was sewn using a SINGER Heavy Duty 4432 Sewing Machine shown in Figure 17. The sewing machine used can complete basic sewing stiches necessary to produce a

mask and is capable of stitches necessary to sew with stretch-capable materials.

Figure 17: Singer Heavy Duty 4432 Sewing Machine

In this iteration, a stretchy, knit fabric was used. The fabric is stretchy due to its spandex content. The stretch was incorporated to help adjust fit ad sizing of the design since the stretch of the material provides better fit and comfort. As an initial design, the sewing techniques used for construction were rough and not well refined.

Because the type and structure of the fabric was not known, it was investigated using an optical microscope in the Gavin Hall laboratory run by Dr. Ramsis Farag. Additionally, the material was weighed to determine the mass of the material. The optical microscope image of the material confirming its knit structure is shown in Figure 18.

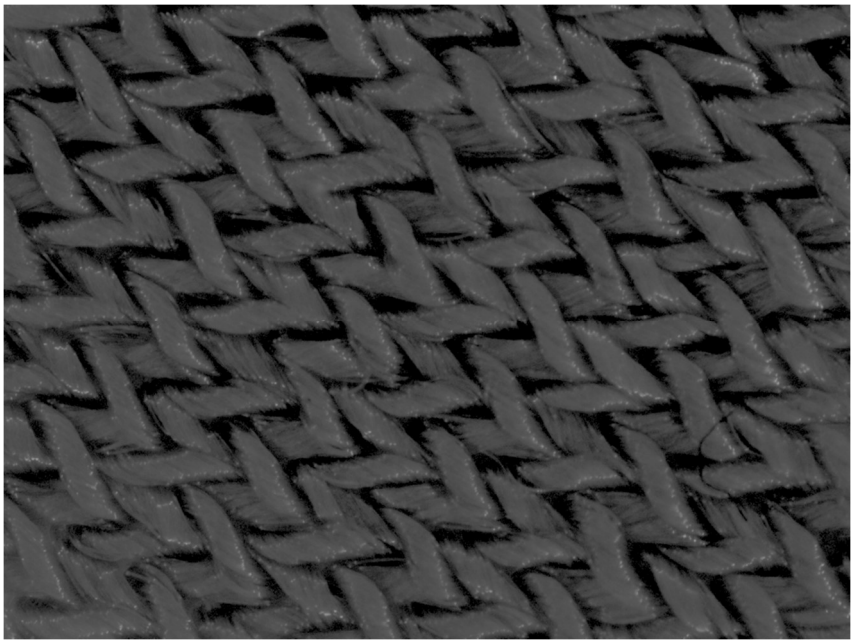

Figure 18: Optical microscope image of knit fabric of prototype-1

The knit material was also investigated using a half-inch folding and magnifying thread counter to calculate numbers of courses and wales per inch, shown in Figure 19.

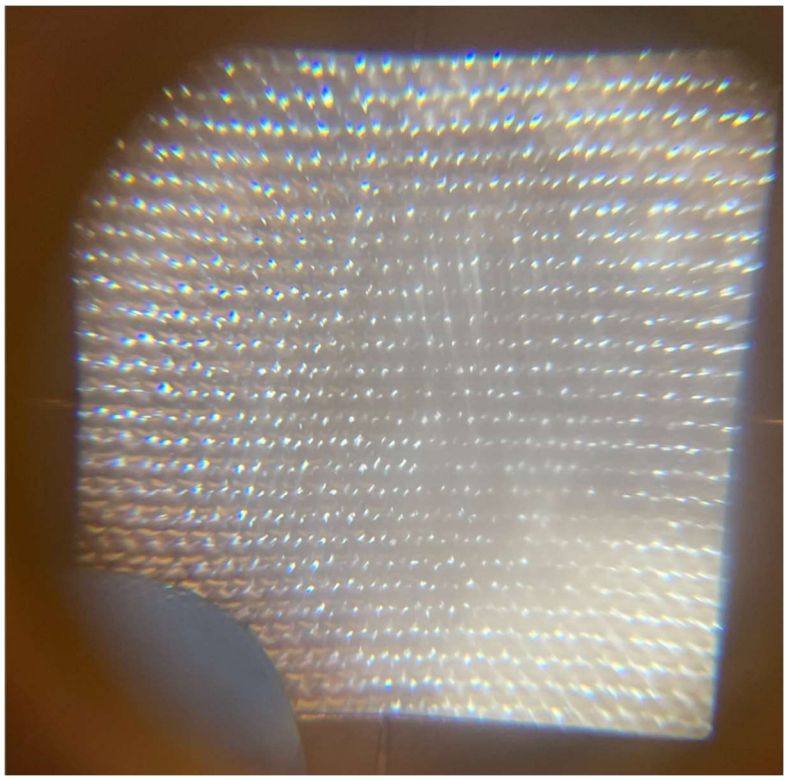

Figure 19: Image used for counting courses and wales of knit fabric

26 courses were counted per half inch for a total of 52 courses per inch, and 19 wales were counted per half inch for a total of 58 wales per inch.

A 3 cm x 3 cm sample was weighed on a Mettler Toledo precision balance scale to determine fabric weight in grams per square meter (GSM). The image demonstrating the weight measurement is shown in Figure 20. The weight found was then converted to GSM using the following unit conversion operation:

$$\frac{188.39\ mg}{3\ cm^2} * \frac{10{,}000\ cm^2}{1\ m^2} * \frac{1\ g}{1{,}000\ mg} = 628.0\ GSM$$

Resulting in a weight measurement of 628 GSM.

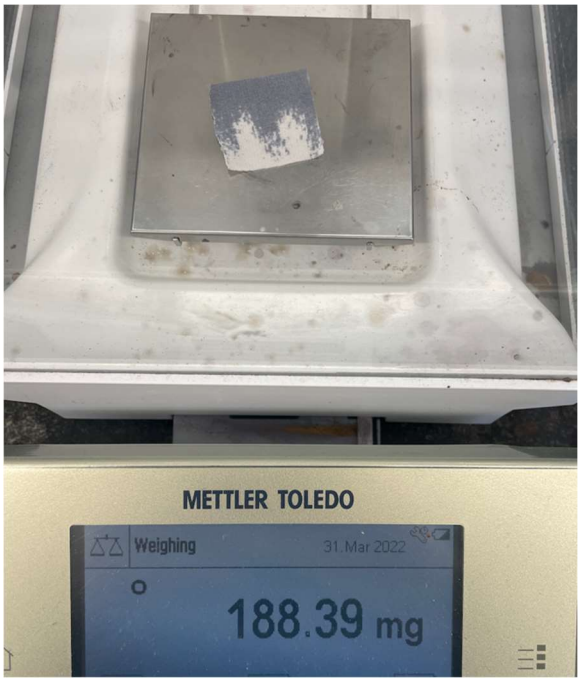

Figure 20: Weight measurement used to calculate GSM of knit fabric

Additionally, varying types of elastic were utilized in the design. The two elastics used in initial construction were a thin, rope-like elastic that suited the small mask size that would be necessary to fit the test mannequin as well as a thicker, flat elastic that would be suitable for a full-sized mask. Both elastics did not have their properties listed when purchased, so they were

also taken to the Gavin lab to be investigated using the optical microscope.

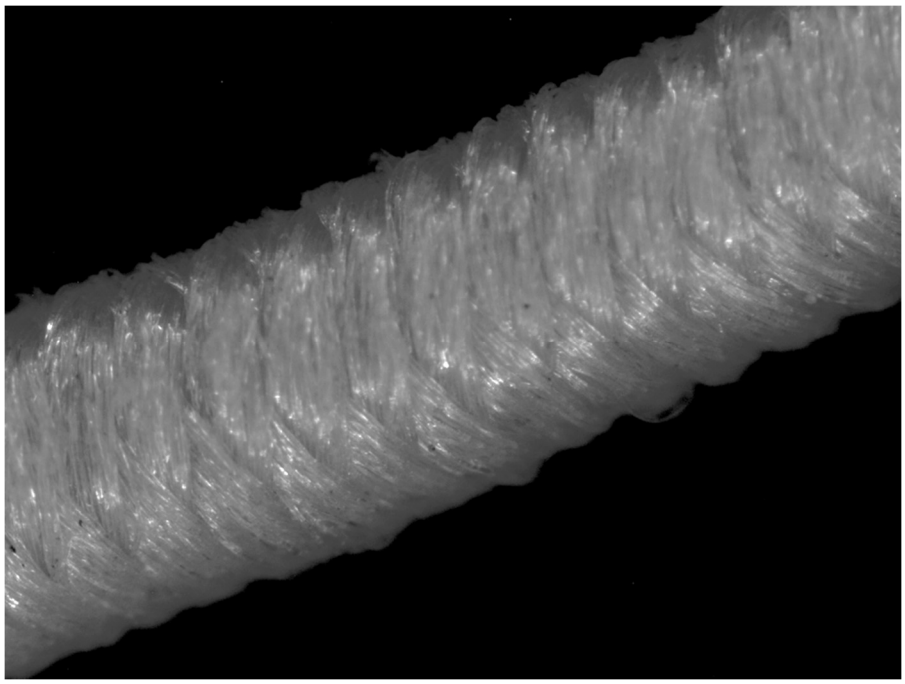

Figure 21: Optical microscope image of braided elastic used in protoype-1

The smaller, cord-like elastic was determined to be a braided structure, or braided thread surrounding an inner rubber length. The image taken of the cord is shown in Figure 22.

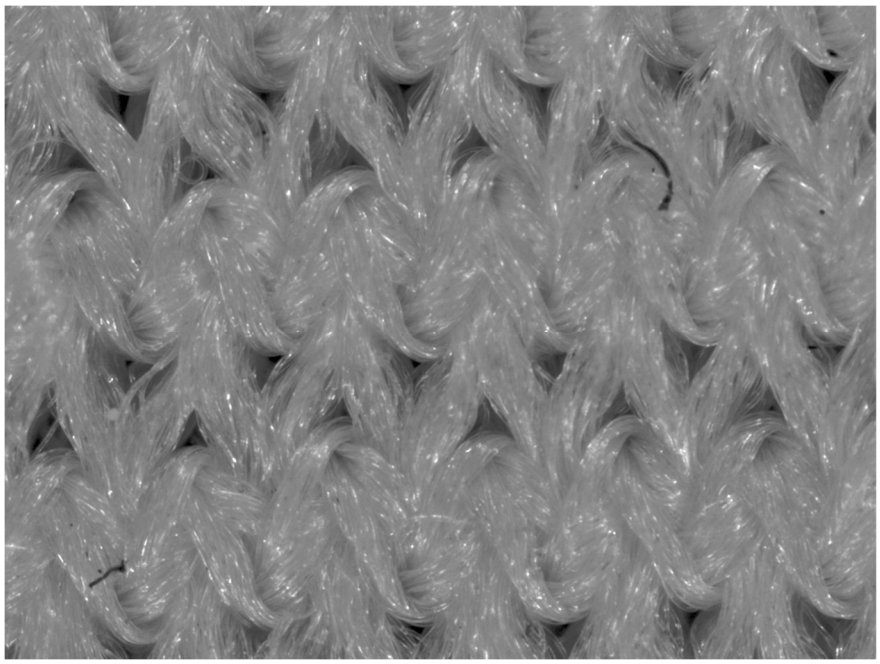

Figure 22: Optical microscope image of knit elastic band

The flat elastic used for the larger, person-sized mask was determined to be a knit-type elastic structure, which likely uses a spandex-blend material which is then knit to form the elastic band. The optical microscope imaging of the band is shown in Figure 22.

3.1.2 Brace Design and Construction

A 3-D rendering of the first brace design produced in SolidWorks is shown in Figure 23.

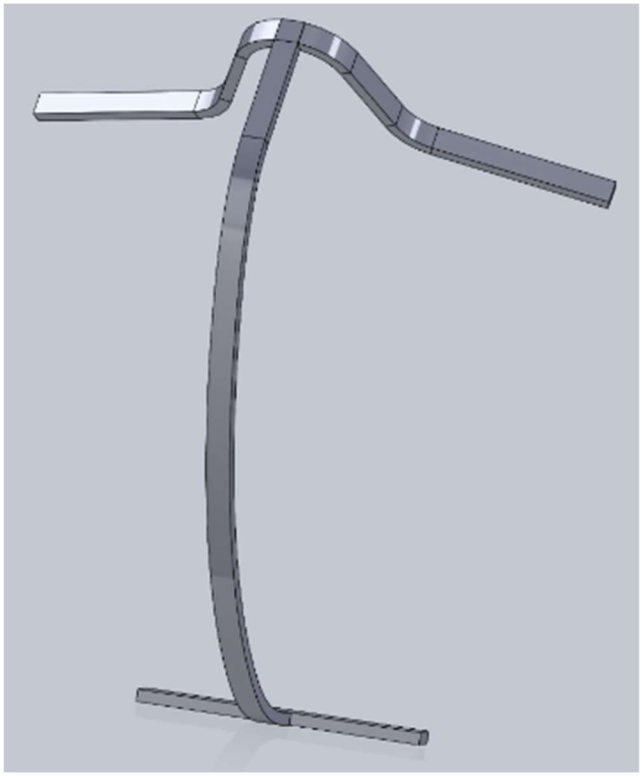

Figure 23: Mask brace for prototype-1

The brace prototype was printed in three sections before assembly using hot glue for a temporary solution. The brace can be produced either by incorporating joints in each piece for assembly or printing as a single piece with water-soluble supports.

The model was constructed by utilizing a photo taken of the mannequin used for construction while incorporating a tape measure in the photo for scale reference. Sketches in SolidWorks were superimposed on the image and the scale was taken from the image. This was

repeated for all three pieces: nosepiece, mouthpiece, and the chin section. Each piece on the image taken is shown in Figure 24.

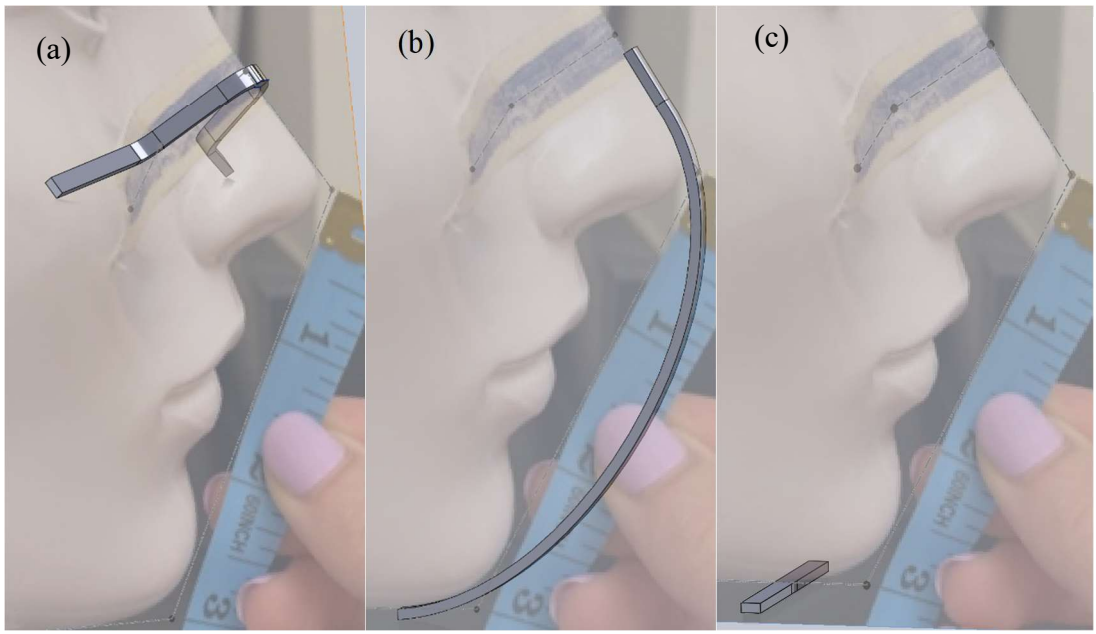

Figure 24: Superimposed images on SolidWorks for brace construction for (a) nosepiece, (b) mouthpiece, and (c) chin section

A separate photo was used to better construct the contour of the nosepiece using marked tape on the mannequin model as shown in Figure 25:

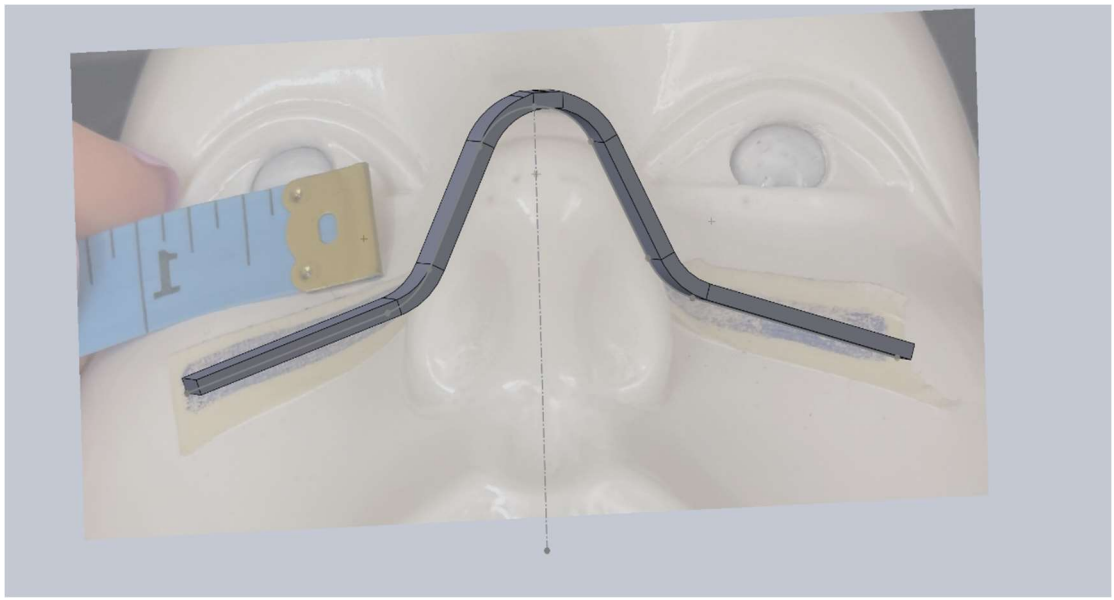

Figure 25: Nosepiece contour on SolidWorks

The design is intended to be a solid one-piece design that could be printed either in three parts and assembled or printed using water-soluble support material. Assembly would have to be done using a glue that would stick to the printed PLA material.

The issues with the initial proposed brace design include the problem of assembly of the three parts or the use of the soluble support material. A large volume of support material would have to be used to produce the brace structure. A demonstration of potential print orientation and support material is shown in Figure 26.

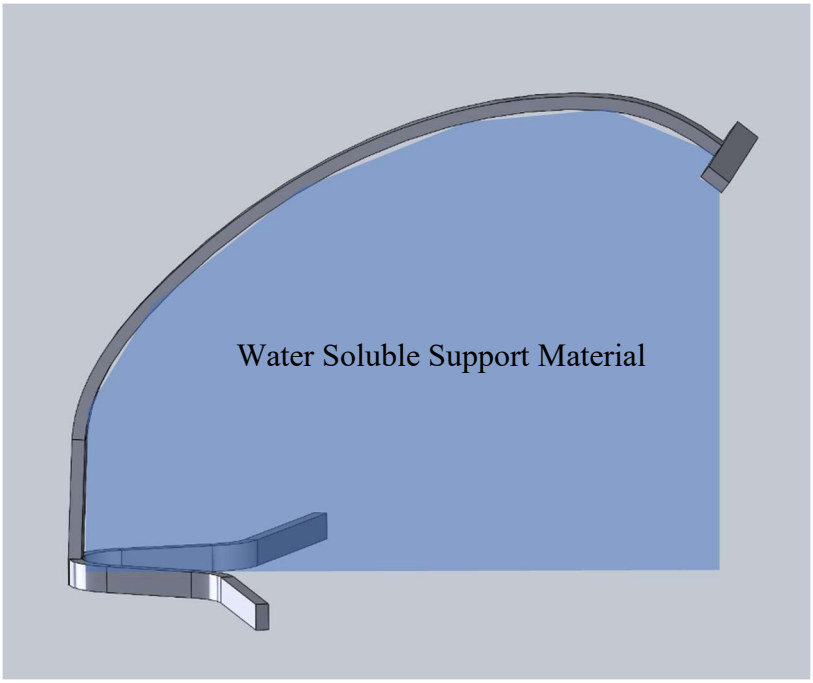

Figure 26: Brace for prototype-1 with support material

Also, if the brace were rotated in orientation to have support material, the layering of the 3-D printing process may sacrifice the integrity of the brace structure and cause areas that may come apart during use or wear. The 3-D printing layering structure is best optimized when each piece is printed flat.

3.1.3 Mask Design and Construction

An initial design was sewn of a knitted fabric to incorporate a channel along the top and

bottom in which the brace would fit into. This method would allow the brace to be removable for machine washing the mask body, as demonstrated by the green nosepiece sample shown in section (a) of Figure 27.

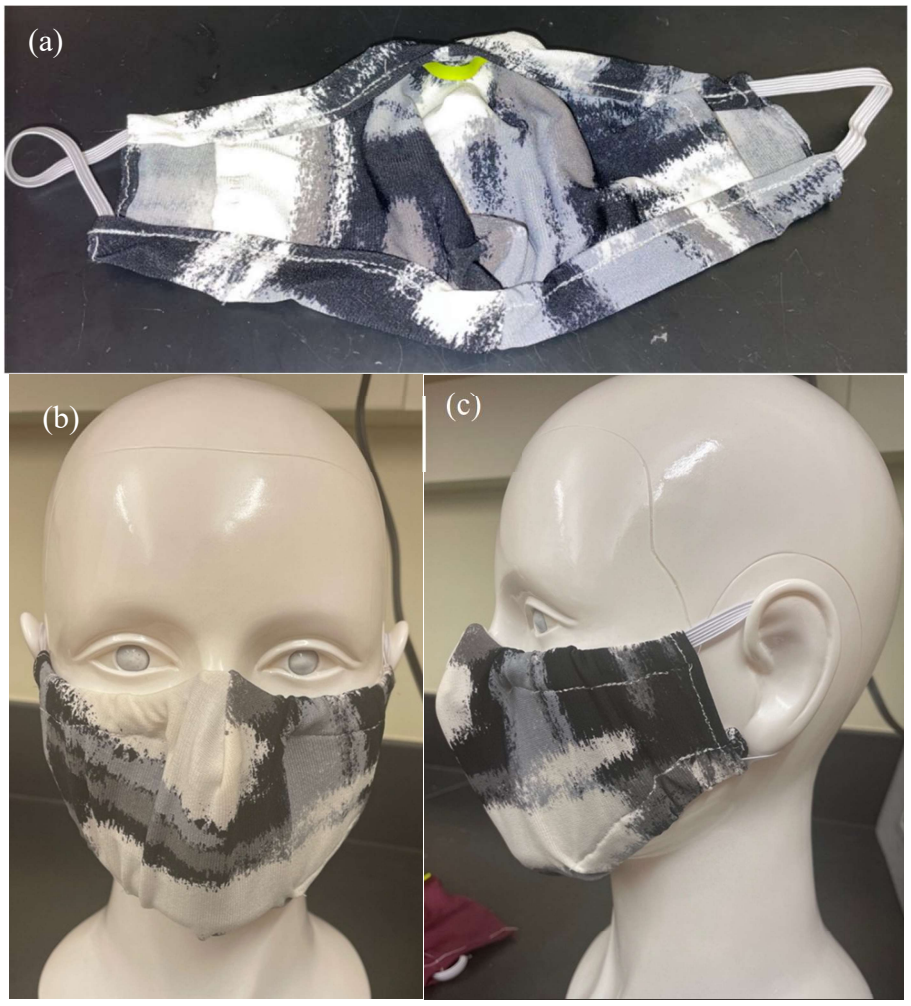

Figure 27: Prototype-1: (a) lying flat, (b) from front, and (c) from side

Issues with the initial mask design and construction include an area of brace that is left without fabric covering which meets the user's skin at the point where the brace touches the nose bridge. Because the brace is a single part design, the "T" shaped sections where the mouthpiece meets the top and bottom of the chin, as highlighted in Figure 28, could rub against the user's skin and cause discomfort during wear.

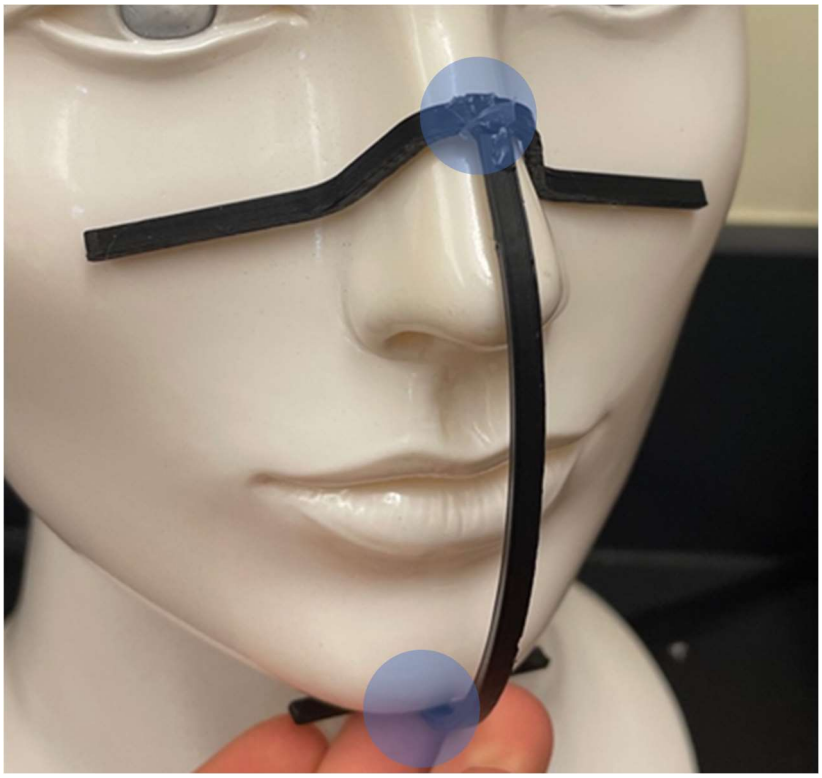

Figure 28: Locations of direct brace contact with skin in the first prototype

Methods of remediation include creating a brace design that is separate and sits inside separate channels such that they may be covered by fabric and not rub the user's face. Another solution would be to construct a more complex pocket design perhaps utilizing Velcro or other means.

Additionally, a new design addition was deemed desirable: the ear loops of masks often catch on other objects such as glasses or keys when kept in a user's pocket or purse. If a design could be produced in which the ear loops are able to retract into the mask structure, then stretch for use, the mask would be less likely to catch on these objects. This feature is especially important when one would want to put the facemask on in a hurry such as when others are approaching.

3.2 Second Prototype

3.2.1 Materials

An updated version of the mask was then produced to help fix problems identified with the first iteration. The same material was used as in the first iteration. The brace was again printed with PLA. The same elastic material was also used. However, Velcro was incorporated to add cushion to the exposed areas of the brace and prevent discomfort to the user.

3.2.2 Brace Design and Construction

Brace design was not changed for this iteration; the one-piece design was still used. This new design incorporating padded channels would eliminate the exposed brace pieces, but the same issues in assembly and printing of a single-piece brace remain.

3.2.3 Mask Design and Construction

The same channels were constructed along the top and bottom of the brace. However, a Velcro strip was added along the middle of both channels to close the gaps and give the channels the ability to wrap around the exposed brace material. The addition is shown in Figure 29.

Figure 29: Prototype-2 and additions

The mask fabric on each side was increased such that the elastic could be wrapped around the design without having traditional exposed loops, thus when worn the elastic would stretch. This provides the desired retractable ear loop design.

Although the padded Velcro strips did prevent the brace from coming into contact with the user's skin, some areas of contact remained, and the Velcro caused issues with the sealing benefits provided by the brace because of the thickness of the padding. It was decided that a new brace design and mask design would be best in combatting these issues.

3.3 Third Prototype

3.3.1 Materials

This mask iteration explored construction possibilities of cotton fabric masks. A 100% cotton material was sourced from Walmart with the brand name Waverly Inspirations in the color “Ink.” This material represents a cotton that would be suitable for the design and desired filtration efficiency as well as easy to find for someone at home if they wished to replicate the mask design. However, full fabric information was not available on the label, so the optical microscope was again used to investigate the weave type of the fabric. An image of the material is shown in Figure 30, confirming that the cotton is plain-weave cotton.

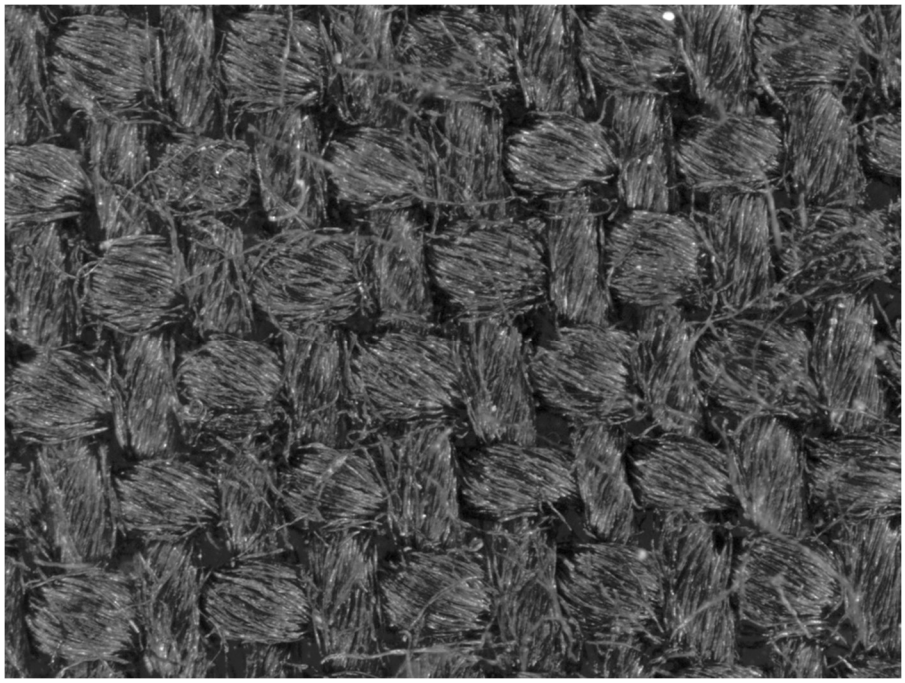

Figure 30: Optical microscope image of plain-weave cotton for prototype-3

The cotton material was investigated using a half-inch folding and magnifying thread counter to calculate yarn density. 70 yarns per inch was counted for the material. The image used for counting is shown in Figure 31.

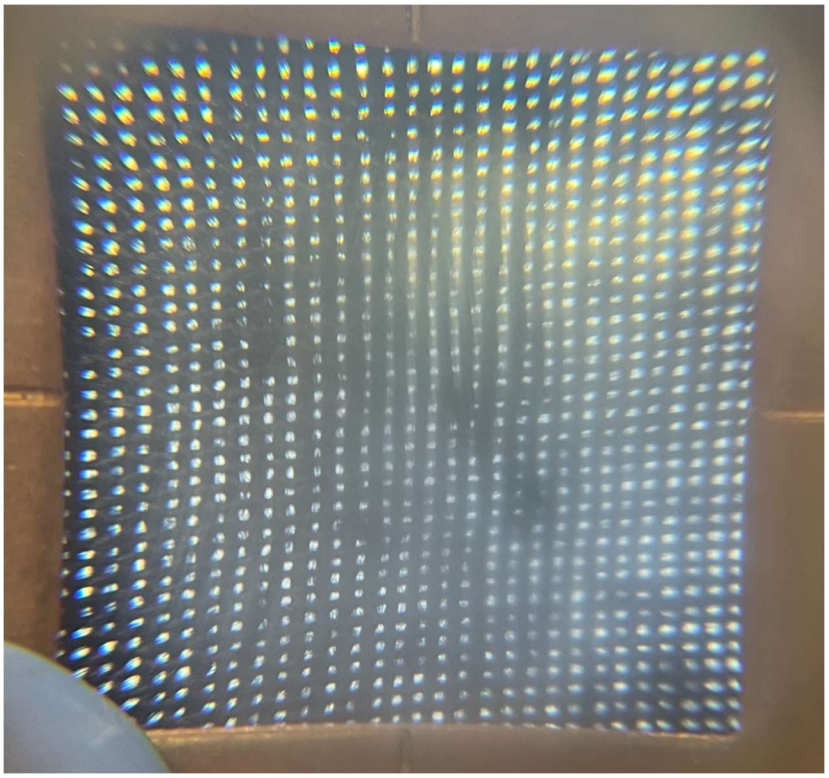

Figure 31: Image for course and wale count of cotton plain-weave fabric

A 3 cm x 3 cm sample was weighed on a Mettler Toledo precision balance scale to determine fabric weight in grams per square meter (GSM). The image demonstrating the weight measurement is shown in Figure 32. The weight found was then converted to GSM using the following unit conversion operation:

$$\frac{123.61\ mg}{3\ cm^2} * \frac{10{,}000\ cm^2}{1\ m^2} * \frac{1\ g}{1{,}000\ mg} = 412.0\ GSM$$

Resulting in a weight measurement of 412 GSM.

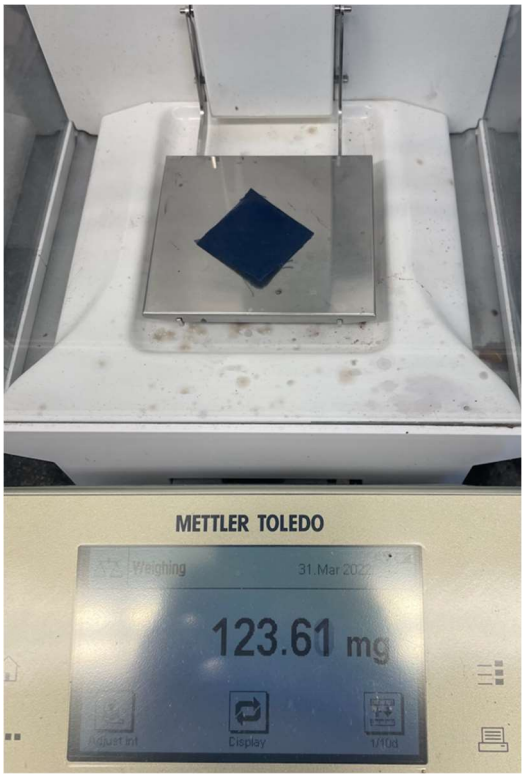

Figure 32: Weight measurement used for weight calculation of cotton fabric

Alterations were made to the brace design to allow for assembly without the use of glue. However, the materials of the brace remain the same at a 3-D print PLA filament.

The inner filter material was determined to be a layer of melt blown filter material in addition to a layer of spunbonded filter material for best filter performance. Both filter materials were taken to the Gavin lab optical microscope to be imaged as well.

The meltblown filter material was also investigated by using the optical microscope to closely observe structure. Meltblown fabrics are a type of nonwoven fabric which utilize either textile, paper, extrusion, or some combination of these types to form and then bond fibers, filaments, polymers, or yarns into flexible and porous structures [8]. A high velocity stream of air is used in production of these fabrics to force filaments away from the face of the spinnerette as shown in Figure 33.

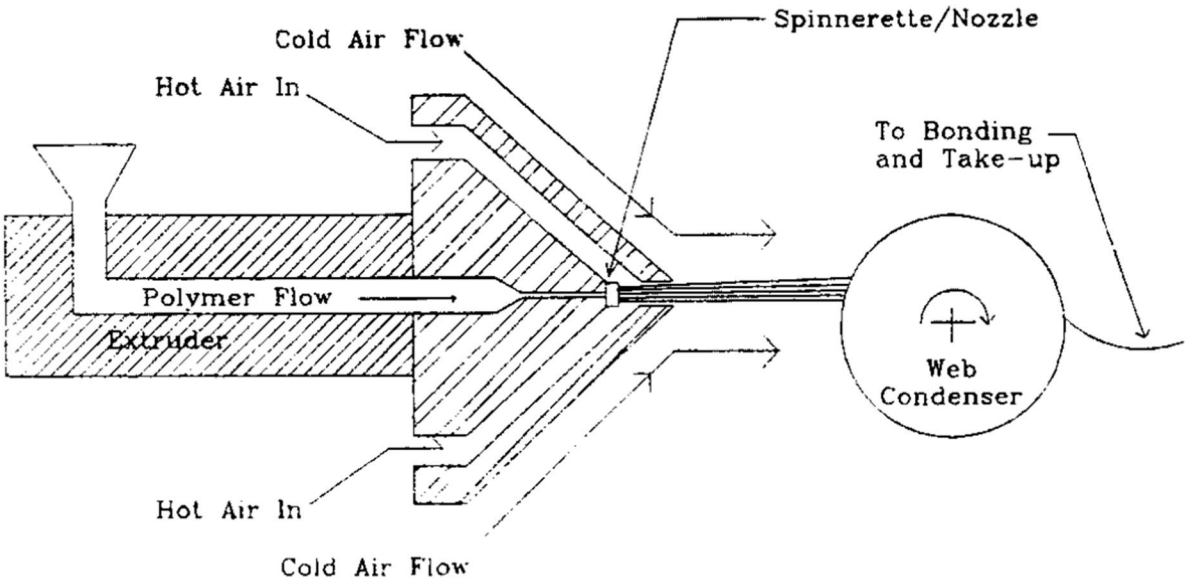

Figure 33: Melt blowing process [8]

Fibers are deposited onto a moving conveyor belt and bonded together, allowing for the creation of a finely woven web-like structure with a large surface area, which is ideal for absorption and filtration.

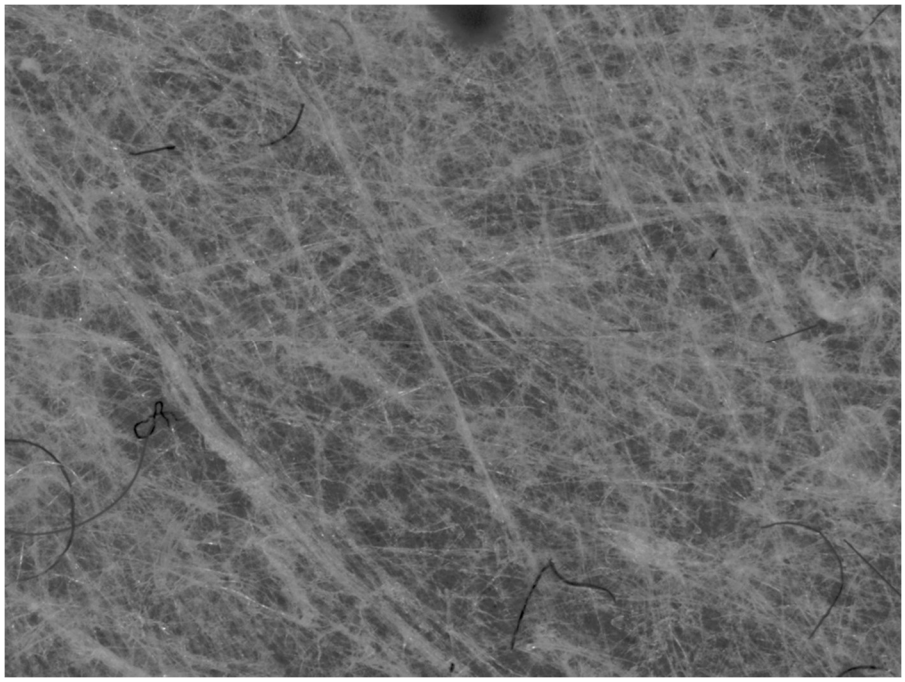

Figure 34: Optical microscope image of meltblown filter fabric

In contrast, spunbonded materials are also nonwoven materials but are manufactured with a lower-velocity airstream. Additionally, electrostatics may be used to keep filaments separated in the web when extruded. An illustration of the spunbond process is shown in Figure 35.

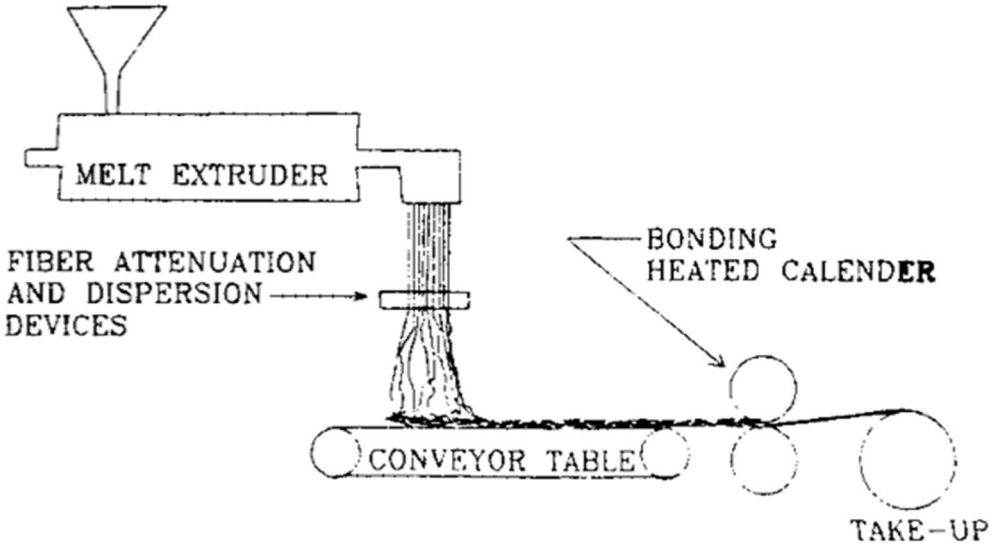

Figure 35: Spunbond process [8]

The spunbonded filter material is shown using the optical microscope in Figure 36.

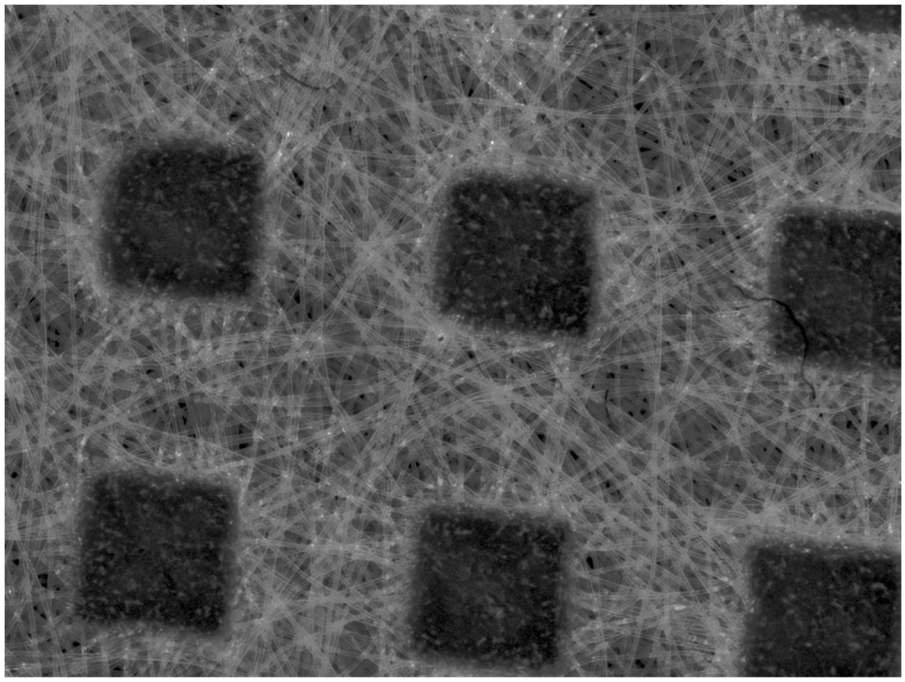

Figure 36: Optical microscope image of spunbonded filter material

Additionally, a new elastic cord was utilized. It was determined that the elastic needed to have additional stretch to fit the user comfortably while also retracting as designed. Therefore, an elastic with similar appearance and functionality to that used commonly in surgical mask elastics was used as shown in Figure 37.

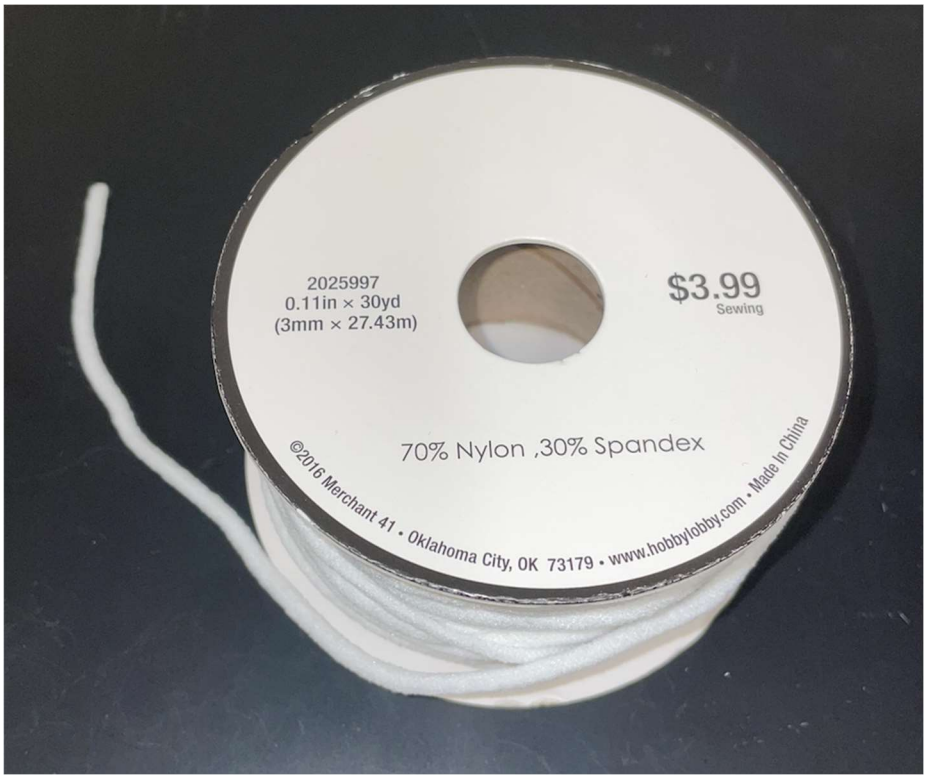

Figure 37: Surgical mask-style elastic cord

The elastic type could not be determined from packaging, so the optical microscope was used to determine the structure of the fabric. However, images were inconclusive, and no knit or weave could be detected from the imaging. The image taken is shown in Figure 38. It could be suggested that the material has been worn and therefore the structure is hidden, but it is likely that the cord is either knit or braided because of its rounded shape.

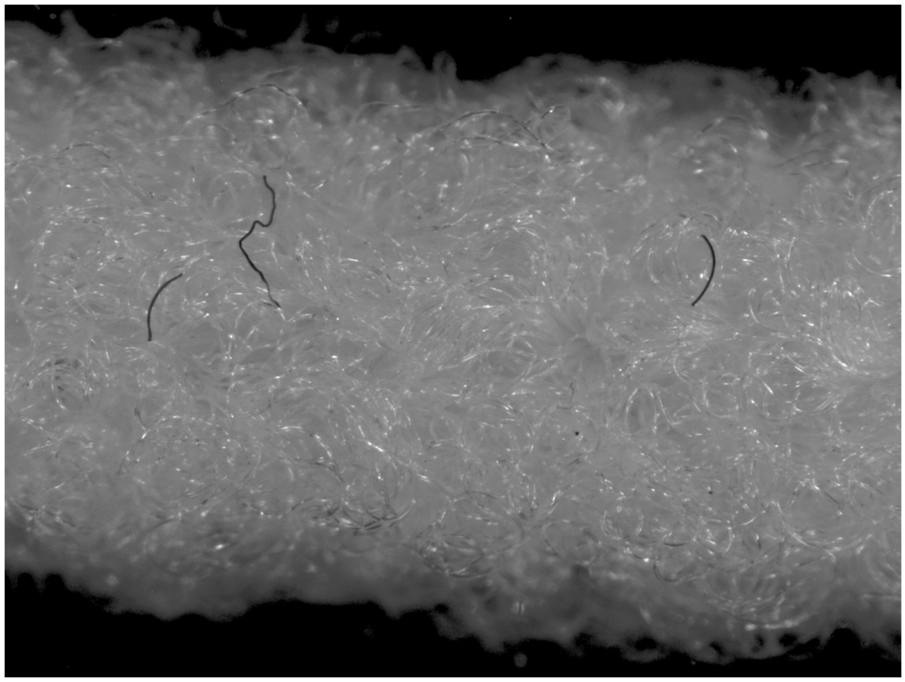

Figure 38: Optical microscope image of unidentified structure elastic cord

3.3.2 Brace Design and Construction

As an alternative to the previous design, and to simplify the design process and size issues, new fitting methods were investigated that do not involve glue. For that reason, snap-fit plastic parts seemed to offer a solution.

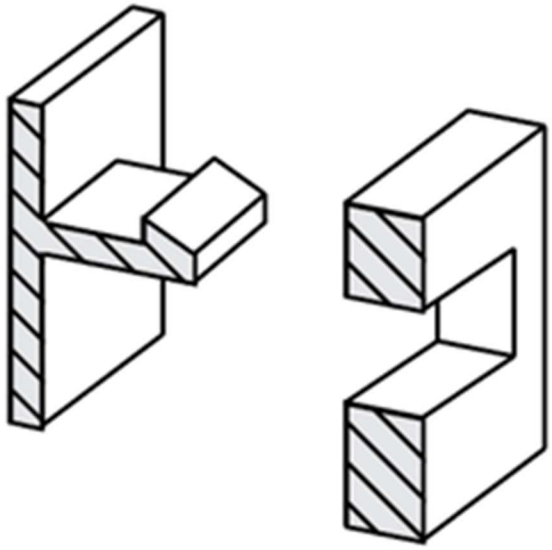

Figure 39: Cantilever Snap Fits [27]

Snap-fit parts are seen often in everyday use, including in buckles on backpacks or other fasteners. This could be applied to the mask fittings using a cantilever-type snap fitting, which can be easily 3D printed [27]. An image representing this is shown in Figure 39.

This design element could be incorporated onto the ends of the mouthpiece of the brace and center of nose and chin pieces. Another important element to consider during this design process is the direction of the layers during printing as demonstrated in Figure 40.

Figure 40: Layer lines related to 3-D printed snap fits [28]

It is important to make sure layers are printed in a way in which they will not break during the fit. This is consistent with current printing methods for the brace and the direction the snap would be printed for each piece to lay flat [28].

The brace is intended to incorporate a clip-like structure for assembly such that pieces could be printed flat and then assembled once for future use. The clip would allow for initial assembly, but the brace could not be taken apart afterwards. The new brace piece designs then must incorporate either the clip structure or the rectangular housing structure for this assembly.

New pieces were constructed in SolidWorks for printing as shown in Figure 41.

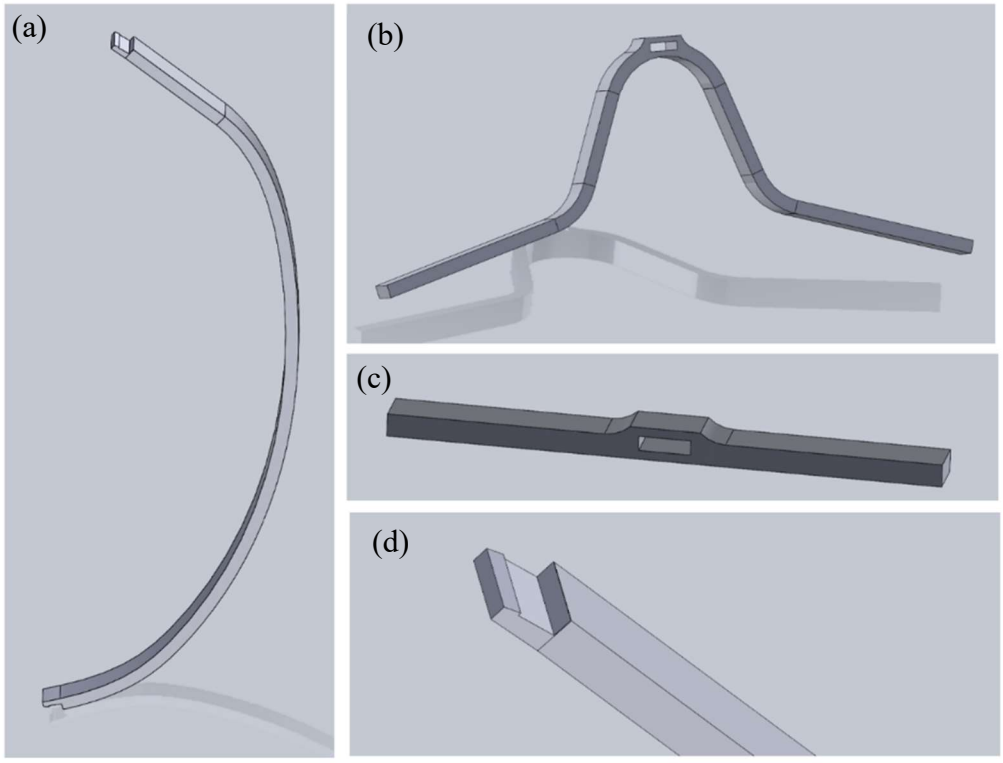

Figure 41: Brace with cantilever snap fittings: (a) on the mouthpiece, (b) on the nosepiece, (c) on the chin section, and (d) a close view of the fitting

After 3-D printing of the pieces, it was determined that at the small scale of the brace dimensions, the resolution of the 3-D printer was not enough to print the cantilever snap fittings with enough detail to be functional. The pieces were rounded and the holes desired were clogged with printed material.

In a newer iteration, it would be advantageous to utilize a smaller filament diameter to increase resolution of the print or consider alternate methods of assembly for the single-piece brace design. Alternatively, a multi-piece brace design could be utilized to simplify the process.

3.3.3 Mask Design and Construction

Multiple approaches to a new mask design were considered. The folded-over technique utilized in the previous iterations using the stretchy fabric caused the mask to become bulky along the nose and chin line. Additionally, the new fabric utilized for its filtration properties is

cotton, which is more difficult to fold for the previous design. First, a new design technique was attempted in which four separate channels for brace pieces were sewn into the interior filter pocket piece before assembly with the outer fabric piece, as shown in Figure 42.

Figure 42: Prototype-3 example - four separate channels

This design would have been successful to hold the upper and lower brace pieces, but this would have a similar problem as the first iteration in which the brace would be making direct contact with the user's skin. It would also be unable to support the retractable ear loop design proposed, which is a necessary feature.

Next, a new approach was made in which smaller panels were added to the sides of the inner filter piece and sewn to the front piece, and afterwards channels were made along the entire top and bottom of the mask. This way, the brace could fit as well as the elastic without causing bulky layering in the fabric, as shown in Figure 43.

This mask design creates direct interaction between the brace and the user's skin and needs to be revised. This calls into question the necessity of a single-piece brace design. To keep the sewing techniques for the mask relatively simple, therefore making replication of the design

easier for mass production or replication at home, it could be considered best to utilize a multi-piece brace design. If this were to be used, the chin piece could be omitted in place of a nosepiece and mouthpiece alone with their own channels inside the mask.

Figure 43: Prototype-3 example - top and bottom channels

3.4 Fourth Prototype

3.4.1 Materials

An updated version of the mask was produced considering the new brace design proposal. This includes outer layers of the same 100% cotton fabric as used for the previous iteration and an inner filter layer of melt blown fabric.

The same PLA was used to produce the new brace design, which consists of two individual pieces.

The inner filter layer was chosen to be one layer of melt blown filter material in the shape of the filter pocket of the mask. The melt blown layer was determined to retain the filtration properties desired without the added breathing difficulty caused by a multi-layer filter.

3.4.2 Brace Design and Construction

The first iteration brace pieces were utilized but printed separately for the mouthpieces and nosepieces to construct this part. Additionally, the length of the mouthpiece was decreased such that it would not extend out of the mask pocket. The updated brace designs are shown in Figure 44.

The brace did help with sealing along the nose bridge as well as keeping the mask away from the user's mouth, as designed, but the nosepiece is only contoured to fit the mannequin exactly. It would be advantageous to alter this piece to be either more flexible to fit a wider range of nose shapes or to be moldable in some state to fit different contours.

Figure 44: Brace design from Prototype-4

3.4.3 Mask Design and Construction

The full design is shown on a mannequin in Figure 45.

Figure 45: Prototype-4 on mannequin

The mask incorporates two channels in which brace sections are inserted to provide a better seal along the nose bridge as well as to keep fabric from touching the user's mouth during use.

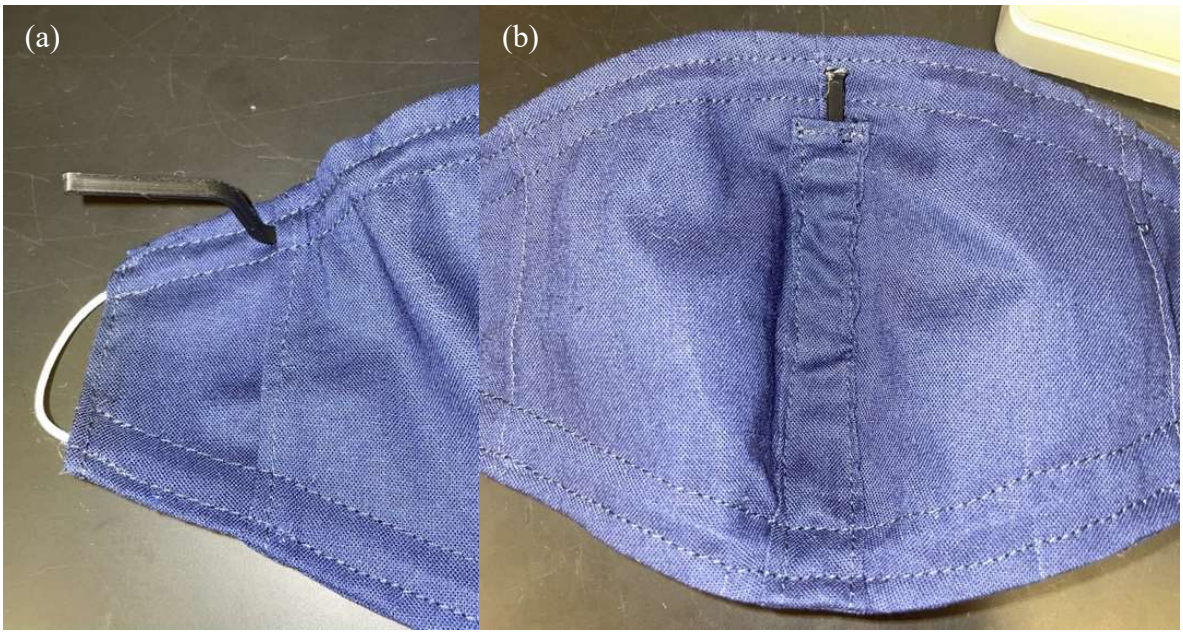

Figure 46: Fourth prototype - brace insert channels (a) at nose and (b) at mouth

Unlike the previous iteration, the channels do not have openings in the center to allow for insertion of the brace pieces. Instead, the brace pieces are inserted along the sides of the channel by the filter pocket and slid into position in the center of the mask. This provides a layer of padding and fabric between the brace and the user's skin without sacrificing the sealing effects provided by the brace piece. These channels can be seen in Figure 46.

The final mask design also incorporates the same retractable ear loops as demonstrated in earlier iterations. This extension is shown in Figure 47.

Figure 47: Fourth prototype - further extended sides for ear loops

3.5 Fifth Prototype

3.5.1 Materials

For the final prototype, the same cotton fabric was used. However, a silver nanoparticle coating was added to the outermost layer of fabric to reduce bacterial contamination. The coating was supplied as a sample through HeiQ Materials AG, and the coating is constructed by combining one-part HyProTecht, the silver nanoparticle coating, with three parts EFFECT VB, an agent to help the coating go into effect. The products can be seen in Figure 48.

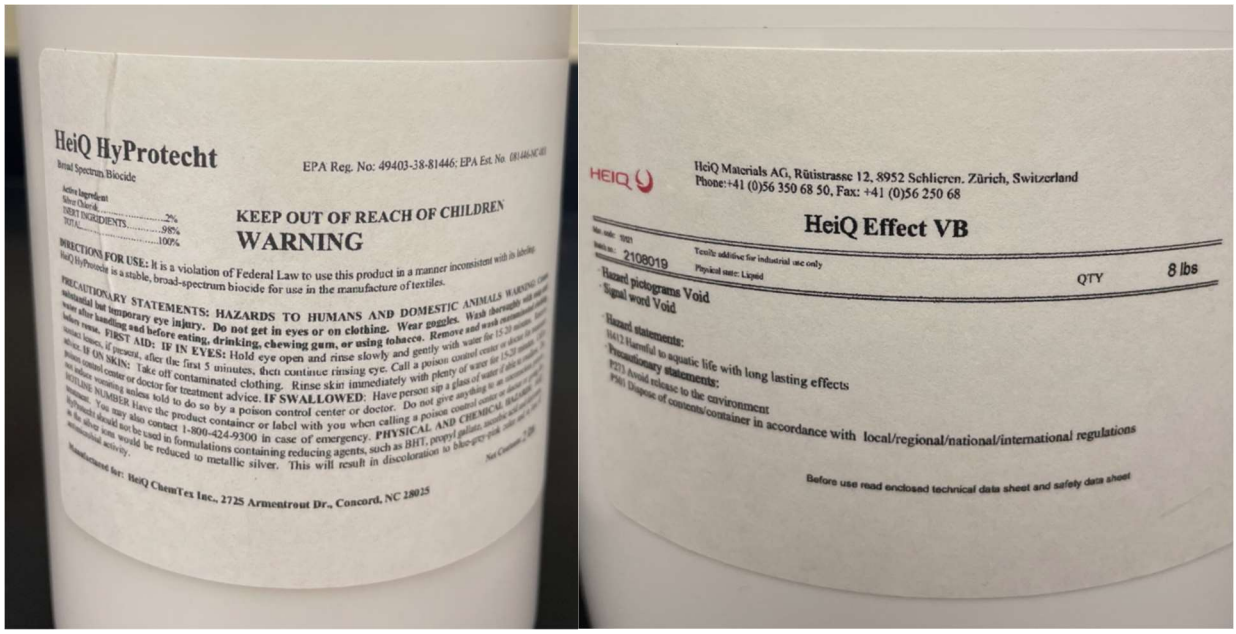

Figure 48: HeiQ products used for silver nanoparticle coating

To apply the coating, the material must be atomized. The atomization process was accomplished using a broadband ultrasonic generator and an ultrasonic nozzle. The broadband ultrasonic generator, which is manufactured by Sono-tek Corp, can be seen in Figure 49.

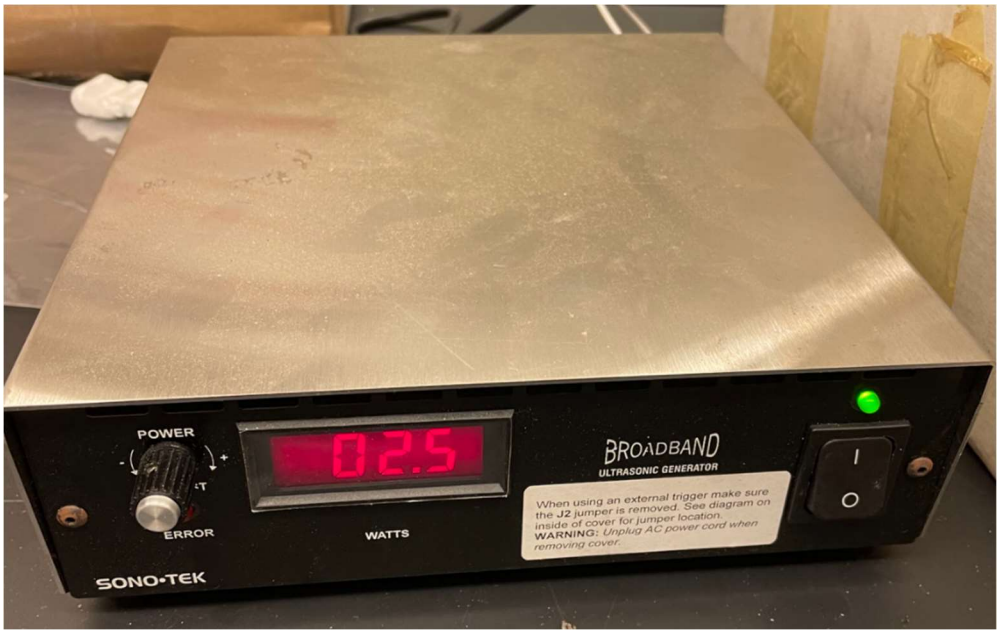

Figure 49: Sono-Tek broadband ultrasonic generator

This generator can generate high frequency electrical energy which is then used to operate atomizing nozzles. The nozzle utilized for the application is shown in Figure 50, which is also manufactured by Sono-Tek.

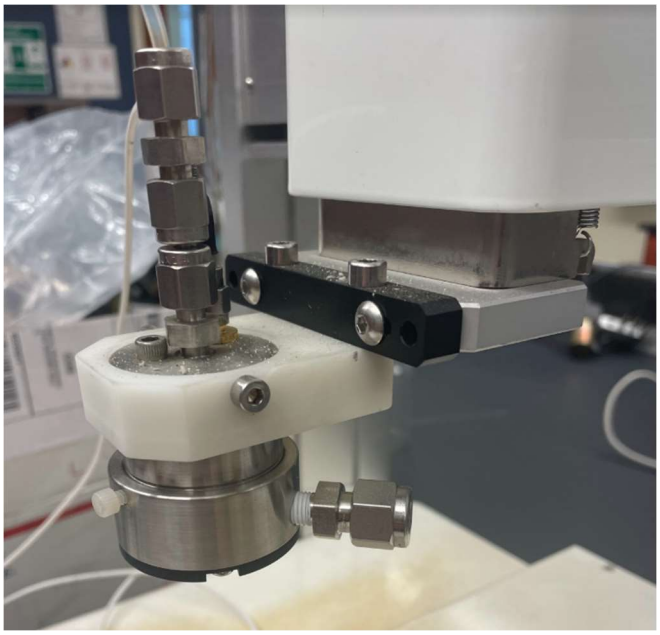

Figure 50: Sono-Tek ultrasonic atomizing nozzle

To apply the coating, the ultrasonic generator is connected to the nozzle as indicated in

the diagram shown in Figure 51.

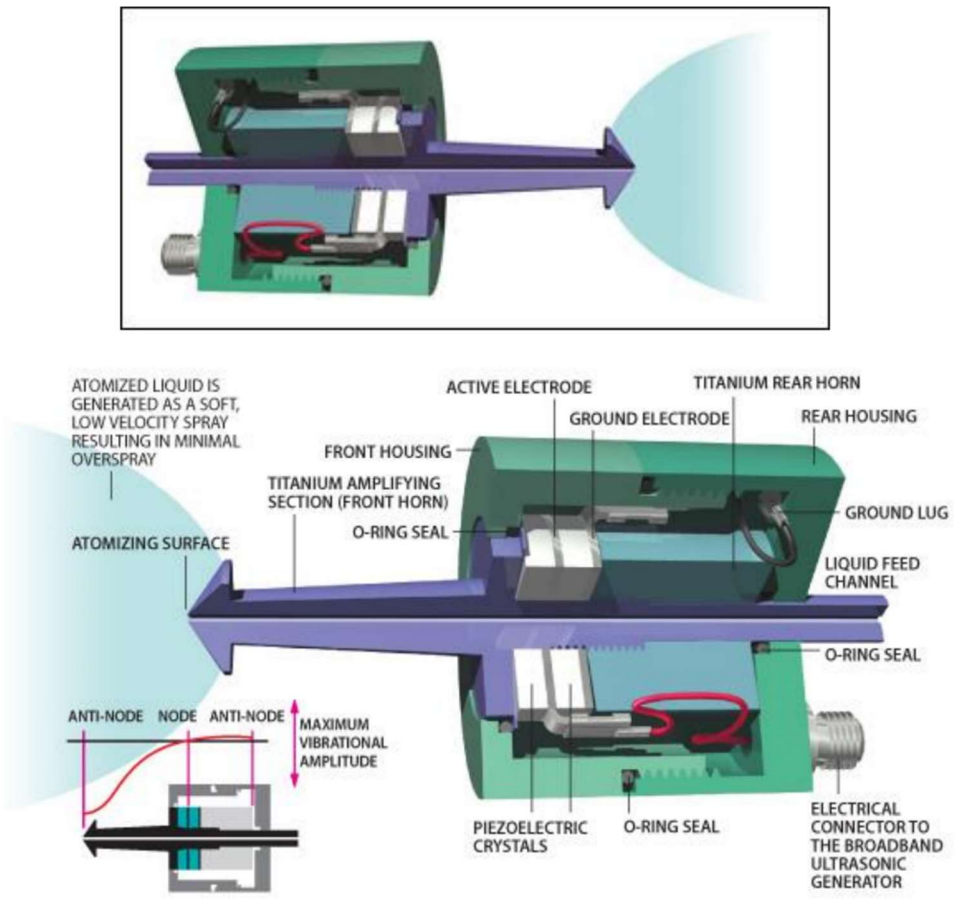

Figure 51: Ultrasonic nozzle diagram with connections [29]

The electrical connector connects the generator to the nozzle. Ultrasonic atomizing nozzles do not involve pressure, unlike other techniques that utilize pressure to spray. Therefore, a low-velocity spray at around 7.5 to 12.5 centimeters per second is produced. This method decreases the amount of overspray produced by causing droplets to settle onto the substrate surface in place of bouncing [29].

The mixed HeiQ HyProTecht solution was contained in a syringe, which was then connected to the ultrasonic nozzle. The ultrasonic generator was powered on to an optimized power of 2.5 W, which was determined to be the ideal power level because it produced a smooth

discharge of small droplets in place of large, collected drops. The difference in optimization of the power level and its effect on spray can be demonstrated in Figure 52.

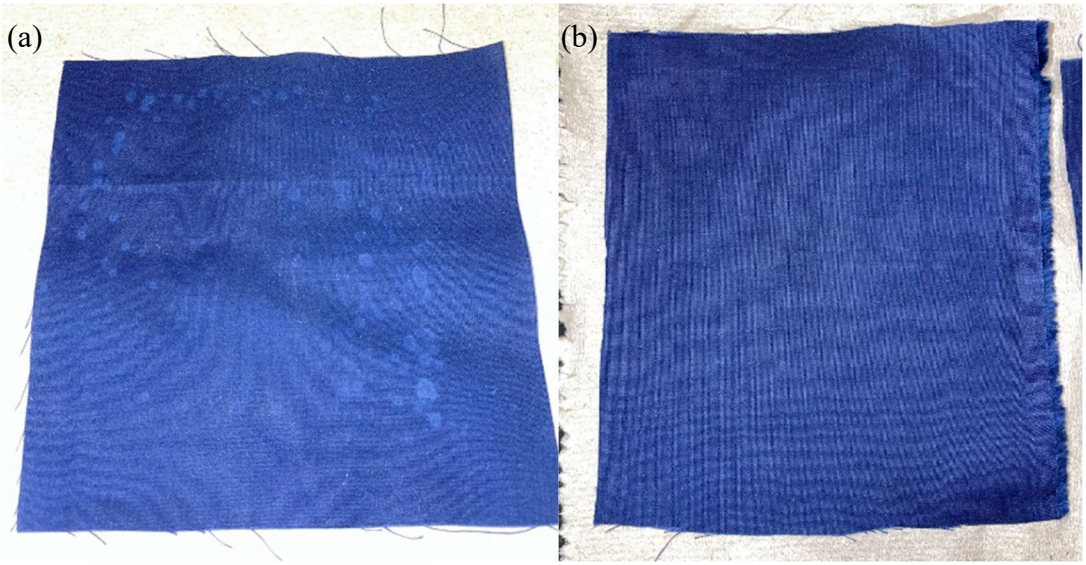

Figure 52: Silver nanoparticle coating applied (a) at high, unoptimized power, and (b) at lower, optimized power of 2.5 W

Optimizing the power level decreased the amount of visible clumping in the coating and produced a much more even, finely sprayed coating as shown in (b). To evenly dispense the coating onto the substrate, a programmable coating system titled the I&J4300-LF Benchtop Dispensing Robot was utilized to automate dispensing. Programming of the robot is done using the included teach pendant, which can be used to construct and load different user-defined programs that can automate the robot to move and dispense coating in desired shapes or locations. The dispenser and teach pendant are shown in Figure 53.

Figure 53: I&J4300-LF benchtop dispensing robot and teach pendant

A simple program was written to dispense a rectangular area of coating onto the fabric squares used for mask construction. The program was entered into the teach pendant into Program 3 as written below [29]:

1. Set up – Line speed – Enter – 30 – Enter

   Set up – XY move speed – Enter – 30 – Enter
2. Menu 2 – Numerical move – Enter

   X1=100 Y1=100 Z1=50
3. Enter (or point) – Line start – Enter
4. Menu 2 – Numerical Move – Enter

   X2=100 Y2=200 Z2=50
5. Enter (or point) – Line passing – Enter
6. Menu 2 – Numerical move – Enter

   X3=200 Y3=200 Z3=50
7. Enter (or point) – Line passing – Enter
8. Menu 2 – Numerical move – Enter

   X4=200 Y4=100 Z4=50
9. Enter (or point) – Line passing – Enter

10. Menu 2 – Numerical move – Enter

    X5=100 Y5=100 Z5=50

11. Enter (or point) – Line end – Enter

12. Enter (or Point) – Brush Area – Enter – Select (1 - Rectangle) – Width – 5 – Enter – 1.X

    2. Y:1 (Rectangle) – Enter

13. Menu 2 – Numerical Move – Enter

    X6= 100 Y6=100 Z6=50

14. Enter (or Point) – Line Start – Enter

15. Menu 2 – Numerical Move – Enter

    X7=200 Y7=200 Z7=50

16. Enter (or Point) – Line End – Enter

17. Enter (or Point) – End Program – Enter

18. Run

    The shape produced then filled by this program looks as shown in Figure 54.

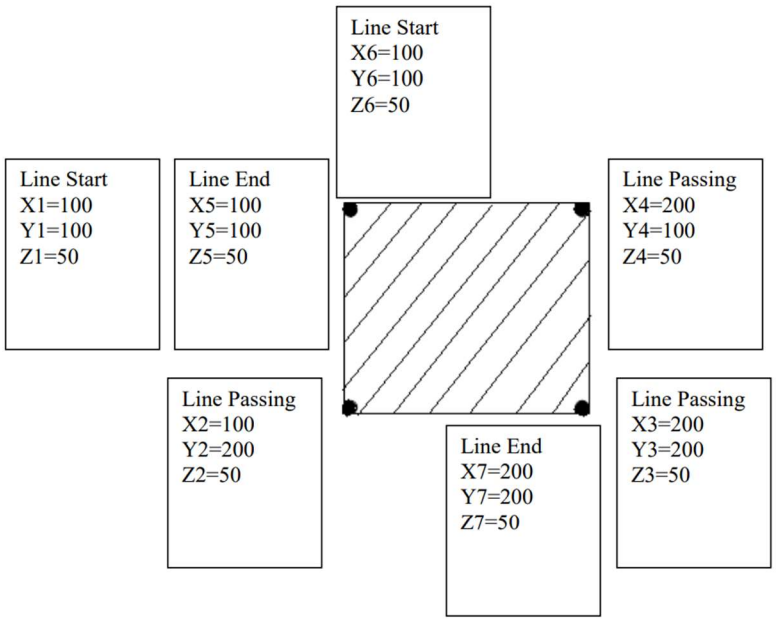

Figure 54: Teach pendant program shape - filled square

The setup for the application is shown in Figure 55, in which the syringe is connected to the nozzle, the nozzle is connected to the generator, and the dispensing device utilizes a user-input program to evenly dispense the coating on the cotton fabric substrate.

Figure 55: Atomization setup for silver nanoparticle coating

When set up and run, the configuration produces an evenly coated cotton substrate fabric square to be used to produce the outer layer of the fifth mask design iteration. The machine in process of coating the substrate is shown in Figure 56.

The same PLA material was used to construct the brace pieces.

The inner filter layer remained as one layer of melt blown filter material in the shape of the filter pocket of the mask

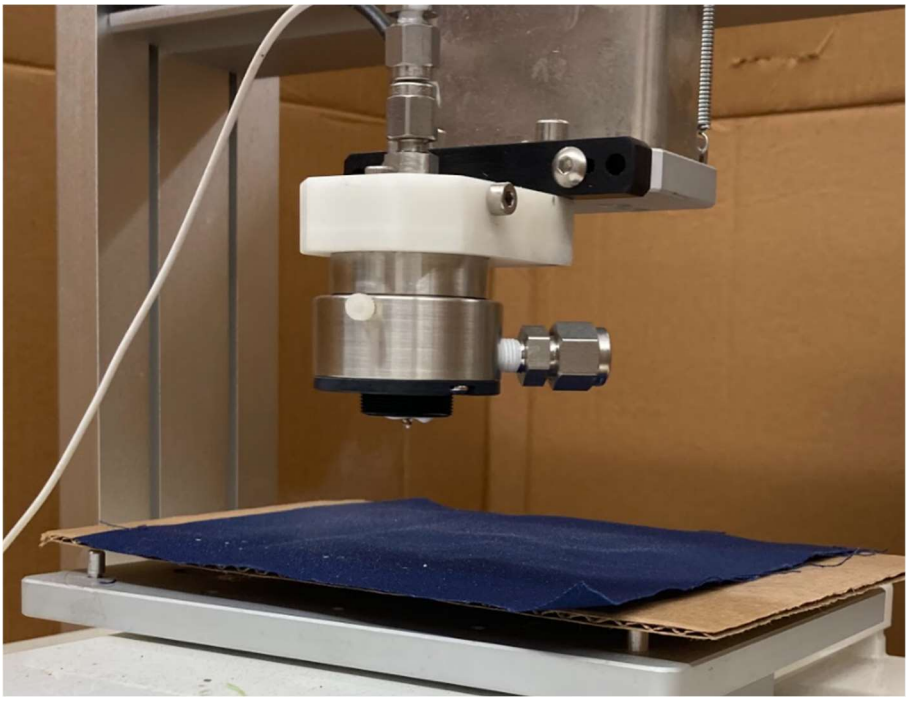

Figure 56: Atomization in process for silver nanoparticle coating

3.5.2 Brace Design and Construction

The brace was altered to best optimize fit and sealing for a variety of different nose bridge shapes. It was observed that the prior art demonstrated the ability to heat printed PLA parts to the threshold of their plastic transition temperature for reforming. Therefore, flat pieces were printed at a variety of thicknesses, then heated on the printer bed to be pressed against the mannequin nose bridge and reformed to that shape. The bed was heated to 70°C until the flat piece began to show warping effects, then was picked up using a pair of tweezers. The piece was then handled after a couple of seconds of cooling and formed against the mannequin's nose or the user's nose. Images of the formed nosepieces with different thicknesses are shown in Figure 57.

The thickness of 1.5 mm was chosen because it held the shape desired the best without preventing a slight ability of give to provide comfort during wear. The thickness of 1 mm did not hold the shape desired, and the thickness of 2 mm did not provide enough give for comfort.

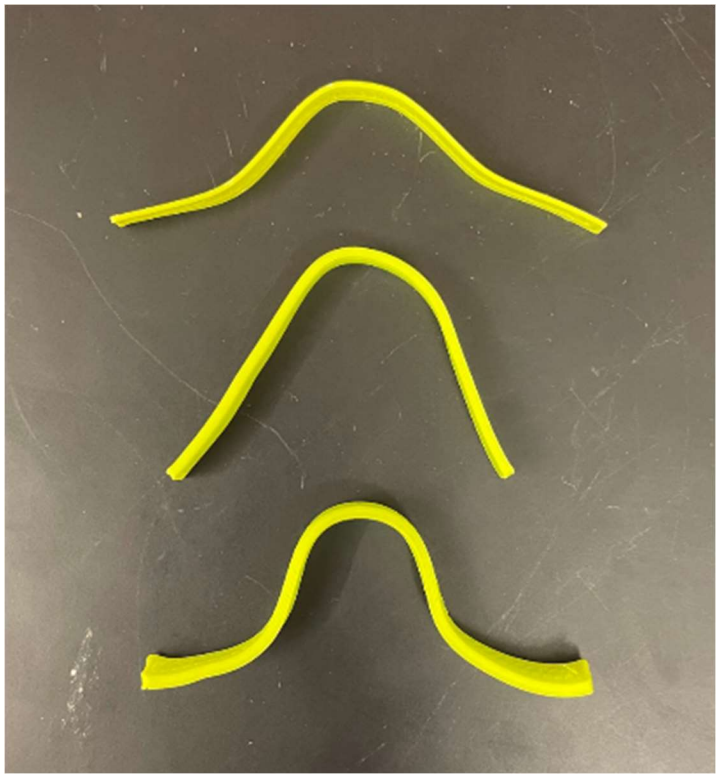

Figure 57: Nosepieces printed flat at different widths then formed to nose bridge shapes: top is 1.0 mm, middle is 1.5 mm, and bottom is 2.0 mm in thickness

The width of the piece was not varied and was set to a width of 0.5 cm as shown in Figure 58.

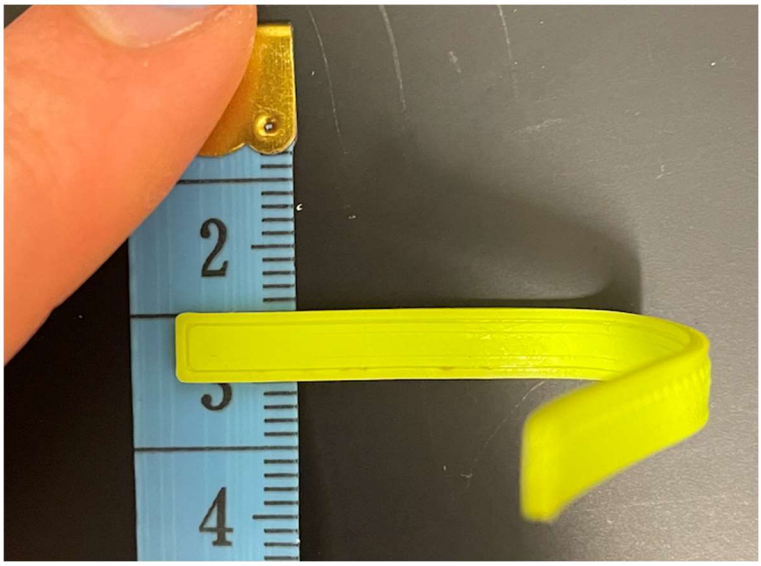

Figure 58: Width of Nosepiece

The central mouthpiece retained the same shape and dimensions as used previously. The thickness of 0.35 cm and approximate length 8.9 cm of the mouthpiece is shown in Figure 59.

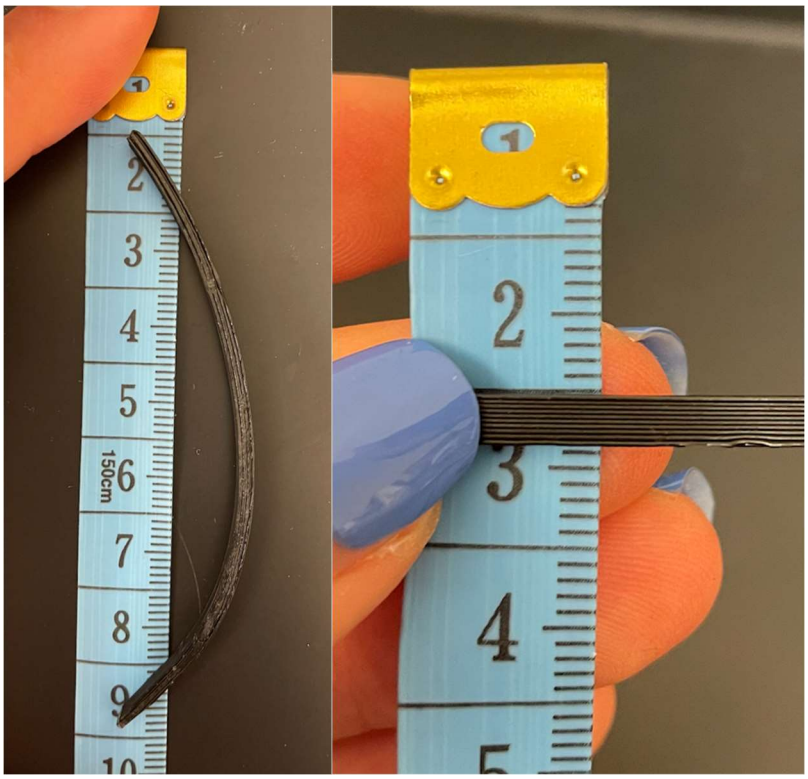

Figure 59: Length and width of mouthpiece

3.5.3 Mask Design and Construction

After the silver nanoparticle coating was applied, the mask was sewn in the same method as the previous iteration. No adjustments were made to the pattern of the design.

The completed design sewn with the coated fabric and containing the new nosepiece constructed is shown in Figure 60.

Figure 60: Prototpye-5 with silver nanoparticle coating

This mask iteration was the final iteration produced. This was then used in performance testing, but the previous mask was sent to the SGS Laboratory for ASTM and ISO testing.

CHAPTER 4: TESTING METHODS AND PROCEDURES

In this section, all testing methods and their procedures will be explained. Various testing methods were utilized to give insight on mask performance at different stages in the design process. First, fabric testing was performed by SGS Laboratories to determine the breathability, initial filtration efficiency, and bacterial filtration efficiency of the fabric composition of the mask body. This was done to determine mask performance if the mask did not have leakage to understand if the textile mask could be constructed with high filtration performance.

Next, leakage testing was performed on multiple mask iterations to determine the leakage of the mask design along the nose bridge and sides of the mask as compared to leakage in a surgical mask. These tests were performed on an experimental setup provided by the students of Dr. Vrishank Rhagav in the Aerospace Engineering Department involving laser illumination and cough simulation.

Finally, a brief performance test was conducted using standard treadmill equipment at the Auburn University Recreation Center to determine effects of wearing the mask during light exercise. This test was performed with a single subject, namely Laine Alby, and did not require the submission of an application to the Institutional Review Boards for the Protection of Human Subjects in Research (IRB) of Auburn University to be performed.

4.1 Fabric Testing

25 sample squares of the fabric composition were produced and sent to the SGS Corporation laboratory for three standard tests to be performed. The tests included were EN14683:2019 Annex C Method which requires 5 mask samples to be performed. At SGS Laboratories, this test costs $250 to be set up and $150 to be performed. ASTM F2299/F2299M-03 requires 5 samples as well, and costs $250 to be set up and $600 to be performed. Finally,

ASTM F2101-19 requires 10 masks for testing, and costs $825 to be performed. Additional fees include fixturing fees at $150 and sample handling fees at $350. For all tests to be performed, it cost $2,575. Samples provided can either be full mask samples or 4” x 4” samples. Although 15 masks are used for the testing, 25 were provided to allow for backup samples.

Because the amount of time it would take to sew 25 full mask samples on a single machine was estimated to be too long and would delay results, 4” x 4” samples were sewn for testing as shown in Figure 61.

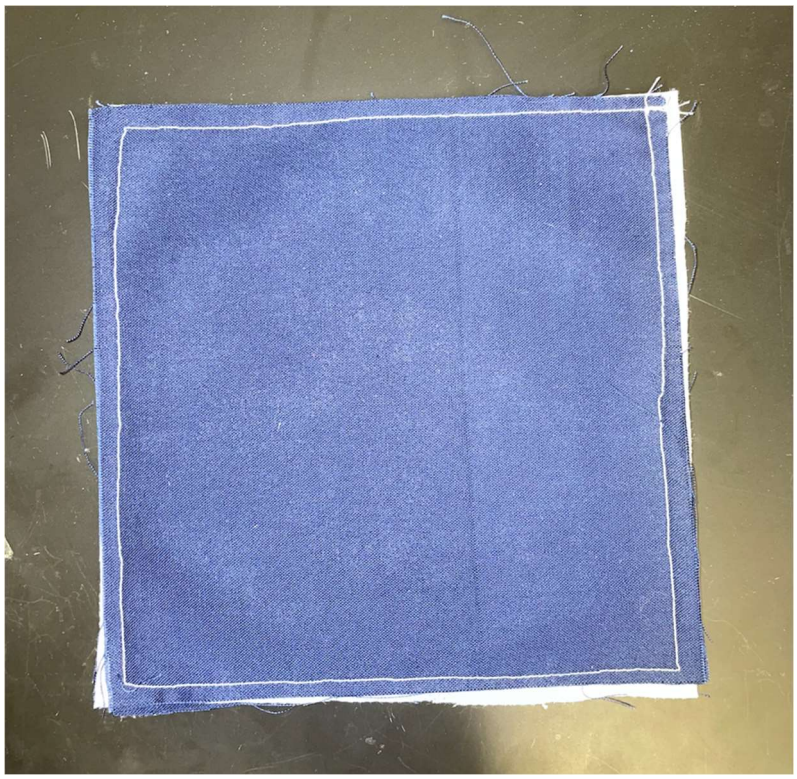

Figure 61: SGS sample square, 4"x4"

The outer layers consisted of the plain weave cotton fabric used for mask prototype-5, and the inner layer consisted of the meltblown filter material layer also used in this mask prototype. The sample sent, however, did not have the HeiQ coating because the coating was not yet available for use. Therefore, it is important to consider that testing results did not consider additional effects of the coating on parameters measured.

The testing was performed in late September of 2021. Because test samples were flat, square samples and not full mask samples, it is also important to consider that parameters calculated would be reflective of a mask composed of this same layering that fit perfectly, without leakage. Therefore, leakage testing is also important to determine if the mask has significant leakage that would compromise these results.

4.1.1 ASTM F2299/F2299M-03

Determining the Initial Efficiency of Materials Used in Medical Face Masks to Penetration by Particulates Using Latex Spheres

This test method is designed to measure an initial particle filtration efficiency of materials used in medical facemasks by using monodispersed aerosols, and particle counting is performed by light scattering in the size range of 0.1 to 5.0 micrometers. Airflow velocities used range from 0.5 to 25 cm/s [30].

The test is performed by passing filtered and dried air through an atomizer to produce an aerosol spray that contains suspended latex spheres. This aerosol is passed through a charge neutralizer, then mixed and diluted with preconditioned air to produce a stable latex sphere aerosol. Then, the material specimen is installed in the test system, airflows are established, and upstream and downstream aerosol counts are sampled and recorded at a 1-minute sampling time and at a minimum of five counts per position. The testing setup is shown in Figure 62.

To calculate the aerosol filtration efficiency for a particular particle size, the following formula is used:

$$\eta(D_p) = \left[1 - P(D_p)\right] * 100 \qquad \text{Eq. 4}$$

where P represents the penetration, D_p represents the particle size, and η represents the downstream particle concentration divided by the upstream particle concentration. This

calculated value is then used as a method of comparison of efficiencies between medical face mask materials.

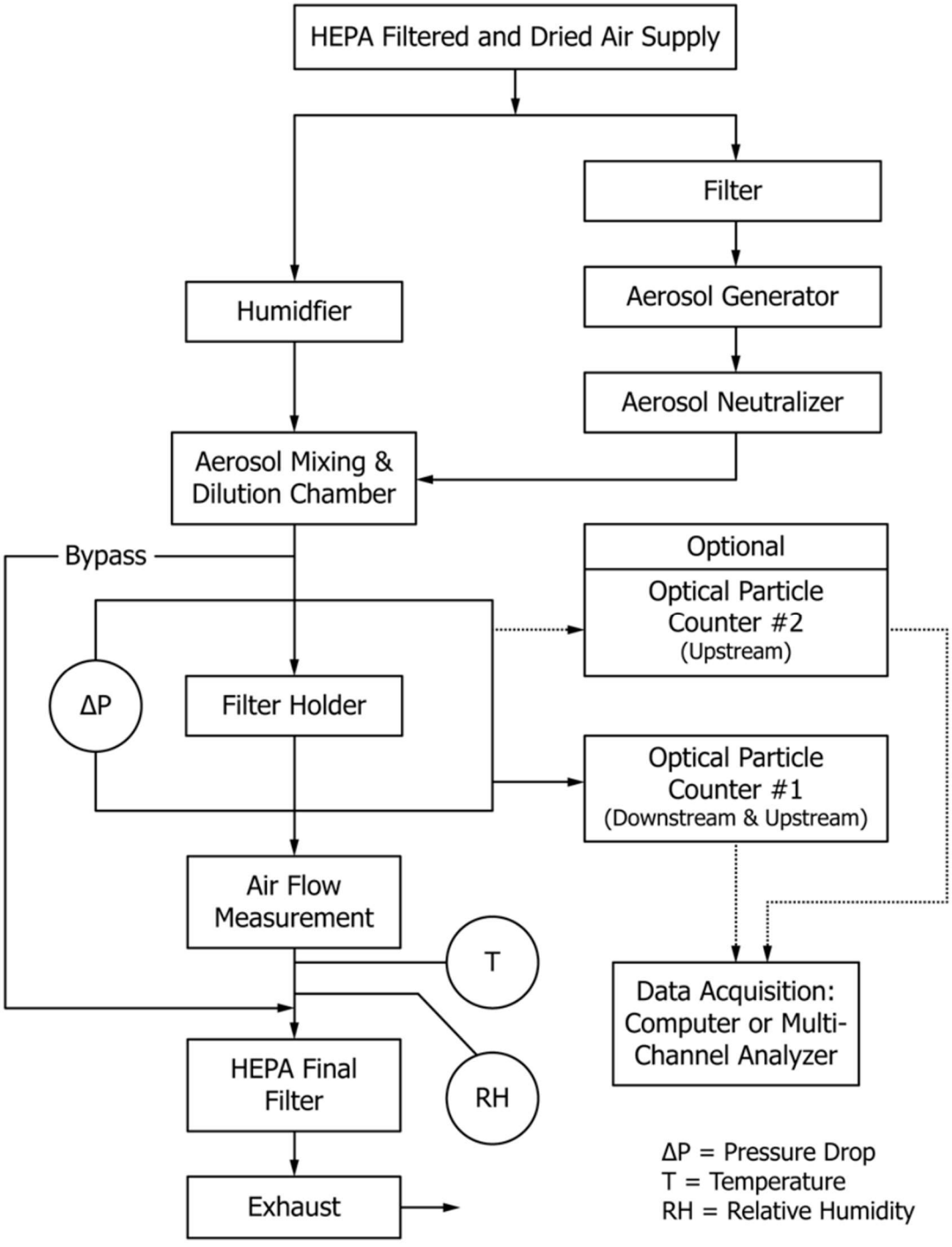

Figure 62: ASTM F2299 Test Method Illustration [30]

It is important to consider that this test method notes its inability to assess the design of

the medical face mask as well as the integrity of the seal of the tested mask on the wearer's face. It also notes that clothing design is a significant factor that also needs to be considered in the effectiveness of the tested mask in combination with particulate penetration results.

4.1.2 EN14683:2019

Annex C Method for determination of breathability (differential pressure)

The test method EN14683:2019 Annex C Method was used for determining breathability, which utilizes the following experimental setup demonstrated in Figure 63.

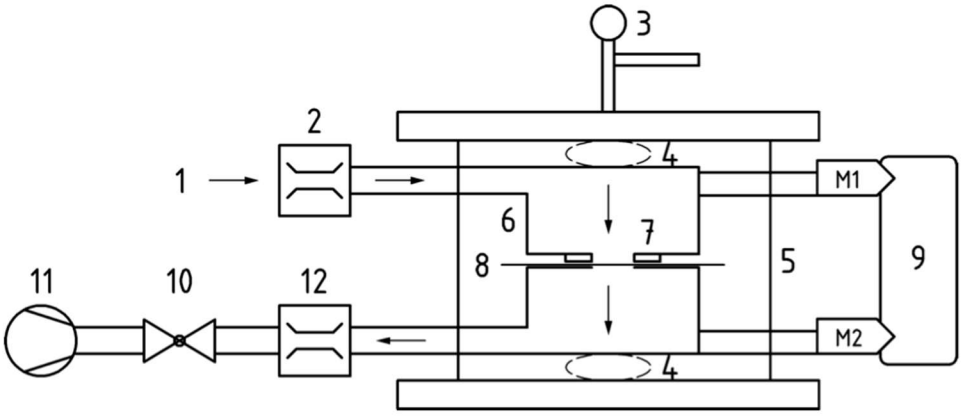

Key

1	air inlet	7	metallic ring (3 mm thick)
2	mass flow meter	8	filter material
3	lever for mechanical clamping	9	differential manometer or M1 and M2 manometers
4	system for final adjustment of the pressure (either at the top or the bottom)	10	valve
5	system ensuring optimal alignment of the 2 parts of the sample holder	11	vacuum pump including a pressure buffer tank
6	sample holder with a metal sealing mechanism	12	mass flow meter for checking leaks (optional)

Figure 63: Test apparatus for measuring differential pressure [31]

This device measures differential pressure that is required to draw air through a surface area at a constant flow rate, therefore measuring the air exchange pressure of the mask material used in testing [31]. The apparatus uses a water-filled manometer to measure the differential pressure, a mass flow meter to measure airflow, and an electric vacuum pump to draw air

through the system. The test specimen is a flat sample of all layers of the face mask material, which is secured to the apparatus with a sample holder consisting of a mechanical clamping system involving metal rings of 25 mm diameters. Samples are conditioned at 21°C and 85% relative humidity for at least 4 hours before testing. Then, flow of air is adjusted to 8 liters per minute, the sample is positioned, and differential pressure is measured for the system.

Differential pressure is then calculated as follows:

$$\Delta P = \frac{X_{m1} - X_{m2}}{4.9} \quad \text{Eq. 5}$$

where X_{m1} represents the lower pressure side of the material, X_{m2} represents the higher-pressure side, 4.9 is the area in square centimeters of the test material, and ΔP is the differential pressure per square centimeter of the material in Pascals.

This test method is also only representative of a flat, square mask sample and does not reflect performance of the mask when in use, considering leakage and other design effects. Therefore, leakage testing is again of importance.

4.1.3 ASTM F2101-19

Test Method for Evaluating the Bacterial Filtration Efficiency (BFE) of Medical Face Mask Materials, Using a Biological Aerosol of *Staphylococcus aureus*

This test method uses a ratio of the upstream bacterial challenge to the downstream residual concentration to determine filtration efficiency of medical face mask materials and produces a bacterial filtration efficiency measurement for the material. The test is performed by clamping the medical face mask material between a 6-stage cascade impactor and an aerosol chamber into which a bacterial aerosol is introduced. This is done using a nebulizer and a culture suspension of the test bacteria *Staphylococcus aureus*. Using a vacuum attached to the cascade impactor, the aerosol is drawn through the face mask material and collected onto six agar plates.

Control tests are performed by omitting the test specimen in the clamp [32]. The test apparatus for the ASTM F2101-19 test is shown in Figure 64.

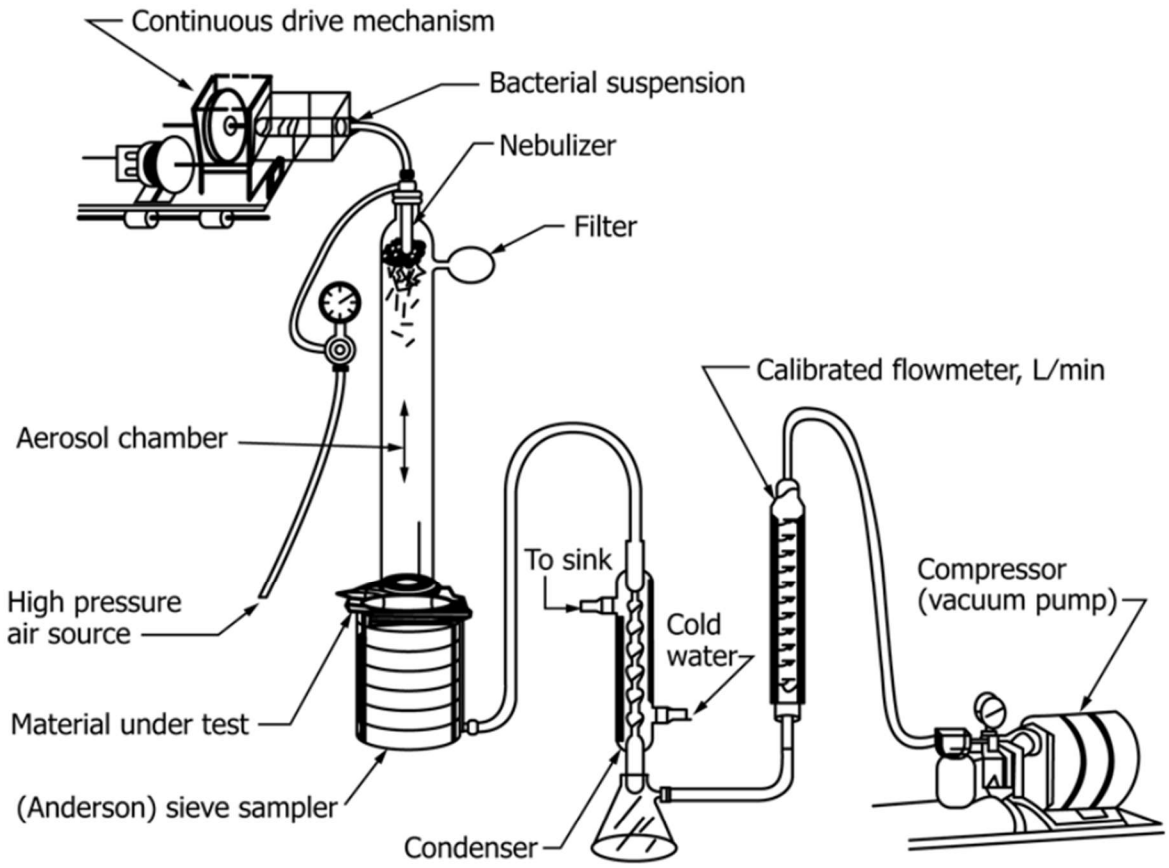

Figure 64: Bacterial Filtration Efficiency Test Apparatus [32]

The calculation for the filtration efficiency percentage is as follows:

$$FE = \left(1 - \frac{T}{C}\right) * 100\% \qquad \text{Eq. 6}$$

where FE is filtration efficiency, T is the plate count total for the test sample, and C is the average plate count total for the test controls [32].

This test method evaluates the bacterial filtration efficiency of different medical face mask materials but does not define acceptable levels of efficiency. Therefore, comparison of the result to commonly available or accepted face mask materials is necessary to determine performance of the test specimen used. Additionally, the test procedure notes that degradation by

stresses such as physical stress, chemical stress, and thermal stress could negatively impact the performance of the mask material, and this is not considered during testing.

4.2 Leakage Testing

The leakage of the current mask design was compared to that of the commonly used surgical face mask in the Aerospace Engineering Laser Lab by the Applied Fluids Research Group at Auburn University. The research group constructed an experimental setup designed to test surgical masks against simulated pulsatile coughs to test the flow pulsatility on the surgical mask and its effectiveness. Their findings indicate that inhaling, exhaling, double, and triple coughs provide leakage through which germs become airborne and are not filtered by the mask [33].

To demonstrate the masks' leakage, the mask is worn by a mannequin head attached to a cough simulator. The setup is shown in Figure 65.

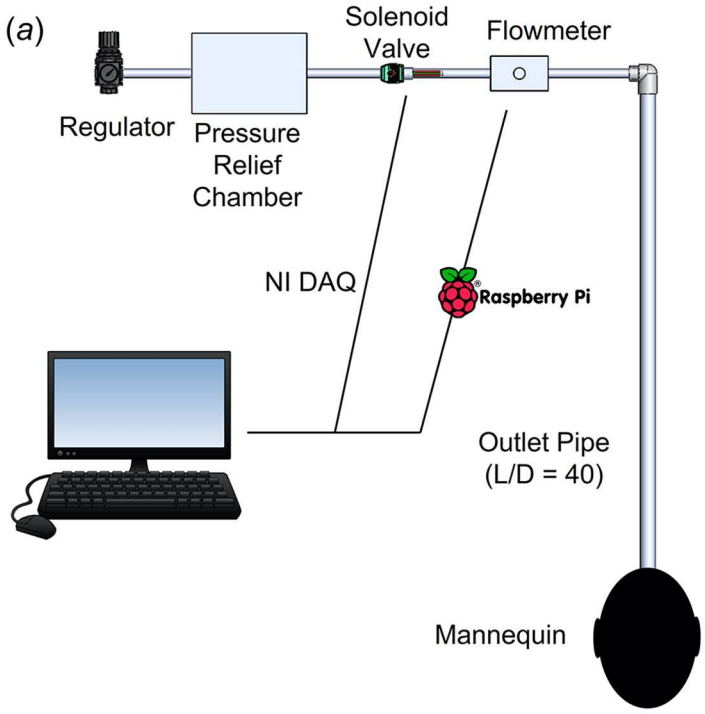

Figure 65: Laser illumination testing setup and configuration for cough simulation [33]

The simulator utilizes a solenoid valve that is run by a National Instruments DAQ to control flow duration. At the wall, a flow regulator controls the air flow rate. This air then runs to an in-line pressure relief chamber to smooth the flow profile to mimic that of a natural cough. The outlet pipe of the simulator extends through the mouth of the mannequin and has a diameter of 2.54 cm and a length L/D of 40 to ensure the flow is fully developed at the end of the tube. The mannequin serves as a representation of the mask fit to a user's face. An image of the setup complete with the mask on the mannequin head is included in Figure 66.

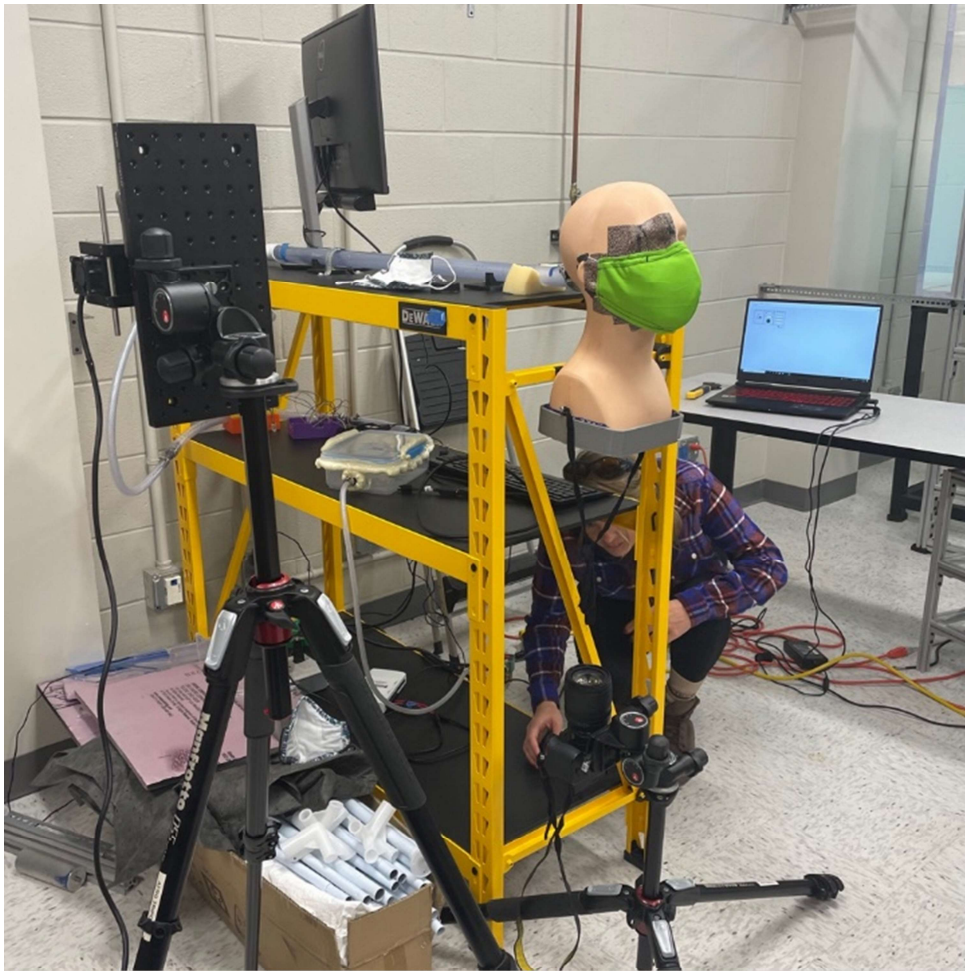

Figure 66: Laser illumination lab setup

In potential flow theory, external flows around bodies are treated as inviscid or frictionless as well as irrotational [34]. Although this is an ideal case and is not practical to real-

life flow of fluids being tested, it can be helpful before testing to visualize the flow of the user's breath through areas of potential mask leakage to help confirm which planes of interest should be investigated for leakage. For example, if we were to consider a gap in the mask between the user's nose and mask, potential flow theory would help to produce a visualization of the breath flow as demonstrated in Figure 67.

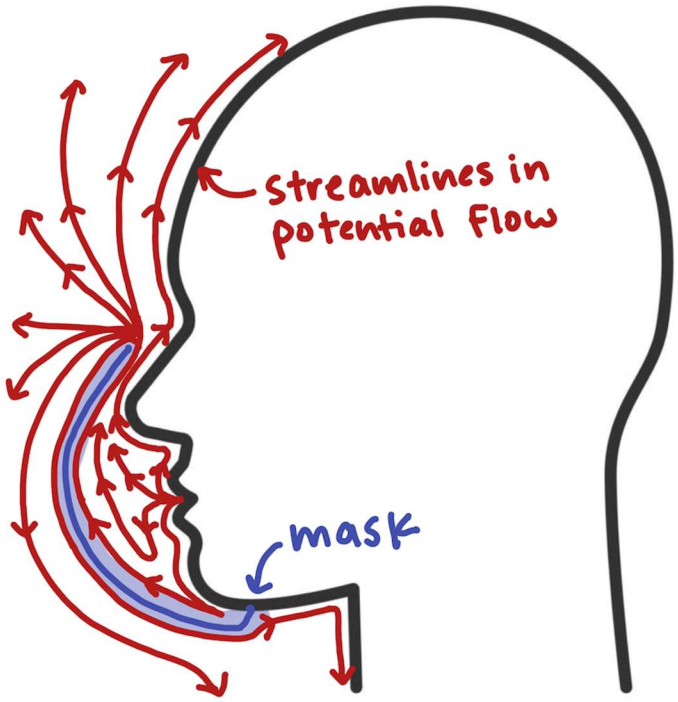

Figure 67: Potential flow theory illustration of breath streamlines

Therefore, it is important to illuminate the sagittal plane for study to demonstrate if a gap is present and if fluid particles are leaking from this area of the mask.

The same can be said about the side of the mask, where gaps are often present when a surgical mask is used. This can be demonstrated by studies who have previously investigated fit modifications to surgical masks to address this gapping area [17].

The laser was used to illuminate leakage along two planes: the sagittal plane for leakage along the nose bridge, and a transverse plane to illuminate side leakage. The camera was then

positioned perpendicular to this plane to capture the leakage illuminated by the laser. The planes are illustrated on a representation of the mannequin head in Figure 68.

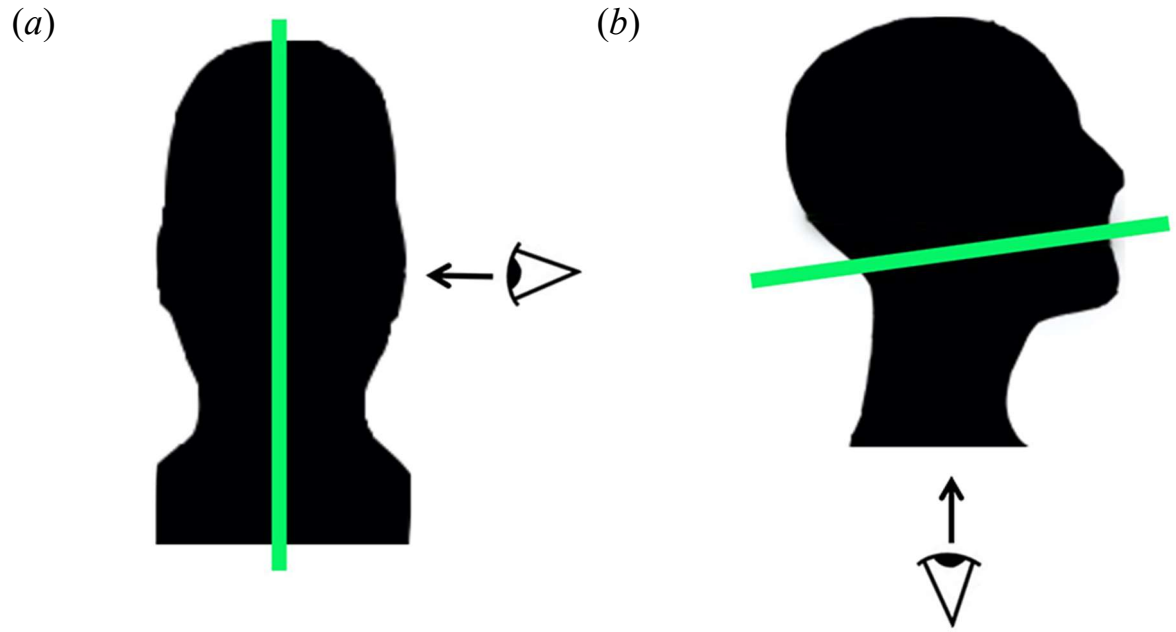

Figure 68: (a) Sagittal plane positioning of laser with camera positioned beside mannequin and facing the plane to capture leakage along the nose bridge, (b) side plane positioning of laser with camera facing plane from underneath mannequin head to capture leakage on the sides of face covering [33]

Therefore, leakage can be compared to that of the surgical mask to determine if it was improved in comparison to the surgical mask. The surgical mask was tested with a single-pulsed cough of duration $T_1 = 0.225$s and cough peak flow rate of 4.5L/s. The leakage is then made visible by smoke flow illumination. The long outlet pipe is filled with smoke from a fog machine while an outlet hole at the end remains open, allowing air inside the tube to exit and smoke to enter, and then the hole is sealed after it is filled with smoke. A 532 nm continuous-wave laser is used to illuminate the planes described in Figure 68 by converting the laser beam into a light sheet. Then, the leakage is captured at 30 frames per second using a Nikon Z50 mirrorless camera. The camera is shown in Figure 69.

Figure 69: Nikon Z50 mirrorless camera used for laser illumination [35]

The designed test produces an image depicting streaklines. In fluid mechanics, a streakline is defined as the locus of all fluid particles passing continuously through a particular point in space [36]. This idea can be demonstrated in using the example of smoke from a chimney being blown by the wind, wherein the wind velocity produces a trail of smoke which visually represents a streakline. The origin of the smoke is the point in which the fluid particles all initially pass.

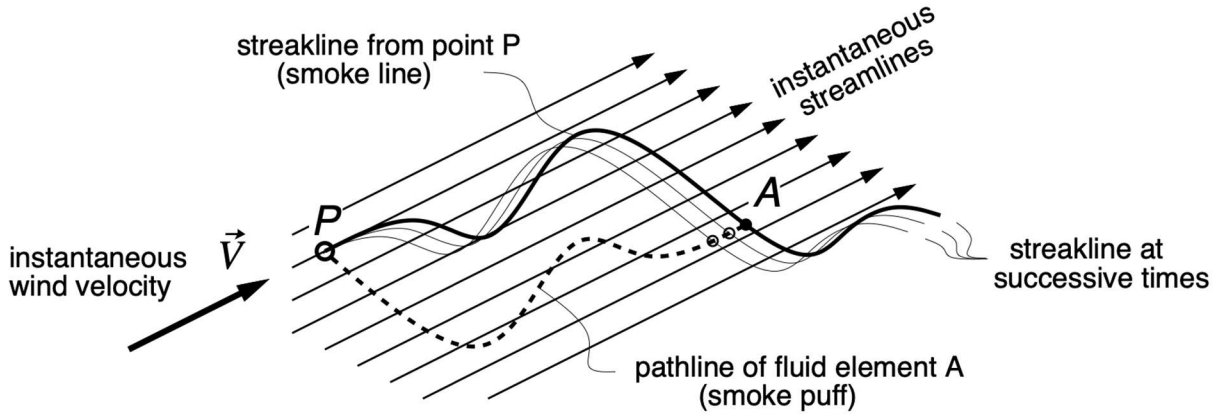

Figure 70: Illustration of Streaklines [36]

Streaklines differ from streamlines, which are defined as lines parallel to the local velocity vector of the fluid particle, and from pathlines, which are defined as the path a fluid particle takes in space as a function of time. The use of a streakline in this case will help demonstrate the directional flow of the fluid particles with time, since in this case we are interested in where the user's breath is travelling as it is emitted. The use of a streamline or pathline in this study is not necessary to determine where in the mask leakage occurs.

After testing, results will be compared to that of a surgical mask at the same time T_1 to identify improvements of the mask design.

4.3 Performance Testing

To test the performance of the masks, and to evaluate the performance effects of the silver nanoparticle coating, a test was performed in which the mask was worn during light exercise. Blood-oxygen percentage was recorded before and after each 10-minute walking session, and heartrate was recorded throughout each session.

The experiment was conducted while wearing no mask, wearing the mask design of prototype-4 without the silver coating as well as prototype-5 with the silver coating. The same nosepiece and mouthpiece were used for each design. Additionally, the same pattern and dimensions were used to produce each tested mask.

Figure 71: Treadmill setup for performance testing

The exercise pace tested was a walking speed of 3.0 miles per hour on a Cybex treadmill located in the Auburn University Student Recreation Building. All walks were conducted at the same speed for the full 10-minute duration. The same test subject was used, namely Laine Alby,

for each test. The testing set up for the treadmill is shown in Figure 71.

The measurement device used for heart rate and blood-oxygen percentages was the Apple Watch Series 6, Model A2291. Plots were then converted into CSV files using WebPlotDigitizer [37].

To minimize the effect of the order of the tests performed, breaks of 15 minutes were taken between runs to return to resting heart rate values.

CHAPTER 5: RESULTS AND DISCUSSION

In this chapter, the results of the three testing types are presented. First, results of the SGS Laboratories testing are presented, demonstrating the initial efficiency, differential pressure, and breathability measurements of the mask. The results will be compared to values of traditional mask materials or others identified by literature to identify benchmark goals for these parameters. These parameters may also be compared with ASTM standards or industry standards mentioned during the literature review.

Next, results from the laser illumination experiment are discussed. Results will be presented from both the novel mask tested as well as a surgical mask, then these results will be compared.

Finally, performance testing results for both blood-oxygen percentage as well as heart rate throughout the exercise period are reported and graphed for discussion. Their results will be compared between the testing iterations, when no mask is worn, the mask without the HeiQ coating is worn, and the mask with the HeiQ coating is worn. The graphs will be analyzed for large changes in heart rate behavior to identify if a mask is putting strain on the user during exercise.

5.1 Fabric Testing

5.1.1 Results

The test results for the Initial Efficiency are shown in Table 1, which has an average initial efficiency of 73.69%. Initial Efficiency values are calculated using latex microspheres having a particle size of 0.1 micrometers, as opposed to Bacterial Filtration Efficiencies which are calculated using a different particle type and size. Filter ID's indicate which sample was utilized in the testing, but all samples are the same composition and dimensions. The ID is simply used

as a means of record keeping at the SGS Laboratory complex. RH represents relative humidity values while BP represents barometric pressure.

Table 12: Initial efficiency test results

Filter ID	Differential Pressure (mmH_2O)	Port	Particles (0.1 μm)	Efficiency (%)	Conditions
24798-1	8.8	Upstream Downstream	203586 52505	**74.21**	Temp: 21.2°C RH: 40.3% BP: 728 mmHg
24798-2	8.1	Upstream Downstream	203770 69142	**66.07**	Temp: 21.0°C RH: 39.4% BP: 728 mmHg
24798-3	8.3	Upstream Downstream	201249 46543	**76.87**	Temp: 20.7°C RH: 38.6% BP: 728 mmHg
24798-4	8.0	Upstream Downstream	202199 42817	**78.82**	Temp: 20.9°C RH: 42.7% BP: 728 mmHg
24798-5	8.5	Upstream Downstream	201145 55396	**72.46**	Temp: 21.7°C RH: 40.9% BP: 728 mmHg
			Average:	**73.69%**	

The breathability or differential pressure test results are shown in Table 13, where an average differential pressure of 5.02 mmH_2O/cm^2 is reported. This breathability value comes at slightly below that of an N95 respirator, but about twice the value of a surgical mask, indicating that the mask is less breathable than a surgical mask but not as difficult as an N95 mask. An N95 respirator has an average differential pressure of 5.5 mmH_2O/cm^2, while a surgical mask has an average differential pressure of 2.24 mmH_2O/cm^2 [38].

Again, in this test the Filter ID is indicative of which sample square was used during each test, and the measurement area indicates a different section of this sample square that was set in the testing ring for each iteration. The differential pressures measured of all five testing areas per filter ID is averaged and represents that of the individual sample. These are then averaged to

represent the fabric composition.

Table 13: Breathability or differential pressure test results

Filter ID	Measurement Area	Differential Pressure (mmH_2O)	Mean Differential Pressure (mmH_2O)	Mean Differential Pressure / Area (mmH_2O/cm^2)	Conditions
24798-6	1 2 3 4 5	27.3 26.5 26.4 24.1 22.5	25.4	**5.2**	Temp: 23.0°C RH: 36.7% BP: 727.9 mmHg
24798-7	1 2 3 4 5	26.1 25.0 24.5 25.0 24.8	25.1	**5.1**	Temp: 23.1°C RH: 36.9% BP: 727.9 mmHg
24798-8	1 2 3 4 5	21.9 21.5 21.7 23.5 21.7	22.1	**4.5**	Temp: 23.1°C RH: 37.7% BP: 727.9 mmHg
24798-9	1 2 3 4 5	26.7 28.0 24.1 24.2 24.5	25.5	**5.2**	Temp: 23.1°C RH: 38.3% BP: 727.9 mmHg
24798-10	1 2 3 4 5	26.0 23.1 24.8 25.4 26.1	25.1	**5.1**	Temp: 23.1°C RH: 38.8% BP: 727.9 mmHg
			Average:	**5.02**	

BFE testing was performed using air at a flow rate of 8 liters per minute and with a standard effective area of 4.9 cm^2. Setup parameters are shown in Table 14.

In this test, the plate count indicated represents the number of particles of test bacteria counted on the sample at the end of the testing period. The unit CFU represents colony forming unit, which is a measurement unit used to demonstrate visible agar colonies on a test sample.

Table 14: ASTM F2101 Testing conditions: bacteria filtration efficiency (BFE), SGS IBR Laboratories

Challenge	Staphylococcus *aureus*
Area of Test Specimen (cm^2)	48.3
Specimen side facing challenge	Inside
Flow Rate (lpm)	28.3
Mean Particle Size (MPS) of challenge aerosol (μm)	3.3
Average plate count of positive control	2239 CFU
Plate count of negative control	0 CFU

The test results for BFE are shown in Table 15, which demonstrate an average efficiency of 99.31%. Testing conditions include a challenge specimen of Staphylococcus aureus, which has a mean particle size of 3.3 micrometers. The average plate count of a positive control in this test is 2239 CFU, while the plate count of a negative control is 0 CFU. This indicates that when a filter or barrier material is not used, 2239 CFU of test particles are counted on the test substrate, while when no bacteria are present during testing, 0 CFU of particles collect on the test substrate.

Table 15: BFE test results

Sample Tested	Results (CFU)				
	1	2	3	4	5
Stage 1	0	1	1	0	0
Stage 2	0	0	0	0	0
Stage 3	0	0	0	1	1
Stage 4	1	1	2	0	0
Stage 5	14	12	17	1	13
Plate Count Total	17	21	22	2	15
% BFE	**99.24%**	**99.06%**	**99.02%**	**99.91%**	**99.33%**
Average % BFE:	**99.31%**				

5.1.2 Discussion

The BFE test results indicate a very high efficiency value at a larger particle size of 3.3 micrometers. In comparison, the mean particle size of COVID-19 has been shown to vary between 50-140 nanometers [39]. The upper end of this size range lies close to that of the latex

particles (0.1 micrometers), but less than that of Staphylococcus aureus (3.3 micrometers). It is also important to consider that the virus is transmitted through respiratory droplets, which are larger than the mean particle size of coronavirus alone and are typically 5-10 micrometers in length. This is much higher than the size of the Staphylococcus aureus particles tested, suggesting that the filtration efficiency of larger respiratory particles is high for the masks tested.

The BFE tested of the novel mask is close to that of tested N95 masks at 99.9%, while surgical masks had an average BFE of 97.48% in testing [40]. Therefore, the novel mask had a BFE very close to that of the N95 mask and much higher than that of the surgical masks tested.

5.2 Leakage Testing

Flow visualization results are shown in Figure 72 for both the surgical mask and novel mask along the sagittal plane as described in the leakage testing procedures. Images were both taken at a time of $T = 2T_1$ for comparison.

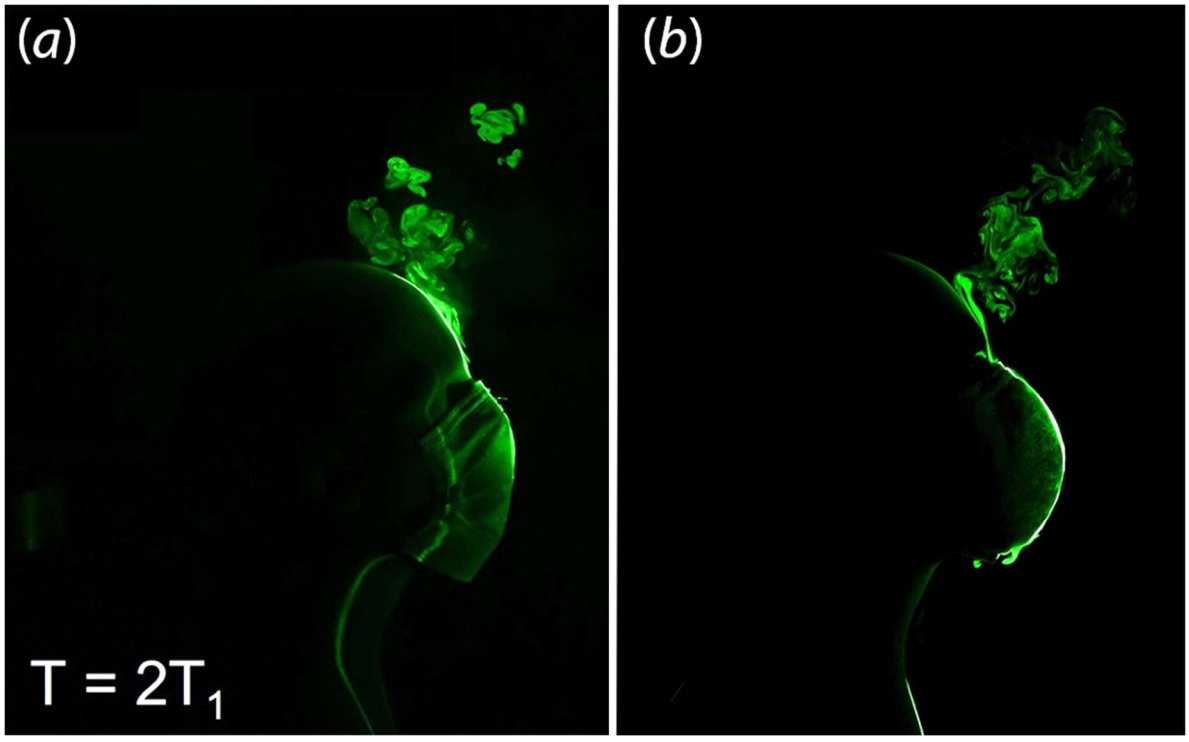

Figure 72: Smoke flow visualization of flow leakage along the sagittal plane for (a) surgical mask and (b) novel mask [33]

It can be seen in both images that flow leakage occurs at the very top of the nose bridge. In the surgical mask case, significant leakage occurs such that the stream is very bright and close to the user's forehead. The stream then continues upward in large plumes. Although the novel mask appears to have a smaller volume of leakage and streams appear to be smaller in width, no concrete conclusions can be drawn confidently from these images because the difference is not incredibly large.

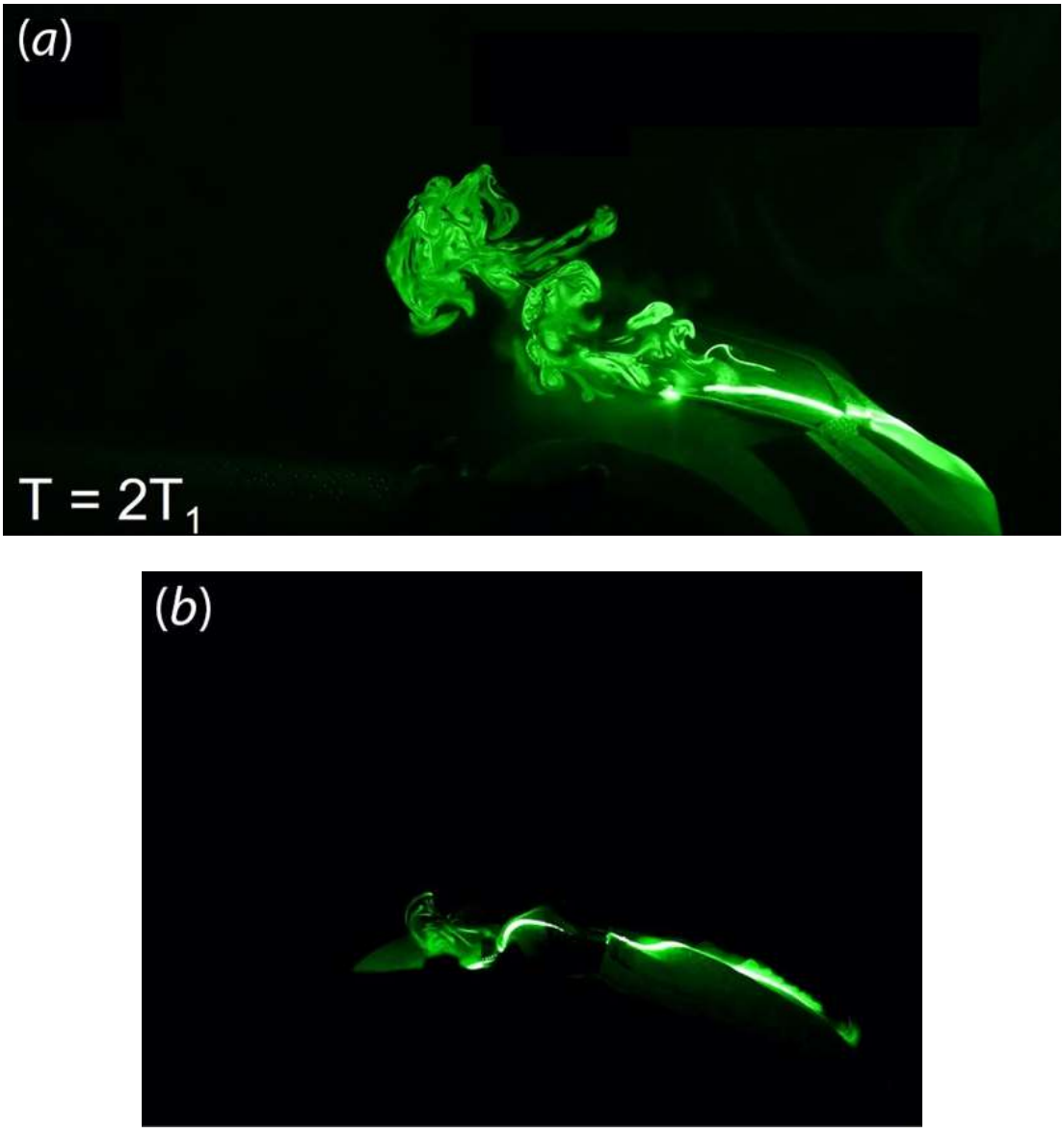

Figure 73: Smoke flow visualization of flow leakage along the side plane (a) surgical mask and (b) novel mask [33]

For the side plane, the resulting images at the same time $T = 2T_1$ can be seen in Figure 73 for both the surgical mask and the novel mask tested.

Here, a significant amount of flow leakage is demonstrated by the surgical mask at the side of the mask by the ears. In contrast, the image of the novel mask demonstrates significantly reduced flow leakage in the same area. This difference can be attributed to the design change of adding additional fabric material on the sides of the mask such that the puckering demonstrated in surgical masks is eliminated, as described in the protoype-4 and prototpye-5 mask manufacturing descriptions.

5.3 Performance Testing

5.3.1 No Mask Worn

The heart rate plot for the performance test run without wearing a mask is shown in Figure 74.

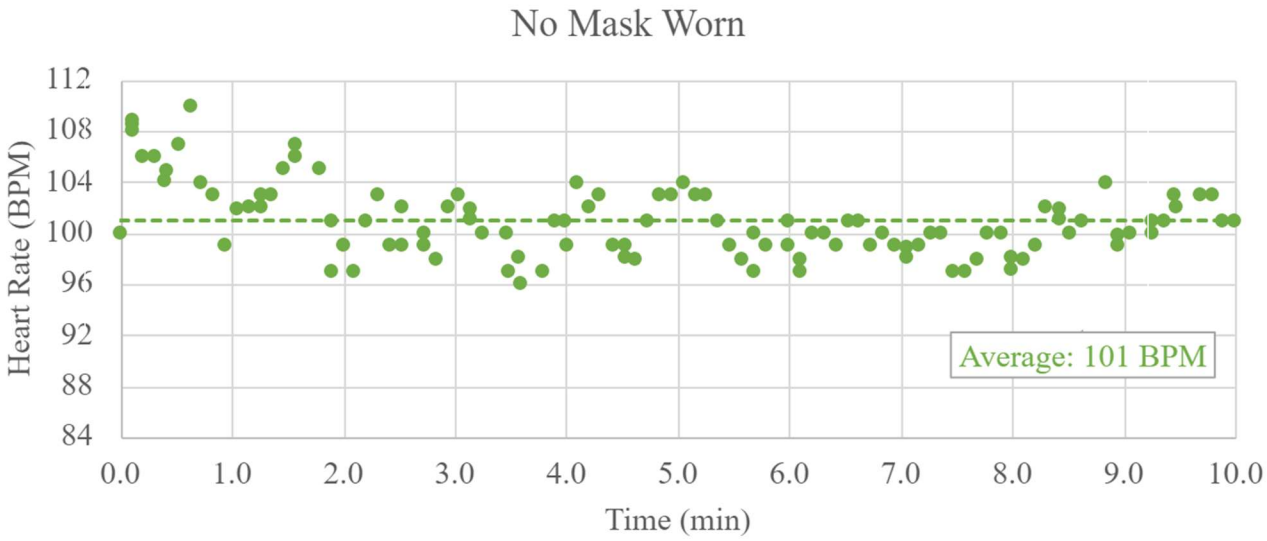

Figure 74: Heart rate plot for performance test without wearing mask

The average heart rate recorded for the 10-minute run was 101 beats per minute, or BPM.

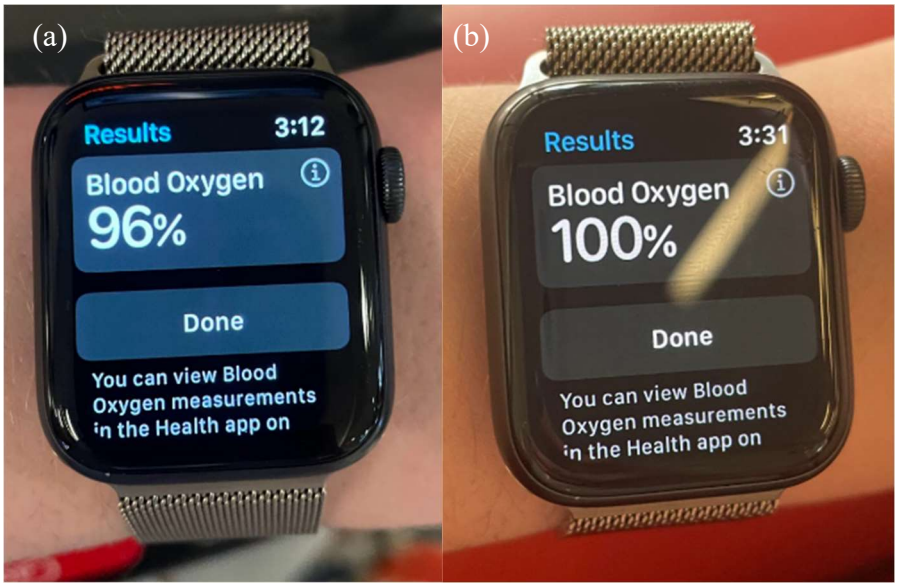

Figure 75: Blood oxygen percentages reported for performance testing without a mask reported

(a) before testing and (b) after testing

The initial blood oxygen measurement reported before the test was 96%, while the blood oxygen reported for after the test was 100%, as shown in Figure 75.

5.3.2 Mask Without Coating

The heart rate plot for the performance test run wearing the mask without the silver nanoparticle coating is shown in Figure 76.

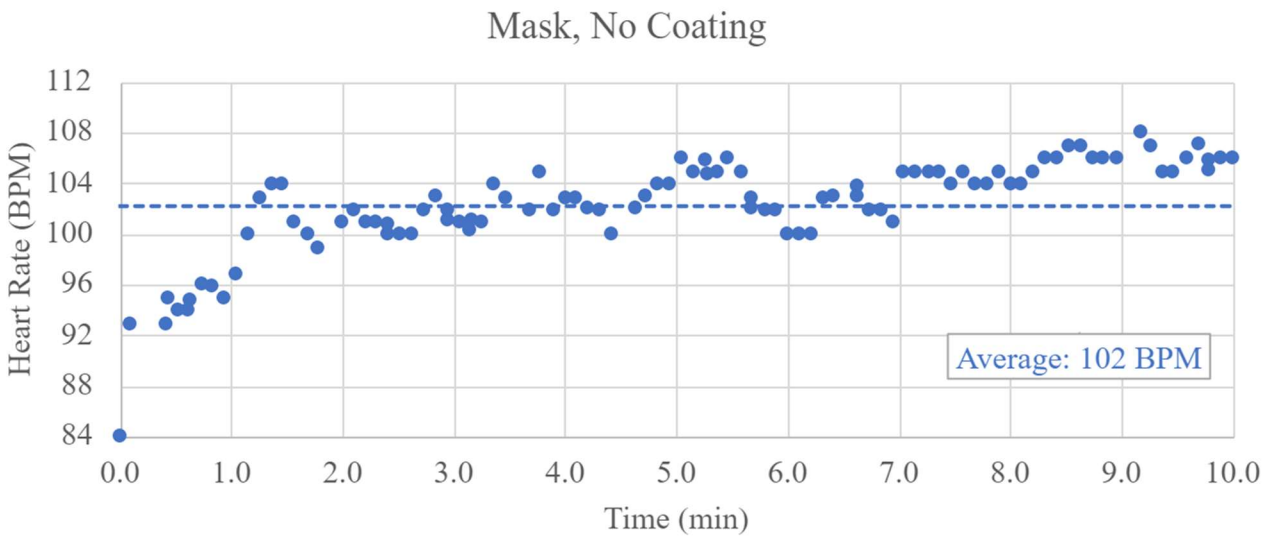

Figure 76: Heart rate plot for performance test of mask without silver coating

The average heart rate recorded for the 10-minute run was 102 BPM.

The initial blood oxygen measurement reported before the test was 100%, while the blood oxygen reported after the test was 99%, as shown in Figure 77.

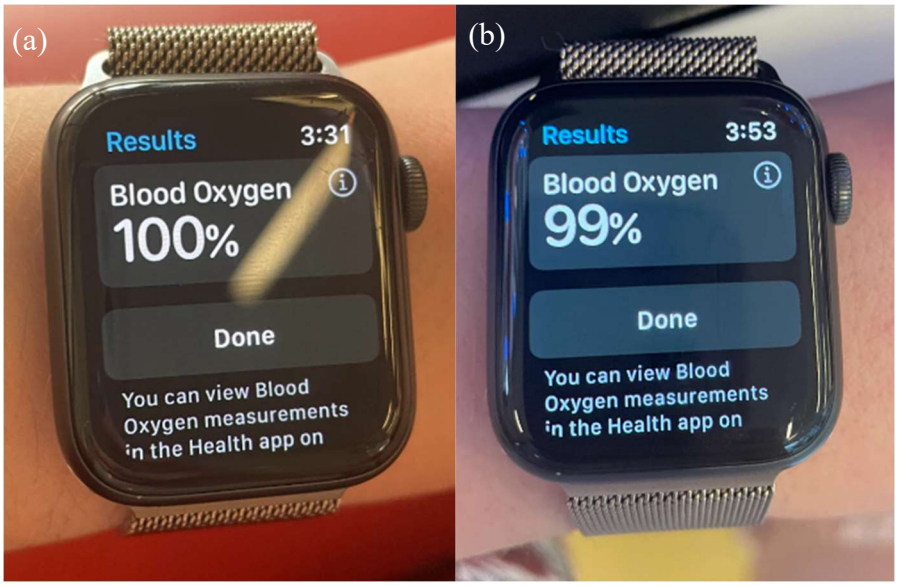

Figure 77: Blood oxygen percentages reported for performance testing wearing mask with no coating: (a) before testing and (b) after testing

5.3.3 Mask with Coating

The heart rate plot for the performance test run wearing the mask with the silver nanoparticle coating is shown in Figure 78.

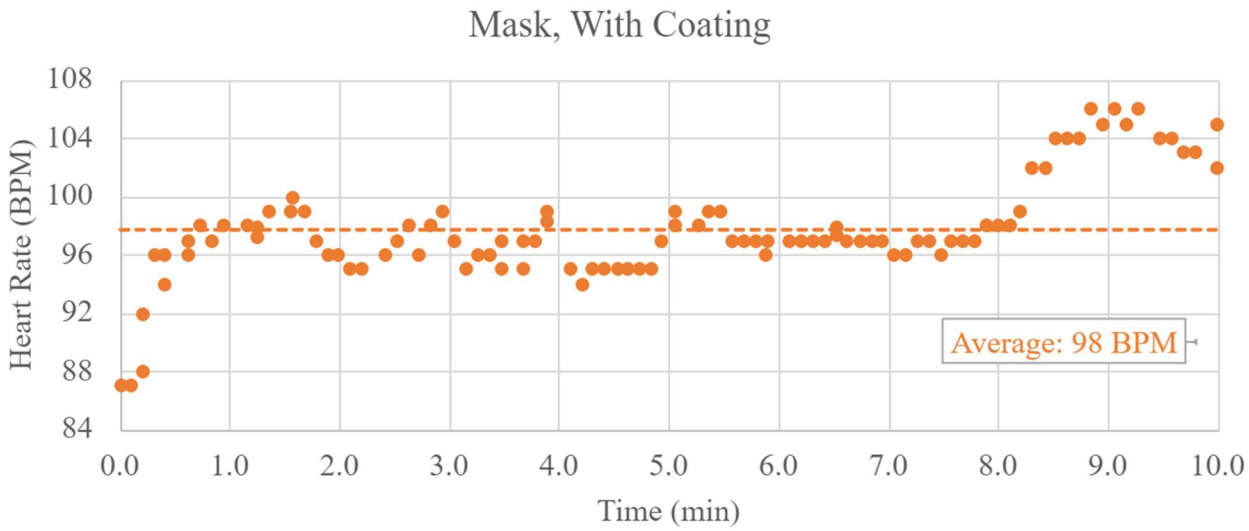

Figure 78: Heart rate plot for performance test of mask with silver coating

The average heart rate recorded for the 10-minute run was 98 BPM.

The initial blood oxygen measurement reported before the test was 99%, while the blood

oxygen reported for after the test was 97%, as shown in Figure 79.

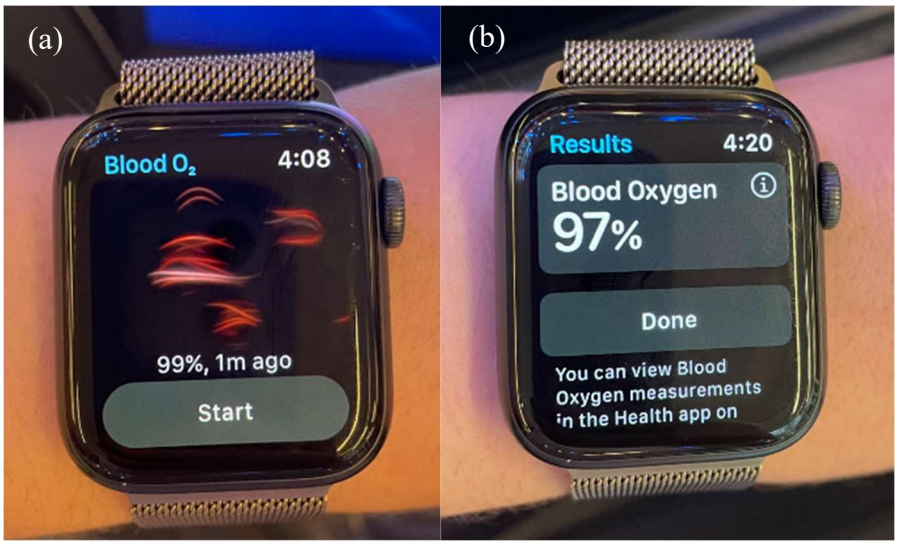

Figure 79: Blood oxygen percentages reported for performance testing wearing mask with coating reported (a) before testing and (b) after testing

5.3.4 Performance Test – Discussion

Figure 80 demonstrates the results of all tests for comparison purposes.

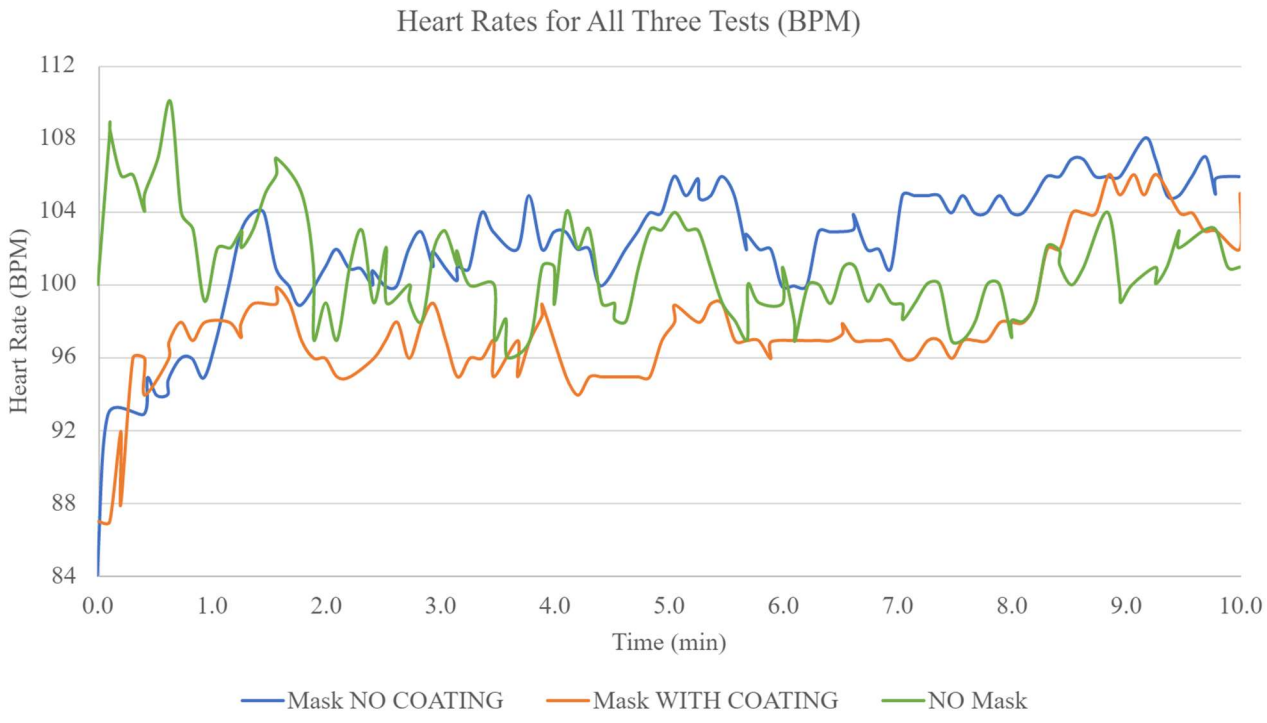

Figure 80: Plot of all heart rate testing

It can be seen in the comparison of the performance tests that each test remained within approximately a 10 BPM range of one another throughout the experiment. The test with the lowest average heart rate was the test performed while wearing the mask that did have the HeiQ coating applied, at 98 BPM, but the mask tested without the coating had only a slightly higher average heart rate of 102 BPM. In contrast, the test performed without wearing a mask had an average heart rate of 101 BPM, which is only 1 BPM lower than that of the test performed while wearing the uncoated mask. The tests all had very similar heart rate performance, and from this data it cannot be said confidently that wearing a mask with or without a coating significantly affects heart rate behavior during light prolonged exercise.

These results support that the novel mask should not cause the wearer added strain or discomfort during activities such as talking or typical breathing if results were not significant during light exercise.

CHAPTER 6: CONCLUSIONS AND RECOMMENDATIONS

6.1 Conclusions

In conclusion, this project resulted in a textile face mask design with enhanced capabilities as compared to other textile masks currently available on the market. Through the employment of various testing methods, including bacterial filtration efficiency, breathability, initial filtration efficiency, laser leakage illumination, and performance testing, various mask iterations were evaluated and improved to perform better. Different engineering methods were utilized, including textile engineering, additive manufacturing, and laser imaging, all to construct a device with the capability of reducing the spread of COVID-19 or another disease if a pandemic such as COVID-19 were to occur again.

The final design, prototype-5, incorporated two layers of plain-weave, 412 GSM cotton fabric with an inner meltblown filter material layer. This design optimized breathability without sacrificing bacterial filtration efficiency, and matched results predicted by literature in the literature review regarding fabric material selection. The brace used was constructed from PLA, and had a thickness of 1 mm. This brace was optimized by being heated and then formed to the user's exact nose contour to prevent leakage. In leakage testing performed by laser sheet illumination of fog particles, this design proved to eliminate leakage along the side of the mask but needs further optimization to eliminate leakage along the nose bridge. In performance testing, the mask did not have a significant effect on the heart rate of a user during light to moderate exercise and was comfortable to wear during that testing. Therefore, a mask was created that accomplished the goals of this project: the mask had high efficiency measurements, was effective in filtering the user's output breath, was comfortable to wear, and was made from reusable and commonly available textile materials.

Although more work is required to produce a mask that eliminates all leakage, this design improves upon designs currently available and provides more protection than a single-use surgical mask. It is the hope of this project that textile face masks can improve such that single-use masks are not relied upon, thereby decreasing waste production, and protecting the environment. With further development, textile masks could be improved upon and be available for healthcare professionals who use this equipment daily but have no reusable resources available.

Continued development in the field of filtration of textiles as they apply to face coverings or filter material is necessary in the world today. The recent pandemic has further emphasized the need for preparation of an event similar to COVID-19 in the future and having devices that can be emulated at home but are proven to be effective is of high importance. Additionally, this work can be applied in other fields in which face coverings and personal protective equipment are necessary to prevent particulate spread and keep the user safe.

6.2 Future Work

The exploration of reusable textiles in filtration applications for face coverings and respirators is a new field brought to light during the COVID-19 pandemic. Many gaps are present in literature which fail to address effects of fabric weave on filtration capacity after wash and wear, as well as capabilities of textile masks for filtration without having to use a removable filter inside. Therefore, many developments and future exploration is needed to fully investigate the possibilities of textiles in this application.

Specifically, regarding this project, various aspects could not be fully explored due to time constraints as well as financial constraints. This includes the fabric testing, illumination testing, and performance testing performed.

The fabric testing would be most advantageous had it been performed for each potential fabric configuration. For example, breathability and filtration efficiency could have been evaluated for the following options: two cotton fabric layers, three cotton fabric layers, two knit fabric layers, three knit fabric layers, two cotton layers with a meltblown filter, two cotton layers with a spunbonded filter, and two fabric layers with a spunbonded and meltblown filter layer. Therefore, each filter layer could be evaluated for its effect on breathability and filtration efficiency, and fabric weave could have been evaluated for its effect as well. This was not possible for the current project due to time constraints, the volume of samples necessary to produce for these tests, as well as the cost of performing all these tests.

Next, illumination testing could be further explored for different nosepiece types. Although leakage was almost eliminated along the side plane, the nose bridge still demonstrated visible leakage and results were not conclusive whether it was decreased as compared to the surgical mask or not. Therefore, additional nosepiece designs could be implemented and tested with the laser visualization setup to see if altering this design could fully eliminate leakage shown here.

Another area that would need additional exploration includes the performance testing aspect of the project. The performance testing experiment would likely need to be replicated numerous times to deliver more accurate results depicting trends of any kind, and it would also be desirable to use instrumentation that provided more significant digits or was known to provide more accurate results than that of an Apple Watch. Additionally, it could be advantageous to run the tests for longer periods of time to observe if prolonged use caused results to diverge and indicate effects of wearing the mask, instead of producing similar results as experienced in this study.

Finally, it would be advantageous to repeat all testing once the mask or mask samples have been washed numerous times. Although the initial testing demonstrates performance of new fabric, if the mask is to be washable and reusable it is important to investigate if the bacterial filtration efficiency and initial filtration efficiency is retained once the fabric has endured wear and repeated washing. Additionally, it is possible that nosepieces lose shape after many uses, and illumination testing after prolonged use of the mask and nosepiece could highlight the effect of this wear on the mask design and its capabilities. The performance testing could also produce different results if the mask is worn and functionality decreases.

Finally, manufacturability of the mask was not evaluated in detail. If the mask is intended to be produced in a large scale, cost analysis of fabric, filter material, brace material, and production methods would be helpful to ensure that the product is both effective and profitable. A goal of the project is to revitalize the textile industry in the state of Alabama, and a mask design with low profitability would not be able to accomplish this goal.

Appendix A:

A1. Mask Pattern

Fit to fill full page when printing image. Can be scaled to accommodate different sizes.

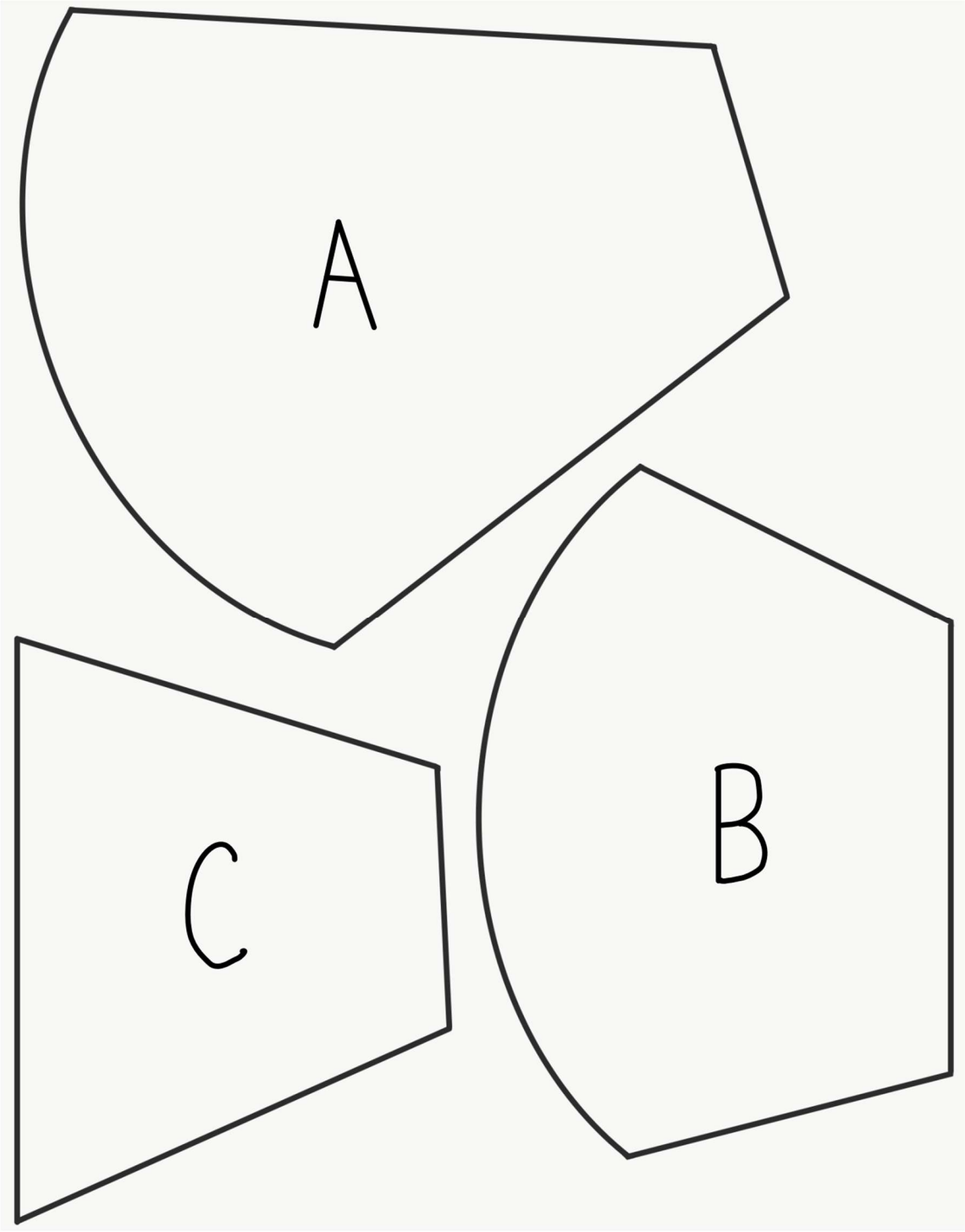

A2. Detailed Mask Instructions

Sewing Instructions:

1. Cut two of each piece detailed in the mask pattern PDF included in this Appendix.

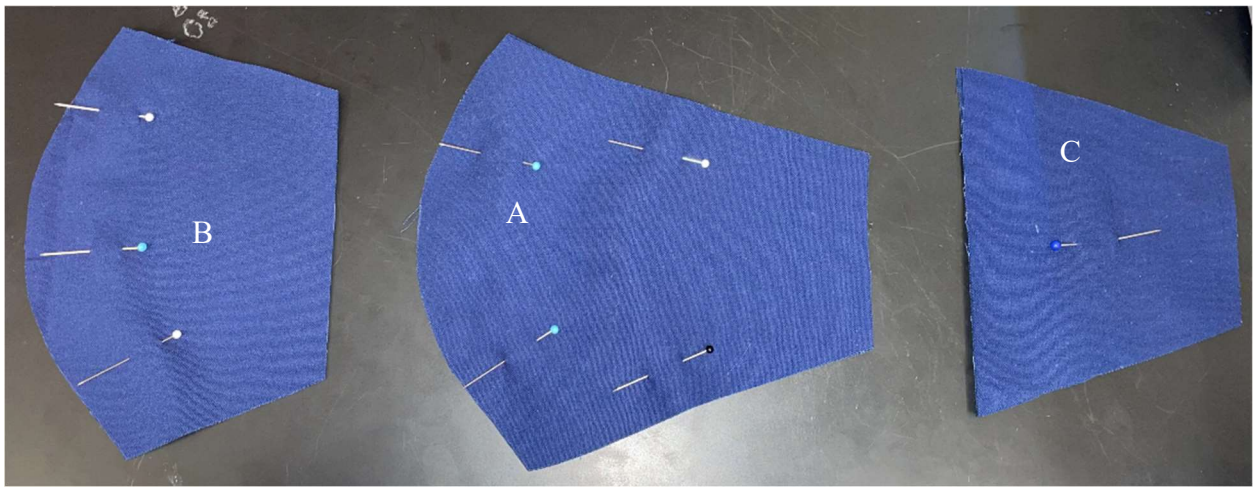

2. Sew along the center line of pieces A and B.

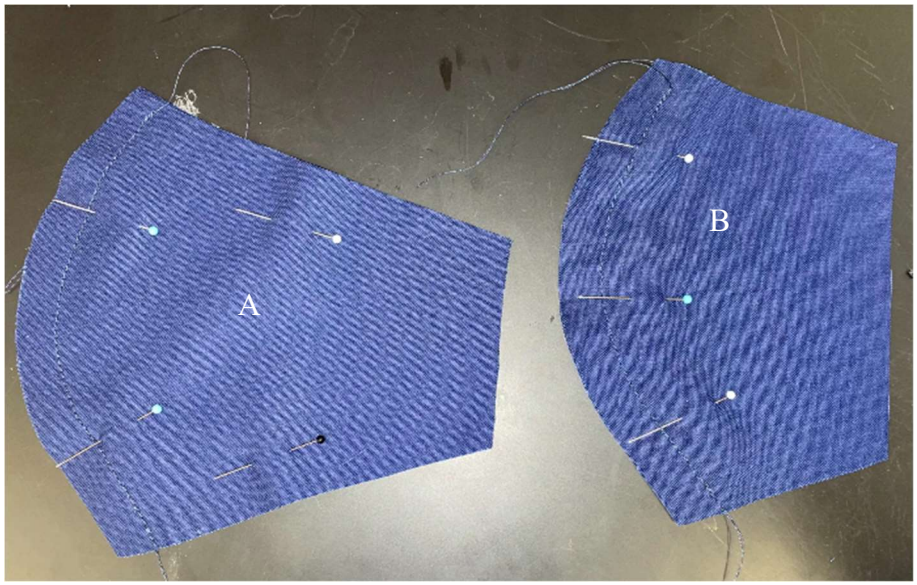

3. Finish raw edges on outer sides of A, B, and C.

4. For the channel holding the mouthpiece in piece B, cut a strip of cotton fabric 1 inch wide and around 7 inches long. Finish the raw top short edge. Attach the piece along the middle seam of piece B about 0.75" down, folding edges to finish them.

5. Finally, pin together pieces A, B, and C in the following order: A, wrong side facing up; B, right side facing up; C, right side facing up. Pieces A B, and C should align along the top and bottom raw edges, while A and C should align along the finished side seams.

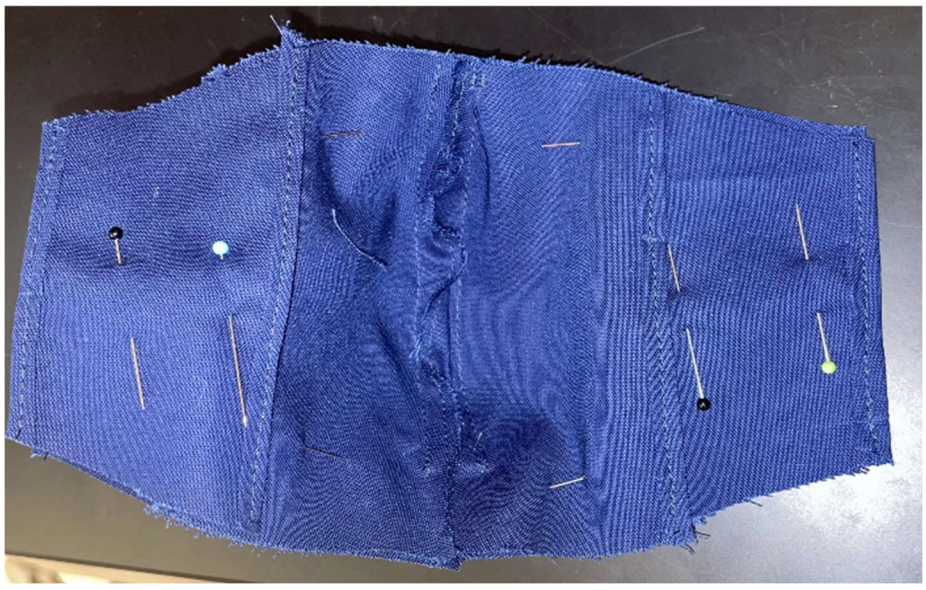

6. Sew along the edge of the top and bottom raw edges to attach all three pieces. Then, flip the mask inside out such that B is now facing outward on the right side as well as A. Piece C should be tucked under B such that the filter pocket is accessible.
7. Sew along the top and bottom close to the edges to close the seams. Sew another line along the previous seam about 1/2" lower to construct a channel for the elastic band and nosepiece.
8. Using a wire or crochet hook, feed the elastic through the outer channel along the top and

bottom of the mask. Knot off the elastic so that no excess material creates extrusive loops that could catch on keys or eyeglasses if in the user's pocket or bag.

3D-Printing Instructions:

1. Print the nose and mouthpiece from the linked STL or SolidWorks files in the article. Pieces should be printed from PLA at 100% infill and should lay flat.
2. Once printed, allow to cool.

Assembly:

1. Feed the nosepiece through the outer, shorter channel at the top of the mask so that it is enclosed by the cotton fabric, then feed the mouthpiece into the central pocket of piece B. Both pieces should be removed during washing.

2. Cut a piece of melt blown filter paper to fit inside the filter pocket if necessary. This filter layer will provide extra filtration when the mask is in use. The filter should be removed for washing and replaced after each use.

Bibliography

[1] H. J. Schunemann, E. A. Akl, R. Chou, D. K. Chu, M. Loeb, T. Lofti, R. A. Mustafa, I. Neumann, L. Saxinger, S. Sultan and D. Mertz, "Use of facemasks during the COVID-19 pandemic," *National Library of Medicine,* 2020.

[2] Y. Wang, Z. Deng and D. Shi, "How effective is a mask in preventing COVID-19 infection?," *Wiley Public Health Emergency Collection,* no. 10163, 2021.

[3] S. E. Eikenberry, M. Mancuso, E. Iboi, T. Phan, K. Eikenberry, Y. Kuang, E. Kostelich and A. B. Gumel, "To mask or not to mask: Modeling the potential for face mask use by the general public to curtail the COVID-19 pandemic," *Infectious Disease Modelling,* vol. 5, pp. 293-308, 2020.

[4] World Health Organization, "WHO Coronavirus (COVID-19) Dashboard," World Health Organization, 2022. [Online].

[5] World Health Organization, "WHO Coronavirus (COVID-19) Dashboard," 2022. [Online]. Available: https://covid19.who.int/.

[6] Centers for Disease Control and Prevention, "Trends in Number of COVID-19 Cases and Deaths in the US Reported to CDC, by State/Territory," 2022. [Online]. Available: https://covid.cdc.gov/covid-data-tracker/#trends_dailycases.

[7] C.-s. Wang and Y. Otani, "Removal of Nanoparticles from Gas Streams by Fibrous Filters: A Review," *Industrial and Engineering Chemistry Research.*

[8] S. Adanur, PhD., Wellington Sears Handbook of Industrial Textiles, Basel: Wellington Sears Company, 1995.

[9] M. W. Okruch, "Experimental observation of the relationship between the pressure drop and flow rate," University of Louisville, Electronic Theses and Dissertations,, 2016.

[10] P. Robertson, "Comparison of Mask Standards, Ratings, and Filtration Effectiveness," Smart Air, 2021.

[11] N95DECON, "Standards for Surgical N95 Filtering Facepiece Respirators and Surgical Masks: COVID-19," 3 August 2020. [Online]. Available: https://static1.squarespace.com/static/5e8126f89327941b9453eeef/t/5f2f458117f1700098c7c8c3/1596933505885/N95DECON_Respirator_Mask_Standards_Technical_Report_200803.pdf.

[12] P. Bilek and P. Sidlof, "Measuring of filtration efficiency of nonwoven textiles in volume from scattered light by seeding particles," *EPJ Web of Confrences,* vol. 45, p. 01014, 2013.

[13] ASTM International, "ASTM International Approves Face Covering Standard, Releases PPE White Paper," ASTM International, 17 February 2021. [Online]. Available: https://newsroom.astm.org/astm-international-approves-face-covering-standard-releases-ppe-white-paper. [Accessed 19 January 2022].

[14] S. F. o. R. ASTM Committee F23 on Personal Protective Clothing and Equipment, "Standard Specification for Barrier Face Coverings, Designation F3502-21," 15 February 2021. [Online]. Available: 10.1520/F3502-21. [Accessed 19 January 2022].

[15] W. C. Hill, M. S. Hull and R. I. MacCuspie, "Testing of Commercial Masks and Respirators and Cotton Mask Insert Materials using SARS-CoV-2 Virion-Sized Particulates: Comparison of Ideal Aerosol Filtration Efficiency versus Fitted Filtration

Efficiency," *Nano Letters,* vol. 20, pp. 7642-7647, 2020.

[16] A. V. Mueller, M. J. Eden, J. M. Oakes, C. Bellini and L. A. Fernandez, "Assessment of Particle Removal Efficiency of Fabric Masks as Alternatives to Standard Surgical Masks for PPE," *Matter,* vol. 3, pp. 950-962, 2020.

[17] F. M. Blachere, A. R. Lemons, J. P. Coyle, R. C. Derk, W. G. Lindsley, D. H. Beezhold, K. Woodfork, M. G. Duhling, B. Boutin, T. Boots, J. R. Harris, T. Nurkiewicz and J. D. Noti, "Face mask fit modifications that improve source control performance," *American Journal of Infection Control,* vol. 50, pp. 133-140, 2022.

[18] H. Whiley, T. P. Keerthirathne, M. A. Nisar, M. A. F. White and K. E. Ross, "Viral Filtration Efficiency of Fabric Masks Compared," *Pathogens,* vol. 9, no. 762, pp. 1-8, 17 September 2020.

[19] A. Konda, A. Prakash, G. A. Moss, M. Schmoldt, G. D. Grant and S. Guha, "Aerosol Filtration Efficiency of Common Fabrics Used in Respiratory Cloth Masks," *ACS Nano,* vol. 14, pp. 6339-6347, 2020.

[20] O. Aydin, B. Emon, S. Cheng, L. Hong, L. P. Chamarro and M. T. A. Saif, "Performance of fabris for home-made masks against the spread of COVID-19 through droplets: a quantitative mechanistic study," *Extreme Mechanics Letters,* vol. 40, 2020.

[21] A. Konda, A. Prakash, G. A. Moss, M. Schmoldt, G. D. Grant and S. Guha, "Response to Letters to the Editor on Aerosol Filtration Efficiency of Common Fabrics Used in Respiratory Cloth Masks: Revised and Expanded Results," *ACSNano,* vol. 14, pp. 10764-10770, 2020.

[22] K. a. R. S. G. a. C. KG, "Face protection, especially protective mask". Germany Patent

DE202020101979U1, 21 April 2020.

[23] S. K. GmbH, "Multi-layer mask with reversible, removable multi-layer filter for repeated use and cleaning options". Germany Patent DE202020101788U1, 4 May 2020.

[24] F. S. &. C. K. GmbH, "Mouth and nose protective mask". Germany Patent DE202020106904U1, 9 December 2020.

[25] J. E. Carstens, "Body conforming textile holder and filter article". United States Patent US7614399B2, 10 November 2009.

[26] P. C. Beller, "A Mask In 15 Minutes: How An Engineer's 3D-Printed Design For COVID-19 Protection Went Viral," General Electric, 21 May 2020. [Online].

[27] J. Low, "How to design snap-fit joints for 3D printing," HUBS B.V., 2022. [Online]. Available: https://www.hubs.com/knowledge-base/how-design-snap-fit-joints-3d-printing/.

[28] Mark Forged, "3D Printed Joinery: Simplifying Assembly," Markforged, 2022. [Online]. Available: https://markforged.com/resources/blog/joinery-onyx.

[29] I. Gocek, "Design, synthesis and characterization of polymeric films and membranes," 10 May 2010. [Online]. Available: https://etd.auburn.edu/handle/10415/2179.

[30] ASTM International, "Designation: F2299/F2299M − 03: Standard Test Method for Determining the Initial Efficiency of Materials Used in Medical Face Masks to Penetration by Particulates Using Latex Spheres," 1 June 2017. [Online]. Available: 10.1520/F2299_F2299M-03R17.

[31] European Committee for Standardization, "EN 14683:2019+AC Medical Face Masks - Requirements and Test Methods," August 2019. [Online]. Available:

https://www.edana.org/docs/default-source/international-standards/nbn-en-14683_2019-ac-2019_e.pdf?sfvrsn=3797c92b_4.

[32] ASTM International, "Designation: F2101 − 19: Standard Test Method for Evaluating the Bacterial Filtration Efficiency (BFE) of Medical Face Mask Materials, Using a Biological Aerosol of Staphylococcus aureus," 1 July 2019. [Online]. Available: 10.1520/ F2101-19.

[33] S. Morris, W. McAtee, J. Capecelatro and V. Raghav, "Influence of expiratory flow pulsatility on the effectiveness of a surgical mask," *Journal of Exposure Science & Environmental Epidemiology,* pp. 1-9, 2022.

[34] A. H. Techet, "2.016 Hydrodynamics," 22 September 2005. [Online]. Available: https://web.mit.edu/2.016/www/handouts/2005Reading4.pdf.

[35] BH Photo Video, "Nikon Z50 Mirrorless Camera with 16-50mm and 50-250mm Lenses," 2022. [Online]. Available: https://www.bhphotovideo.com/c/product/1511295-REG/nikon_1632_z_50_mirrorless_digital.html/?ap=y&ap=y&smp=y&smp=y&lsft=BI%3A514&gclid=CjwKCAjwrqqSBhBbEiwAlQeqGgOgaI4bcCroeZ6QPvqeZpPwsaAnIZsSZkgIP-Jt-q42RcmXJAtgABoChkAQAvD_BwE.

[36] K. P. Burr, "Fluids - Lecture 8 Notes," 23 August 2003. [Online]. Available: https://web.mit.edu/16.unified/www/FALL/fluids/Lectures/f08.pdf.

[37] A. Rohatgi, "WebPlotDigitizer," August 2021. [Online]. Available: https://automeris.io/WebPlotDigitizer.

[38] F. G. Morais, V. K. Sakano, L. N. de Lima, M. A. Franco, D. C. Reis, L. M. Zanchetta, F. jorge, E. Landulfo, L. H. Catalani, H. M. Barbosa, V. M. John and P. Artaxo, "Filtration efficiency of a large set of COVID-19 face masks commonly used in Brazil," *Aerosol*

Science and Technology, vol. 55, no. 9, 2021.

[39] Y. M. Bar-On, A. Flamholz, R. Phillips and R. Milo, "SARS-Cov-2 (COVID-19) by the numbers," 2020. [Online]. Available: doi:10.7554/eLife.57309.

[40] S. Rengasamy, R. Shaffer, B. Williams and S. Smit, "A comparison of facemask and respirator filtration test methods," *Journal of Occupational and Environmental Hygiene,* vol. 14, no. 2, 2017.